

Electronic Thesis and Dissertation Repository

2-1-2021 2:00 PM

The Development of Region-Specific Decellularized Meniscus Bioinks for 3D Bioprinting Applications

Sheradan Doherty, *The University of Western Ontario*

Supervisor: Flynn, Lauren, *The University of Western Ontario*

A thesis submitted in partial fulfillment of the requirements for the Master of Engineering Science degree in Biomedical Engineering

© Sheradan Doherty 2021

Follow this and additional works at: <https://ir.lib.uwo.ca/etd>

Recommended Citation

Doherty, Sheradan, "The Development of Region-Specific Decellularized Meniscus Bioinks for 3D Bioprinting Applications" (2021). *Electronic Thesis and Dissertation Repository*. 7606.
<https://ir.lib.uwo.ca/etd/7606>

This Dissertation/Thesis is brought to you for free and open access by Scholarship@Western. It has been accepted for inclusion in Electronic Thesis and Dissertation Repository by an authorized administrator of Scholarship@Western. For more information, please contact wlsadmin@uwo.ca.

Abstract

The incorporation of meniscus extracellular matrix (ECM) into a 3D printable bioink has the potential to promote tissue regeneration by providing biological cues that direct cell survival, proliferation, and lineage-specific differentiation. This study developed region-specific meniscus ECM bioinks and assessed their effects on the viability, retention, and differentiation of adipose-derived stromal cells (ASCs). A novel meniscal decellularization protocol was developed and demonstrated effective removal of cellular content and preservation of key ECM constituents. When incorporated into alginate-based bioinks, the decellularized inner and outer meniscus demonstrated cell-instructive effects supporting ASC retention, and enhancing differentiation towards a fibrochondrogenic phenotype when cultured with chondrogenic differentiation medium. These studies provide relevant new insight supporting that region-specific ECM can be harnessed to direct cell phenotype and function within tissue-engineered scaffolds.

Keywords

Decellularized meniscus, meniscus, extracellular matrix (ECM), tissue engineering, adipose-derived stromal cells, naturally-derived materials, cell-based therapy, chondrogenesis, cell-instructive biomaterials, bioprinting, osteoarthritis

Summary for Lay Audience

The meniscus is the most commonly injured structure in the knee joint. With a limited capacity for self-repair, injury often requires surgical intervention. Due to a lack of repair techniques, the leading procedure used in this treatment is the complete or partial removal of the damaged tissue, otherwise known as a meniscectomy. The meniscus plays an important role in ensuring the health of the knee joint, and therefore, its removal is associated with wear and tear of the joint that ultimately leads to the onset of osteoarthritis (OA). OA inflicts significant health and economic burdens on society, as it is the second most prevalent chronic condition in Canada. As such, there is a critical need for an effective treatment that promotes regeneration and restores the function of the meniscus. Three-dimensional (3D) bioprinting is a technique that can be used to fabricate customizable meniscus implants. However, one limitation of this approach is that the standard materials being used do not incorporate biological cues to direct cells in the repair process. This project focuses on incorporating meniscus-specific proteins and a regenerative cell population into a printable bioink. Overall, these proteins may enhance cell survival and direct the differentiation of the encapsulated cells to help regenerate injured meniscal tissues. This thesis developed a new protocol for isolating meniscus-specific proteins with minimal changes to their native characteristics. A modified liquid form of these proteins was then incorporated into a printable bioink with regenerative cells derived from human fat tissue. As a first step towards testing the potential of this therapy, gel beads were made from the protein-containing bioinks and cultured for 28 days. For comparative purposes, an additional bioink that did not contain meniscus proteins was also cultured for 28 days. The results indicated that the incorporation of meniscus proteins into the bioink promoted the cells to remain inside of the beads and provided evidence that the regenerative cells were directed towards meniscus-like cells. These studies represent a key first step in developing a 3D bioprintable therapy to regenerate damaged meniscus.

Co-Authorship Statement

The meniscus decellularization protocol applied in this project was based on a protocol previously developed by Anna Kornmuller for processing porcine auricular cartilage. All experimental work included in this thesis was completed by Sheradan Doherty, with the exception of the immunohistochemical staining and imaging presented in Figure 3.5, which was performed by Dr. Pascal Morissette Martin on samples prepared by Sheradan Doherty. In addition, Dr. Morissette Martin helped to establish the immunohistochemical staining protocols for the alginate-based beads. However, the staining and imaging presented in Figures 3.10. and 3.11 were completed by Sheradan Doherty.

Acknowledgments

First and foremost, I would like to express my sincere gratitude to my supervisor, Dr. Lauren Flynn. Thank you for providing me with endless support, guidance, patience, and commitment. Thank you for teaching me skills required to think critically and to be confident in my work; these will follow me in all of my future endeavours. I admire your intelligence, work ethic, and success as a scientist. I am proud to call myself a member of your team and value my time spent under your supervision.

Thank you to Aspect Biosystems for an enjoyable and informative internship, and for generously providing essential materials for these studies. Especially thanks to Dr. Spiro Getsios, Dr. Valerio Russo, Dr. Sheng Pan, Dr. Kamal Khan, and Dr. Katherine Thain.

To my advisory committee, Dr. Tom Appleton and Dr. David Hess, thank you for your insightful feedback and criticism, and dedication in guiding this project to completion.

To all members of the Flynn lab, I am so grateful for the opportunity to have worked with each one of you. Thank you for always taking time out of your busy schedules to help and support me, both in and outside of the lab.

To my roommates-turned-best-friends, Megan and Sarah, thank you for being the ones I got to come home to at the end of my days. I will cherish our memories, and countless hours of laughter, couch time, and country music forever.

Thank you to my family, especially my parents, Thom and Annie, for your love and encouragement throughout my life and education. Thank you for providing me with every opportunity to pursue my interests and goals, and for continuously supporting and trusting my decisions. I love you.

Lastly, I would like to thank my dog, Seamus. Whether it be a video or a visit home, when times were tough, and work was hard, your spunky, loving, and playful personality never failed to brighten my day.

Table of Contents

Abstract	ii
Summary for Lay Audience	iii
Co-Authorship Statement	iv
Acknowledgments.....	v
Table of Contents.....	vi
List of Tables.....	ix
List of Figures.....	x
List of Appendices	xii
List of Abbreviations	xiii
Chapter 1	1
1 Literature Review.....	1
1.1 The Meniscus	1
1.1.1 Structure and Function	1
1.1.2 Vascularization and Innervation.....	2
1.1.3 Biochemical Composition and Organization	3
1.1.4 Cells of the Meniscus.....	4
1.2 Clinical Significance	5
1.2.1 Traumatic and Degenerative Changes to the Meniscus	5
1.3 Current Clinical Interventions.....	6
1.4 Regenerative Interventions Targeting the Meniscus	9
1.4.1 Three-Dimensional (3D) Bioprinting	12
1.5 Decellularized Tissue Bioscaffolds.....	15
1.5.1 Overview of Tissue Decellularization.....	15
1.5.2 Methods for Characterizing Decellularized Tissue	16

1.5.3	Cell-Instructive Effects of Decellularized Tissues	17
1.5.4	Meniscal Decellularization Protocols	18
1.6	Adipose-derived Stromal Cells (ASCs).....	19
1.6.1	Donor and Depot Effects on ASCs.....	21
1.6.2	ASC Chondrogenesis	21
1.7	Project Overview.....	22
1.7.1	Project Rationale.....	22
1.7.2	Hypothesis	23
1.7.3	Specific Aims	23
Chapter 2	25
2	Materials and Methods	25
2.1	Materials	25
2.2	Meniscal Decellularization	25
2.3	Characterization of Decellularized Tissues	27
2.3.1	Histological Analyses	27
2.3.2	Biochemical Analyses.....	27
2.3.3	Scanning Electron Microscopy.....	29
2.3.4	Immunohistochemical Analyses.....	30
2.4	Human Adipose-Derived Stromal Cell (ASC) Isolation and Culture	30
2.5	Fabrication of Composite Alginate-ECM Beads	32
2.5.1	Pepsin Digestion of Cryomilled Meniscus.....	32
2.5.2	Cell Encapsulation within Alginate-Based Beads	32
2.5.3	Characterization of Bead Size	33
2.6	<i>In vitro</i> Assessment of Human ASCs Encapsulated in the Bioinks.....	33
2.6.1	Confocal Analysis of Cell Viability and Density using the LIVE/DEAD® Assay.....	33

2.6.2	Gene Expression Analysis.....	34
2.6.3	Immunohistochemical Characterization of ECM Markers within Alginate-Based Beads.....	36
2.7	Statistical Analyses.....	37
Chapter 3	38
3	Results	38
3.1	Comparison of Protocols to Decellularize Porcine Meniscal Tissues.....	38
3.2	Immunohistochemical Characterization of the ECM Composition within the Decellularized Meniscus.....	45
3.3	Bead Synthesis Through Dropcasting of the Alginate-Based Bioinks.....	47
3.4	Viability and Retention of Human ASCs Encapsulated and Cultured in the Alginate-Based Beads.....	47
3.5	Chondrogenic Gene Expression in the Human ASCs Cultured in the Alginate-Based Beads	51
3.6	Immunohistochemical Analysis of Chondrogenic ECM Expression in the Alginate-Based Beads.....	53
Chapter 4	56
4	Discussion.....	56
Chapter 5	65
5	Conclusion	65
5.1	Summary of Findings	65
5.2	Conclusions and Significance.....	67
5.3	Future Directions.....	67
References	69
Curriculum Vitae	94

List of Tables

Table 1.1: Comparison of commonly-used bioprinting techniques.....	14
Table 2.1: RT-qPCR Primer Sequences.....	36

List of Figures

Figure 1.1. Anatomy of the meniscus.....	2
Figure 1.2. Regional variations in vascularization and cell types within the meniscus.....	3
Figure 1.3. Transcriptional control of chondrogenesis.....	22
Figure 2.1. Schematic of meniscus extraction and separation of inner and outer regions.....	25
Figure 3.1. Cell extraction was enhanced in the meniscus samples processed with decellularization Protocol A.....	39
Figure 3.2. Collagen content remained similar in the inner region and was enriched in the outer region following decellularization with both protocols.....	41
Figure 3.3. Protocol A enhanced the retention of glycosaminoglycan (GAG) content in the processed tissues.....	43
Figure 3.4. Scanning electron microscopy (SEM) images of native and decellularized meniscus showing that all samples had a complex fibrous ECM ultrastructure.....	44
Figure 3.5. Immunohistochemical analyses confirmed the presence of key ECM components following decellularization.....	46
Figure 3.6. Macroscopic image of alginate-based beads post-encapsulation shows similar appearance of all formulations.....	47
Figure 3.7. LIVE/DEAD staining confirmed that the human ASCs remained highly viable following encapsulation and culture in proliferation media for 28 days.....	49
Figure 3.8. LIVE/DEAD confirmed that the human ASCs remained highly viable following encapsulation and culture in chondrogenic differentiation media for 28 days.....	50
Figure 3.9. Chondrogenic ECM gene expression was enhanced in the human ASCs encapsulated within the alginate-based beads following 28 days of culture in chondrogenic differentiation medium.....	52

Figure 3.10. Immunohistochemical staining showing limited ECM marker expression within the alginate-based beads following 30 days of culture in proliferation medium..... 54

Figure 3.11. Immunohistochemical staining showing enhanced ECM marker expression within the composite alginate + ECM beads following 28 days of culture in chondrogenic medium..... 55

List of Appendices

Appendix A: Supplementary Data	89
Appendix B: Research Ethics Board Approval	92
Appendix C: Figure Permissions	93

List of Abbreviations

3D	Three-dimensional
ABAM	Antibiotic-antimycotic
ACAN	Aggrecan
ACL	Anterior cruciate ligament
ALG	Alginate
ASC	Adipose-derived stromal cell
BCP	Basic calcium phosphate
BMI	Body mass index
BMP	Bone morphogenic protein
BMSC	Bone marrow-derived stromal cell
BSA	Bovine serum albumin
CMI	Collagen meniscus implant
COMP	Cartilage oligomeric matrix protein
CT	Computed tomography
CXCL6	Chemokine ligand 6
DAPI	4',6-diamidino-2-phenylindole
dH ₂ O	Deionized water
DIM	Decellularized inner meniscus
DMEM/F12	Dulbecco's Modified Eagle Medium: Nutrient Mixture F-12
DMMB	Dimethylmethylene blue
DNase	Deoxyribonuclease
DOM	Decellularized outer meniscus

dsDNA	Double-stranded DNA
ECM	Extracellular matrix
EDTA	Ethylenediaminetetraacetic acid
FN	Fibronectin
GAG	Glycosaminoglycan
GDF-5	Growth differentiation factor-5
GUSB	Glucuronidase beta
IHC	Immunohistochemical
IL-8	Interleukin-8
KRB	Kreb's Ringer Buffer
KS	Keratan sulphate
LAB	Laser-assisted bioprinting
LN	Laminin
MAT	Meniscus allograft transplant
MMP	Matrix metalloproteinase
MRI	Magnetic resonance imaging
MSC	Mesenchymal stem cell
OA	Osteoarthritis
OHP	Hydroxyproline
PBS	Phosphate buffered saline
PCL	Posterior cruciate ligament
PFA	Paraformaldehyde
PMSF	Phenylmethylsulfonyl fluoride

PRP	Platelet-rich plasma
RNase	Ribonuclease
RPL13A	Ribosomal protein L 13a
RUNX2	Runt-related transcription factor 2
SDS	Sodium dodecyl sulphate
SEM	Scanning electron microscopy
SOX-9	Sex-determining region Y-related high motility group box 9
SPB	Sorenson's phosphate buffer
SVF	Stromal vascular fraction
TBST	Tris-buffered saline with 0.1% tween
TCPS	Tissue culture polystyrene
TE	Tris-EDTA
TGF- β	Transforming growth factor- β
WHO	World Health Organization

Chapter 1

1 Literature Review

1.1 The Meniscus

1.1.1 Structure and Function

The menisci are a pair of crescent-shaped fibrocartilaginous structures that play a fundamental role in the knee. Historically, these tissues were once considered to be vestigial, however, they are now recognized as being essential for the proper function and health of the joint [1]. Each knee contains a medial and lateral meniscus positioned between the femoral condyle and the tibial plateau [2]. Macroscopically, healthy menisci appear white, smooth, and glossy [1].

In most adult humans, the medial meniscus ranges from 40-45 mm in length and covers 51-74% of the medial articular surface, whereas the lateral meniscus is 32-35 mm in length and covers 75-93% of the lateral articular surface [3], [4]. Though both structures are semi-lunar and wedge-shaped, the lateral meniscus is more rounded and exhibits greater variety in size and shape [5]. The main ligaments that anchor the menisci are the medial and lateral collateral ligaments, the transverse ligament, and attachments at the anterior and posterior horns [5] (Figure 1.1).

Due to their unique anatomy, the menisci are highly specialized at enabling articulation between the femoral condyles and tibial plateau. Furthermore, the menisci reduce stress on underlying cartilage by converting vertical compressive forces to radial tensile forces [5]–[7]. The maintenance of the structural integrity of the menisci is crucial, as they must withstand the transmission of up to several times a person's body weight between the femur and tibia [8]. In addition to providing joint stability, as well as facilitating load transmission and shock absorption, the meniscus also plays a vital role in supplying nutrition and lubrication to the knee joint [1].

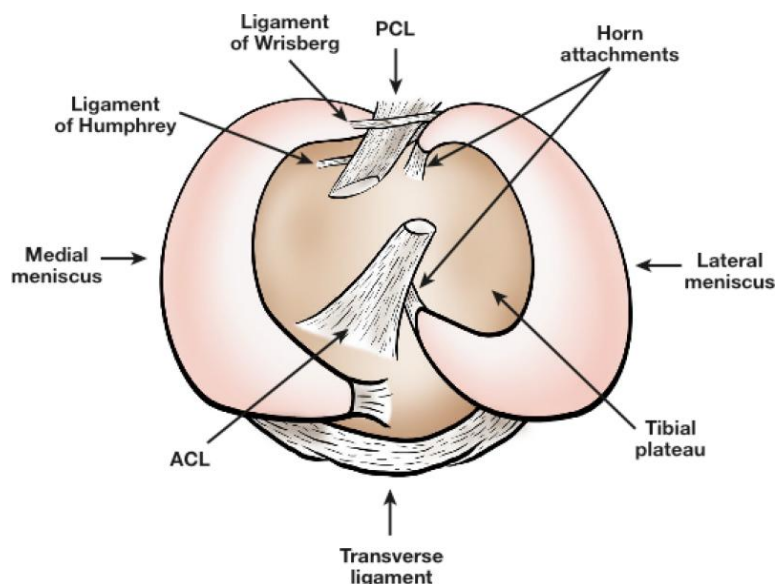


Figure 1.1. Anatomy of the meniscus. Superior view of the meniscus anchored by horn attachments and surrounding ligaments. Abbreviations: ACL=anterior cruciate ligament, PCL=posterior cruciate ligament. Image obtained with permission from [5].

1.1.2 Vascularization and Innervation

During fetal development and shortly after birth, the meniscus is fully vascularized. However, at approximately 3 months of age, the menisci become increasingly avascular, suggesting that an abundant blood supply is required for early meniscal development [9]. At approximately 10 years of age, meniscal vascularization reaches full maturity, wherein only the peripheral 10-30% of the outer meniscus border contains blood vessels and nerves (Figure 1.2) [5]. This organization results in the formation of 2 distinct regions separated by a transitioning section. More specifically, the peripheral region that is relatively vascularized is termed the red-red zone, the inner completely avascular region is termed the white-white zone, and the middle transition region is termed the red-white zone [2]. The medial, lateral, and middle genicular arteries provide the major vascularization to the outer menisci [1]. The remaining portion of each meniscus receives nourishment via the diffusion of nutrients from the synovial fluid [1]. There is a direct relationship between the vascularization and self-healing capacity of the tissue, which predisposes the white-white region to permanent post-traumatic and degenerative lesions [5].

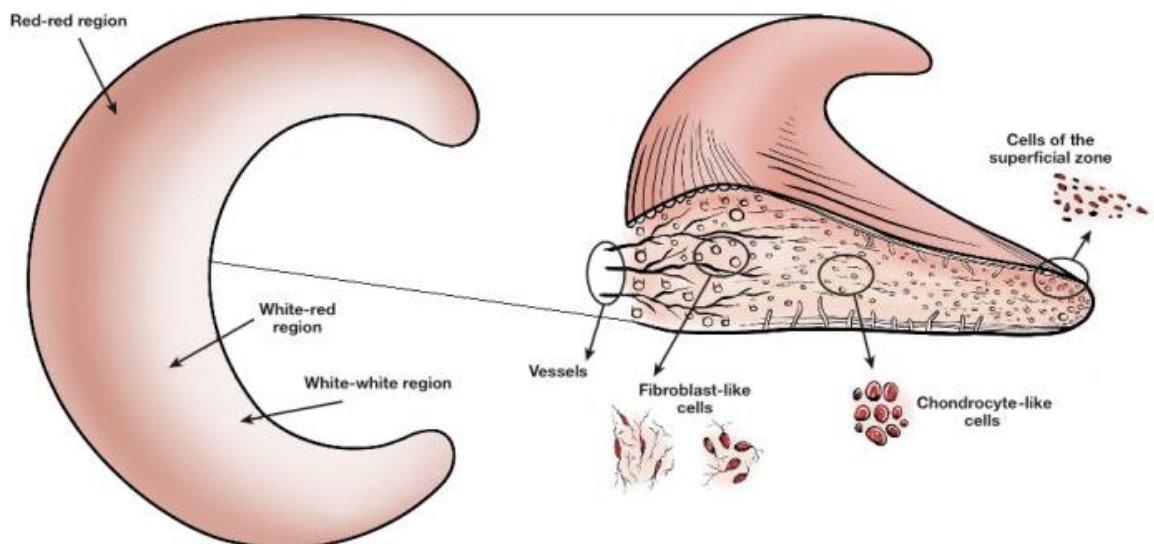


Figure 1.2. Regional variations in vascularization and cell types within the meniscus. The red-red region found in the outer periphery is well-vascularized. The innermost white-white region does not contain vasculature. The white-red region serves as a transition zone between the red-red and white-white regions. The outer region of the meniscus contains fibroblast-like cells, whereas the inner region contains chondrocyte-like cells. Image obtained with permission from [5].

1.1.3 Biochemical Composition and Organization

The meniscus has a unique three-dimensional (3D) ultrastructure and biochemical composition, which contribute to its complex mechanical properties. In the normal, healthy meniscus, water is the most abundant component, accounting for approximately 70% of the total wet weight. The remaining 30% is a combination of organic matter including collagens (~75%), proteoglycans (~17%), cellular content (2%), adhesion glycoproteins (<1%), and elastin (<1%) [10]. The cells and macromolecules of the menisci exhibit a unique zonal organization that gives rise to the two distinct regions, inner and outer, which have varying biochemical composition and structure [11].

Collagens: Collagen fibers in the menisci are arranged in 3 distinct layers: superficial, lamellar, and deep. The superficial layer is a thin layer of randomly oriented fibers. In the lamellar layer, situated just below the superficial layer, most collagen fibers are also randomly oriented, with the exception of the peripheral portions, where they are oriented radially. In the deep zone, collagen fibers are mainly circumferentially oriented with a smaller amount of radially oriented fibers, called tie fibers [12]. In the inner region of

bovine meniscus, collagen comprises approximately 70% of the dry weight, of which 60% is collagen type II and 40% is collagen type I. In the outer region, collagen type I makes up approximately 80% of the dry weight, with other collagen types (II, III, IV, VI, XVIII) present at less than 1% [1], [5], [13].

Proteoglycans: Proteoglycans are heavily glycosylated molecules consisting of a core protein with covalently attached glycosaminoglycans (GAGs) [14]. The main proteoglycan in meniscus is aggrecan [15]. GAGs within the extracellular matrix (ECM) are responsible for maintaining hydration and imparting a high capacity to resist compressive loads. The highest GAG content is found within the inner portion of the meniscus, which serves as the primary weightbearing area [1]. Specifically, in dry weight, the inner portion of the porcine meniscal body contains 8% GAG, whereas the outer portion contains only 2% [16]. In normal human adult meniscus, the GAG profile is comprised of chondroitin-6-sulphate (40%), dermatan sulphate (20-30%), chondroitin-4-sulphate (10-20%), and keratan sulphate (15%) [1].

Adhesion glycoproteins: Adhesion glycoproteins serve an important role in the meniscus ECM, although they only account for less than 1% of the dry weight. These bioactive components are responsible for binding matrix molecules to cells and other ECM components. The main adhesion glycoprotein present in the human meniscus is fibronectin [1], [17].

1.1.4 Cells of the Meniscus

The meniscus contains a heterogenous population of cells. During early development, all meniscal cells present the same morphology, however, following tissue maturation, the cells display an obvious regional variation in phenotype and ECM production [9]. In the inner region, mature cells are round and surrounded by a cartilage-like ECM [18]. The notable abundance of collagen type II and GAG is similar to hyaline cartilage and the cells in this region are classified as “chondrocyte-like” or fibrochondrocytes [18]–[20]. In contrast, the cells located in the outer vascular portion of the meniscus are more similar to fibroblasts in structure and function, with a spindle-shaped morphology [17], [18]. The matrix surrounding these cells is more ligament-like, enriched in collagen type I, and the

cells in the outer region are classified as “fibroblast-like” (Figure 1.2) [5]. Based on the phenotypes and distribution of cells in the meniscus, the inner portion of the tissue possesses cartilage-like behaviour that contributes to the compressive properties, and the outer portion exhibits fibrous-like properties, which contribute to the tensile behaviour of the tissue [18].

1.2 Clinical Significance

The meniscus is the most frequently injured structure in the knee joint and with a limited capacity for self-repair, meniscal injuries are one of the most common orthopaedic conditions requiring treatment through surgery [21]–[23]. Due to the lack of meniscal repair techniques, degenerative tears are often treated by partial or complete removal of the meniscus, otherwise known as meniscectomy. These procedures have been shown to alter the biomechanics of the joint, ultimately accelerating the onset of osteoarthritis (OA) by increasing wear and stress on the articular cartilage [6], [12].

OA is a long-term chronic disease that is associated with pain, swelling, and the deterioration of cartilage in joints. According to the World Health Organization (WHO), OA imposes a substantial burden on society, as it is the eleventh leading cause of disability worldwide, with the knee being the most affected joint [24]. Specifically, OA is the second most prevalent chronic condition in Canada, affecting 14% of the adult population, and it is associated with a heavy financial burden on the Canadian health care system, costing approximately 4.4 billion dollars annually [25].

1.2.1 Traumatic and Degenerative Changes to the Meniscus

Changes to the meniscus can be classified into two main categories: traumatic and degenerative [24]. Traumatic lesions often occur in younger active individuals as a result of a sports-related injury or some form of excessive force to a previously healthy joint [24]. In this case, it is most common to observe longitudinal tears that are parallel to the circumferential fibers, as well as occasionally radial tears that are perpendicular to the circumferential fibers [26], [27]. In contrast, degenerative lesions develop slowly and typically involve horizontal cleavages, flap, or complex tears or meniscal maceration in middle-aged to elderly individuals [26]–[28].

Recently, researchers have identified differences in the gene expression of molecular markers of OA related to the tear pattern of injured meniscal tissues [29]. In this study, samples of torn meniscus were acquired from the white-white zone of 48 patients aged 15-60 (37 with degenerative tears and 11 with traumatic tears) by partial meniscectomy and used for total RNA extraction and quantitative PCR. Most notably, it was found that interleukin-8 (*IL-8*), a cytokine that has been linked to OA, and chemokine ligand 6 (*CXCL6*), involved in mediating neutrophil recruitment to inflammatory sites, along with the matrix metalloproteinases (MMP) MMP1 and MMP3, were expressed at significantly higher levels in traumatic tears compared to degenerative tears [29]. In contrast, collagen type I expression was significantly higher in degenerative tears. Interestingly, there were no differences between the gene expression of OA markers in tears of the medial versus lateral menisci [29].

Additionally, calcification of the meniscus is a common finding amongst patients with OA and is thought to directly contribute to joint degeneration [30]. Specifically, basic calcium phosphate (BCP), which includes hydroxyapatite, octacalcium phosphate, and tricalcium phosphate, is the predominant form of crystals found within the menisci [30], [31]. The prevalence of BCP crystals in the synovial fluid of osteoarthritic knees has been found to be at least 60% [32]. Though the exact mechanisms through which calcium crystals contribute to OA are not fully understood, some *in vitro* studies support that BCP crystals can have many biological effects including the ability to induce cell mitosis, MMP secretion, and prostaglandin synthesis [33].

1.3 Current Clinical Interventions

The heterogenous nature of the meniscus gives rise to regionally-dependent healing properties. Specifically, lesions and tears to the outer vascularized tissue are able to heal, whereas there is a limited capacity for self-repair following damage to the inner avascular region, and medical intervention is often required. In fact, the surgical treatment of meniscal injuries is one of the most common procedures in the orthopaedic field [34]. For example, in the United States this accounts for over one million surgical procedures performed annually [34]–[36].

Meniscectomy: Due to a lack of repair techniques, meniscal injuries are most often treated by the complete or partial removal of the damaged meniscus, otherwise known as meniscectomy [22]. Previously, it was believed that removal of the meniscus would have no consequences as it was thought to be a vestigial structure within the knee joint. However, beyond the 1960s, long-term data following meniscectomy revealed subsequent complications including joint-space narrowing, altered biomechanics of the joint, and overall joint degeneration that accelerates the onset of OA [6]. Studies have shown that the complete removal of the meniscus results in a 40-70% reduction in the femur-tibia contact area, and a corresponding 100-300% increase in stress on the cartilage [37], [38].

Following the recognition of these adverse effects, surgeons have resorted to the partial excision of the tissue in an effort to prevent further tissue damage and minimize changes to the joint [39]. Partial meniscectomies are typically effective at alleviating short-term clinical symptoms including pain and joint swelling [40]. However, even the removal of minimal tissue compromises proper joint function by altering the load-bearing and load-distributing capacities of the meniscus [38], [39]. Furthermore, in a biomechanical study of partial versus total meniscectomies, it was shown that a linear correlation exists between the amount of meniscal tissue removed and increased stress on the joint surfaces [38]. This was further confirmed by other work that concluded knee function is inversely related to the amount of tissue resected [38]. Although the biomechanical changes to the joint following a partial meniscectomy are less severe, the procedure still leads to early cartilage wear and reduced functioning of the knee.

Other surgical interventions: In light of these findings, efforts have focused on developing techniques to repair damaged tissue, promote healing, and conserve normal joint function. A common method believed to fulfill these requirements involves suturing the torn tissue via an arthroscopic procedure [41], [42]. Briefly, surgeons insert a thin tube containing a camera and light into a small incision near the knee, allowing the surgeon to suture the torn tissue [41]. In addition to this traditional suturing method, other meniscal repair options include a range of meniscal fixators [42]. While these techniques

can be effective in the vascularized outer periphery of the meniscus, healing in the inner avascular region remains a challenge.

To overcome the reduced healing capacity in the inner region, methods to promote vascular inflow to the damaged tissue have been investigated. One method involves creating vascular access channels from the outer to the inner region. This is done by the use of needles that penetrate the outer region of the meniscus and are subsequently directed inwards towards the damaged tissue. Ultimately, this creates pathways that allow for the ingrowth of fibrovascular tissue to the damaged area [42]. The generation of these tunnels requires extensive skill and precision, as the surgeon must avoid over-penetration of the tissue that can cause further damage [42]. Clinical studies on humans have shown that these channels can be effective at healing tears less than 2 mm but have also been shown to alter the highly specific organization of the meniscus fibers, which compromises its structural integrity [41], [43], [44].

Alternatively, fibrin clot augmentation is another repair method in which an autologous fibrin clot is inserted into the site of the damaged tissue. This approach takes advantage of the platelet-rich matrix and associated biological factors provided by clots, which may act as chemical mediators to encourage tissue repair, as well as provide a structure on which this can occur [45]. Clots are typically prepared by obtaining a sample of the patient's peripheral blood and physically manipulating it to promote coagulation. The resultant clot is then arthroscopically inserted into the site of injury [45]. A study performed by Arnoczky *et al.* surgically induced tears in the avascular region of 6 dogs and used fibrin clots to repair them. After 6 months, the injured area had been filled with tissue that histologically resembled fibrocartilage, though it was noticeably distinct from the adjacent uninjured tissue [46]. In humans, small scale studies with limited patients have reported complete meniscal repair [47], [48]. Nevertheless, there is a lack of standardization between protocols and therefore, most surgeons are reluctant to select this approach.

A similar method of meniscal tissue repair involves the use of refined platelet-rich plasma (PRP). This technique delivers PRP extracted from autologous blood, which is

thought to be more concentrated in platelets and associated growth factors compared to fibrin clots [49]. Theoretically, PRP provides greater regenerative properties and the denser matrix is more easily manipulated into the knee. A recent study used the PRP method to treat meniscal tears that were induced in the avascular region of rabbit menisci. After 12 weeks, PRP delivered within a gelatin hydrogel was able to significantly repair defects compared to those treated with platelet-poor plasma within the same hydrogel and the hydrogel alone [49]. In humans, a study was conducted on 35 patients wherein 20 received an arthroscopic repair and the remaining 15 received the same procedure with the addition of PRP. No improvements were noted in the PRP-treated group as Clinical outcomes and reoperation rate were similar [50]. Analyses focusing on larger sample sizes and the long-term effects of biomechanical properties of this intervention are still required.

For complex meniscal defects that cannot be treated by conventional surgical techniques, meniscus allograft transplantation (MAT) has attracted increasing interest by surgeons [51],[52]. Clinical results indicate this procedure is effective at relieving pain and providing functional improvement to the joint in the short-term [52]. However, the reported success rates of MAT vary tremendously, ranging from approximately 12% to 100% (mean 60%) [52]. A notable factor that may contribute to the success of a MAT is the method of graft preservation used. For example, some studies have shown that deep-frozen grafts are less likely to elicit a negative and prolonged immune response due to lower cell viability and therefore, reduced immunogenicity when compared to fresh or cryopreserved grafts [53], [54]. In addition to the potential for disease transmission and eliciting a negative immune response in the host, other drawbacks to allograft transplantation include limited donor availability, and challenges associated with sizing and lack of customization of the grafts [55].

1.4 Regenerative Interventions Targeting the Meniscus

Regenerative interventions targeting the menisci aim to restore the composition and biomechanics of the native tissue. In theory, a scaffold that mimics the native meniscal environment should be used as a method to deliver and/or support regenerative cells as

they direct tissue repair. Although some cell-free approaches exist, cell-based strategies are emerging as an attractive alternative to promote meniscal repair and regeneration [21], [40], [56]. The effectiveness of these strategies depends heavily on the reparative capacity of the cells and the efficiency of their delivery method [21]. As such, a considerable amount of research has focused on exploring the application of various cell types and corresponding delivery platforms to be used.

In particular, mesenchymal stromal cells (MSCs) from bone marrow [57], adipose tissue [58], and synovium [59], as well as chondrocytes [55] and meniscal cells [60] have been studied. MSCs are an appealing cell source because they secrete a large variety of immunomodulatory molecules, and may contribute to the healing process within injured tissues through paracrine-mediated mechanisms [61]. Chondrocytes and meniscal cells are also of interest due to their ability to produce meniscus ECM [40]. However, there is no consensus on the optimal cell source due in part to a lack of comparative review, and every source has associated strengths and limitations.

Scaffolds used in meniscal tissue engineering can be broadly classified as synthetic polymer scaffolds (e.g. polyurethane, polycaprolactone, polylactic acid, polyglycolic acid, polylactic co-glycolic acid), hydrogels, or tissue-derived scaffolds (e.g. collagen, hyaluronan, decellularized ECM)[5], [62]. Ideally, the scaffold used should be mechanically robust to support the knee joint and alleviate pain as tissue regeneration occurs.

Synthetic polymers have advantages mostly related to their tuneability, mechanical properties, and virtually limitless supply, however, they lack innate biomimetic and bioactive properties [5]. The most widely researched synthetic meniscal scaffold is the cell-free polyurethane-based Actifit implant. It has been shown *in vivo* that this scaffold degrades over 4 to 6 years [63], during which time its porous nature is thought to allow for regrowth of the meniscus stemming from the native meniscal rim [64]. This implant is only available to patients who have previously undergone a partial meniscectomy. Several short-term studies have shown the safety and some tissue ingrowth, however, data beyond 5 years reports a high failure rate and there is no long-term data to suggest

the implant prevents joint degeneration [63], [64]. Additional research is required in this field to determine if synthetic polymer scaffolds are capable of influencing robust meniscal repair prior to scaffold degradation *in vivo*.

Hydrogels are three-dimensional networks of natural and/or synthetic hydrophilic polymers that attract and retain large amounts of water. Hydrogels present several attractive features supporting their use in meniscal tissue engineering applications [15], [65]. Notably, they can be used for the delivery of cells and growth factors, they facilitate the diffusion of oxygen, nutrients, and waste in and out of the construct, and the highly hydrated environment can mimic features of the inner load-bearing region of the meniscus [66]. One recent study focused on an injectable alginate dialdehyde-gelatin hydrogel seeded with rabbit meniscal fibrochondrocytes [66]. When injected into an *ex vivo* porcine meniscus tear, the hydrogel became well-integrated into the tissue, as determined by histological staining, and supported cell retention, as determined by quantitative assessment of DNA content within the hydrogel [66]. While most current hydrogel research in the field presents preliminary work, hydrogels exhibit promising qualities like the capacity to support high cell viability and in many cases, minimally invasive delivery methods.

Tissue-derived scaffolds can be further classified into two categories: ECM component scaffolds, which consist of purified forms of ECM macromolecules that can be applied alone or in combination through a bottom-up approach to obtain scaffolds with a well-defined composition, or decellularized ECM scaffolds, which include a complex array of ECM components depending on their native tissue sources [5]. The collagen meniscus implant (Ivy Sports Medicine, Montvale, New Jersey), also referred to as the CMI, is a commercially-available ECM component implant composed of type I bovine collagen [51]. The CMI is a porous natural scaffold that may be seeded with regenerative cell populations and implanted into the meniscus, subsequently, allowing for cellular ingrowth and subsequent matrix deposition. Although patients have reported positive outcomes, such as pain alleviation, a number of drawbacks are associated with the CMI [67]. First, it is only an option for patients who have undergone partial meniscectomy. Second, scaffold shrinkage and shape incongruency are common following implantation.

Furthermore, the biomechanical properties of the implant do not reflect those of the native meniscus [68].

Decellularized ECM scaffolds represent a promising approach to tissue regeneration. An increasing body of research provides evidence that these bioactive scaffolds promote tissue repair by providing biological cues that direct cell proliferation, migration, and differentiation [69]. To date, the use of meniscus ECM has predominantly focused on its incorporation into hydrogels [11], [70], [71]. These studies have reported enhanced upregulation of collagen type I and collagen type II expression, and GAG production, in bone-marrow MSCs that were cultured in chondrogenic differentiation medium in ECM-containing hydrogels in comparison to controls without the addition of ECM [11]. Furthermore, the meniscus ECM-containing hydrogels have been shown to help support the cell survival of encapsulated MSCs, fibroblasts, and chondrocytes [11], [70], [71]. In theory, the use of decellularized meniscus ECM represents a tissue-specific bioactive platform that shows promise in providing cells with instructive cues to direct their response and augment meniscal regeneration [23]. However, as a relatively recent focus in the field of meniscus engineering, additional research is required to determine the most effective use of ECM in order to harness its capacity to promote tissue regeneration.

1.4.1 Three-Dimensional (3D) Bioprinting

Three-dimensional (3D) bioprinting, which involves the incorporation of cells and other biocompatible materials within a bioink, is emerging as a promising tool in regenerative medicine. Bioprinting holds the potential to modernize biological research and approaches to healthcare by enabling the design of functional living tissues *ex vivo* for use in applications including disease modeling and tissue engineering [72]–[74]. Most notably, 3D bioprinting allows for the production of personalized constructs with pre-designed patterns, architecture, size, and material distribution [75]. More specifically, this customization can be achieved by acquiring magnetic resonance imaging (MRI) or computed tomography (CT) scans of the tissue of interest, which can then be used to model the overall volume and shape of the construct to be manufactured [76].

To date, 3D bioprinting has been used to create many scaffolds for therapeutic applications. Typically, bioinks are predominantly composed of natural or synthetic polymers, or some form of composite material. Common natural polymers used in this application are alginate, hyaluronic acid, gelatin, agarose, and nanocellulose [76]. In particular, alginate has been extensively studied and used in many biomedical applications due to its adaptability, low toxicity, relatively low cost, and mild gelation conditions [77]. Synthetic polymers that have been applied for bioprinting include polyesters, polyvinyl alcohol, polycaprolactone, and polyurethanes [76].

Over the past decade, several bioprinting technologies have been developed and are classified into three groups based on their printing technique: inkjet, microextrusion, and laser-assisted bioprinting [75]. Inkjet bioprinters are the most commonly used for both biological and non-biological applications. These systems use thermal or acoustic forces to eject drops of bioink out of the printer and onto a substrate that forms the final construct [75], [76]. Microextrusion bioprinters function using robotically controlled extrusion of a material through a head onto a substrate. Dispensing systems used in these printers are pneumatic or mechanical (piston or screw) [75], [76]. Lastly, laser-assisted bioprinting (LAB) is the least common method used to print biological materials. LAB uses a laser source to irradiate an absorbing layer coated with bioink. As the bioink evaporates, it reaches a receiving substrate in droplet form [75], [76], [78]. Advantages and disadvantages of each bioprinting mechanism are outlined in Table 1.1.

Aspect Biosystems Ltd. is a Canadian biotechnology company that is commercializing a propriety microfluidic-based Lab-on-a-Printer™ technology for 3D bioprinting of tissues for regenerative medicine applications. Their innovative RX1 printers incorporate disposable microfluidic printheads containing microscale channels. This design allows for the extrusion of bioink and crosslinker in tandem, resulting in uniform polymerization as the materials exit the nozzle and, therefore, precise construct formation [79], [80]. Furthermore, Aspect's printing technology enables rapid switching between biomaterials during the printing process, allowing for the creation of multidimensional and biologically relevant constructs [79]. Unlike alternative printing technologies, the RX1 bioprinters only expose cells to low shear stresses to reduce cell death [79], [81]. Of

relevance to this project, Aspect Biosystems Ltd. is currently applying their innovative approach to bioprinting to fabricate polyvinyl alcohol-based meniscus implants [82].

Table 1.1: Comparison of commonly-used bioprinting techniques.

	Advantages	Disadvantages	References
Inkjet	Fast printing speed; Relatively low cost; Widely available	Frequent nozzle clogging; Non-uniform droplet sizes; Low droplet directionality	[75], [76], [78]
Microextrusion	Many materials may be printed; Greater spatial control than inkjet; Ability to deposit high cell density	Slow printing speed; Intermediate cost; Lowest cell-viability due to extrusion pressure and increased gauge of nozzle	[75], [76], [78]
Laser-assisted	Nozzle-free avoiding clogging; High control of ink droplets; Can print wide range of viscosities	High cost printer; Potential for metallic particle contamination; Medium printing speed; Cumbersome	[75], [76], [78]

Three-dimensional bioprinting has proven to be widely successful in supporting cell viability and recreating the internal ultrastructure and external appearance of various tissues [83]. However, one limitation of current bioink formulations is that they lack biological cues that provide instruction for cell attachment, proliferation, differentiation, and ultimately, tissue regeneration [83]. Therefore, the addition of tissue-specific ECM, obtained by tissue decellularization, into bioinks is becoming an increasingly researched

topic and shows promise in enhancing biological activity within 3D bioprinted constructs [74], [83]–[87]. Based on these findings, it is speculated that the incorporation of meniscus ECM into a printable bioink may represent a more effective treatment.

1.5 Decellularized Tissue Bioscaffolds

1.5.1 Overview of Tissue Decellularization

Xenogenic and allogenic cellular antigens are recognized as foreign material to a host and in turn may elicit a prolonged inflammatory response or immune-mediated rejection of the implanted tissue. However, ECM components including the structural and functional proteins are generally well conserved across species and well-tolerated upon introduction in a new host [88]. Therefore, tissue decellularization is a method that aims to remove the cellular and nuclear content within a specific tissue, while preserving the native ECM composition and ultrastructure as much as possible. The extraction of cells and nuclear content requires unique methods tailored to the specific physical and biochemical characteristics of the tissue of interest [88]. To maximize cell removal and ECM retention, most decellularization protocols involve a combination of physical, chemical, and enzymatic treatments [88].

Physical methods of tissue decellularization: Physical methods for decellularizing tissue include freeze-thaw cycles, pressure, sonication, and agitation [88], [89]. Freeze-thaw cycles are used to lyse cells by the formation of ice crystals that disrupt cellular membranes. However, freeze-thawing needs to be followed by processes that can remove remaining cellular and nuclear materials such as extraction with detergent [88], [89]. Mechanical agitation, sonication, and the application of pressure are all methods that assist in the extraction of cellular components from the ECM by increasing the exposure of the tissue to other reagents [88], [89].

Chemical methods of tissue decellularization: Chemical treatments used to decellularize tissues include hypertonic or hypotonic solutions, alkaline or acidic solutions, polar solvents, and detergents. Hypertonic and hypotonic solutions are often used in combination with a chelating agent, such as ethylenediaminetetraacetic acid (EDTA).

This combined treatment causes osmotic shock resulting in cell lysis and allows for the removal of cellular remnants by sequestering divalent cations that are necessary for cell-cell and cell-ECM attachments [88], [89]. Treatment with hypertonic and hypotonic solutions is relatively gentle and is therefore used in combination with other treatment methods [88]. Alkaline or acidic treatments are used to solubilize cellular components by altering the pH of the tissue [90]. However, these treatments may cause extraction of soluble factors from the ECM, as well as hydrolytic degradation of biomolecules including collagens, thereby altering the ECM ultrastructure and mechanical properties [89]. Polar solvents, including alcohols, are effective at extracting and dissolving lipids from tissues, but may dehydrate proteins and cause matrix stiffening [91]. Lastly, detergents solubilize cell membranes and dissociate DNA from ECM proteins and are therefore widely used in tissue decellularization [92]. The use of detergents has been associated with the loss of proteins, GAGs, and growth factors. Further, the presence of residual detergent can cause cytotoxic effects both *in vitro* and *in vivo* [23], [88], [89].

Enzymatic methods of decellularization: Enzymes that have been used in tissue decellularization protocols include proteases (e.g. trypsin and collagenase), nucleases (e.g. deoxyribonuclease (DNase) and ribonuclease (RNase)), and lipases. Proteolytic enzymes, such as trypsin, disrupt integrins thereby releasing cells from the ECM and partially digest dense ECM to promote greater penetration of other reagents [88]. Tissue exposure to proteases should be limited to minimize degradation of the ECM [89]. DNase and RNase degrade residual DNA and RNA following cell lysis, which reduces the risk of adverse effects upon implantation of the decellularized tissue [89]. In general, enzymes have been shown to possess immunogenic properties and must be extensively washed out following digestion [89].

1.5.2 Methods for Characterizing Decellularized Tissue

Following decellularization, it is imperative to characterize the tissue to verify the removal of cellular components and ensure the retention of ECM proteins and ultrastructure [93]. Within the field of tissue engineering, there is a critical need for the establishment of standard characterization methods and guidelines regarding the

acceptable amount of residual cellular debris to ensure that decellularized tissue scaffolds can be safely implanted into new hosts [69], [93].

Tissue decellularization may be assessed using a variety of biochemical, microscopic, immunohistochemical (IHC), and histological techniques. To assess the presence of residual cells, cell nuclei may be visualized using 4',6-diamidino-2-phenylindole (DAPI) staining [94], which is often coupled with DNA quantification using the Quant-iT™ PicoGreen® double-stranded (dsDNA kit) [95]. To assess the composition of the decellularized ECM, IHC and enzyme-linked immunosorbent assays (ELISAs) are techniques used to identify ECM components [93]. IHC is particularly useful for qualitative assessment of ECM marker expression and distribution, whereas ELISAs quantify the presence of target proteins. Mass spectrometry is also emerging as a key characterization method because a single experiment yields large-scale protein detection [93]. Lastly, biochemical quantification of GAG and collagen content may be analyzed using the dimethylmethylene blue (DMMB) and hydroxyproline assays, respectively [93], [96]. To further compliment these assays, GAGs and collagen may be visualized using histological techniques such as toluidine blue staining, which stains GAGs purple, and picrosirius red staining, which stains densely packed thicker collagen fibers red-orange and thinner collagen fibers yellow-green [97]. Lastly, scanning electron microscopy is commonly used to visualize the ECM ultrastructure.

1.5.3 Cell-Instructive Effects of Decellularized Tissues

ECM is highly tissue-specific and demonstrates unique properties that can direct cell phenotype and function within the tissue [69]. Building from this knowledge, decellularized tissue bioscaffolds have been developed with the aim of directing cell responses and promoting tissue regeneration by closely mimicking the native tissue environment [69], [98].

Many research groups have shown that ECM-derived scaffolds are capable of regulating cell behaviour including cell survival and differentiation. Compositional properties may direct cellular processes through direct binding of cells to bioactive ECM components, or by the presence of ECM degradation products, called matrikines [69], [99]. Matrikines

are generated by enzymatic activity and their production is associated with the recruitment of host cells, and the modulation of cell adhesion, migration, and differentiation [100], [101]. Furthermore, fragments of some ECM products have been shown to upregulate MMPs, which can subsequently degrade ECM components, like GAGs, thereby releasing sequestered growth factors that act to regulate cell behaviour [102], [103].

Each tissue type exhibits unique biomechanical properties that influence cell adhesion, proliferation, migration, and differentiation [69], [103], [104]. Cells sense mechanical forces through adhesion complexes, which in turn directs cell behaviour by the activation of signalling cascades [105]. The impact of decellularization protocols on the mechanical properties of native ECM is highly variable [69]. Therefore, there is a need for the refinement of protocols to minimize changes and better preserve biomechanical properties of the native ECM.

The distinct structural properties of tissues are another key mediator of cell behaviour that may be important to conserve in the decellularization process [69]. In particular, this includes the basement membrane, which plays a role in guiding cell migration and growth patterns [106]. Additionally, since cells exhibit preferential binding to specific substrates, surface topography may be another factor to consider as it can influence host cell binding to the implanted material [107]. Furthermore, scaffold porosity should be considered to allow for nutrient and oxygen diffusion, as well as provide channels in which cell migration can occur, thereby influencing cell interactions that guide differentiation [108].

1.5.4 Meniscal Decellularization Protocols

The increasing rate of injuries to the meniscus and lack of effective repair techniques have led researchers to develop a variety of decellularization protocols for the meniscus. In 2017, Shimomura et al. developed a bovine meniscus decellularization protocol that processed the inner and outer regions independently [11]. This protocol mainly focused on the use of cellular extraction with the non-ionic detergent, Triton X-100, with an enzymatic digestion step using DNase and RNase. Following decellularization, a

significant loss in DNA content was quantified using the PicoGreen® assay. In the current study, this protocol served as a comparator because Triton X-100 is considered to be gentler than other ionic detergents such as sodium dodecyl sulphate (SDS) [109].

Decellularization protocols targeting the meniscus have extensively employed the use of SDS [68], [71], [110], [111]. SDS is effective at extracting cells, however, it is also commonly associated with the denaturation of collagen, removal of GAGs and growth factors, and residual detergent may elicit cytotoxic effects [109]. Following treatment with SDS, meniscal decellularization protocols have reported extensive loss of GAG content [68], [110], [111], in some cases upwards of ~60% [68]. Furthermore, some of these studies have also reported altered mechanical properties associated with changes to the native collagen content [68], [110], [111]. The combined use of sonication and SDS treatment to decellularize meniscus was also reported in one protocol [110]. This study noted noticeable changes in ECM organization, altered mechanical properties, and significant loss of GAGs.

Other protocols have incorporated the use of proteolytic enzymes including trypsin and collagenase [23], [112], [113]. These enzymes are known to degrade collagens and GAGs, ultimately affecting their bioactivity [88], [109]. The studies reported that GAG content was completely removed, and SEM imaging revealed altered ECM ultrastructure [112], [113]. Less frequently, meniscal decellularization protocols have used peracetic acid [112], which has been shown to denature proteins and strip tissue of growth factors [109].

Building from these findings, this project focused on the use of the non-ionic detergent, Triton X-100, in addition to an enzymatic digestion using DNase and RNase, in an effort to maximize cell extraction while retaining native ECM composition.

1.6 Adipose-derived Stromal Cells (ASCs)

In the late 1960s, research conducted by Friedenstein *et al.* first reported evidence of plastic-adherent bone marrow-derived mesenchymal stem/stromal cells (BMSCs) that were capable of expansion and differentiation towards osteogenic lineages [114]. This

work initiated further investigation into the procurement of other MSCs within adult tissues, ultimately leading to the discovery of numerous MSC tissue sources, with the three most commonly investigated sources being bone marrow, adipose tissue, and peripheral blood [115]. Although BMSCs have been extensively studied for MSC-based therapies, there exists notable drawbacks to their use including their low yield, with an estimated frequency of 1 BMSC for every 3.4×10^4 cells within the bone marrow nucleated cell population, and pain during collection [116]. For these reasons, adipose-derived stromal cells (ASCs) are an attractive alternative.

ASCs are obtained from subcutaneous fat stores in the body, which are readily accessible via minimally invasive procedures. It is common for ASCs to be harvested from procedures such as lipoaspiration or from tissue waste generated during elective breast or abdominal reduction surgeries. In comparison to bone marrow, adipose tissue can be collected in much larger quantities per single intervention. Furthermore, ASCs are notably more abundant than BMSCs, with approximately 5×10^3 ASCs per gram of adipose tissue as compared to between 1×10^2 to 1×10^3 BMSCs per gram of bone-marrow [117].

Various protocols to isolate ASCs from adipose tissue exist and commonly include mechanical processing, enzymatic digestion, and separation steps using centrifugation to yield a heterogeneous stromal vascular fraction (SVF), rich in pre-adipocytes, endothelial progenitor cells, macrophages, blood cells, fibroblasts, pericytes, smooth muscle cells, and ASCs [118]. ASCs are identified as the adherent population when the SVF is expanded on tissue-culture polystyrene (TCPS). The scientific community has outlined three requirements to identify ASCs. First, the cells must be isolated from adipose tissue and adherent to TCPS. Second, they must possess an immunophenotype that is at least 80% positive for CD105, CD90, CD73, CD29, and CD44, as well as less than 2% positive for CD31 and CD45. Lastly, the cells should be able to differentiate towards the three mesenchymal lineages: adipogenic, chondrogenic, and osteogenic [119].

1.6.1 Donor and Depot Effects on ASCs

Recently, studies have identified increased donor age, body mass index (BMI), and donor health as factors linked to decreased proliferation and differentiation capabilities and an increase in the expression of cell senescence markers [120]–[122]. Some potential differences have also been noted between male and female donors [123]. Furthermore, increasing evidence regarding the collection of ASCs from subcutaneous or visceral depots has shown a direct impact on ASC characteristics [104]. For example, studies have shown that ASCs from the upper arm and medial thigh depots consistently exhibited greater proliferation and differentiation towards the adipogenic lineage when compared to those from the abdomen or trochanter [104]. In contrast, others have reported enhanced adipogenesis in ASCs from subcutaneous, pericardial, and thymic remnant adipose tissue depots, while osteogenic differentiation was augmented in ASCs from the omentum [123]. Taken together, these findings highlight the need for research assessing the effects of donor age, sex, BMI, health, and tissue excision site on ASC proliferation and differentiation capacities, as well as immunophenotype.

1.6.2 ASC Chondrogenesis

As mentioned previously, ASCs are capable of differentiating towards the adipogenic, chondrogenic, and osteogenic lineages *in vitro*, which has been confirmed using a combination of immunofluorescence, gene expression analysis, and specific functional assays [119]. Generally, this is achieved through culturing in media that is supplemented with lineage-specific induction factors [124]. Commonly used protocols for chondrogenic differentiation of ASCs involve the supplementation of culture media with dexamethasone, ascorbate-2-phosphate, TGF- β 1, and insulin [125], [126].

The chondrogenic differentiation of ASCs (Figure 1.3) can be enhanced by high cell density and cell-cell contact, which is typically achieved by culturing the cells in 3D aggregates [125]. These conditions closely mimic mesenchymal condensation observed *in vivo* during cartilage development. Sex-determining region Y-related high motility group box 9 (SOX9) is an essential transcription factor in chondrogenesis. SOX9 induces

the transcription of SOX5 and SOX6, which act to further enhance the activity of SOX9, maintaining cartilage phenotypes and preventing hypertrophy [127]. SOX9 induces chondrogenesis by upregulating cartilage-matrix specific genes to help maintain pre-chondrocyte phenotypes [128].

In early chondrogenesis, transforming growth factor beta (TGF- β), as well as bone morphogenic proteins (BMPs), promote cellular condensation, which commits the cells towards a pre-chondrocyte phenotype [129]. Following condensation, the cells begin to differentiate into highly proliferative chondroblasts. At this stage, matrix deposition changes, with reduced collagen I expression, and the upregulation of collagen II, aggrecan, and cartilage oligomeric matrix protein (COMP) [130]. In the late stages of chondrogenesis, chondrocytes enlarge and become pre-hypertrophic, followed by terminal differentiation into hypertrophic chondrocytes preceding osteochondrogenesis. Chondrocyte hypertrophy is characterized by a minimum 10-fold increase in cell volume, cartilage mineralization, and the upregulation of runt-related transcription factor 2 (RUNX2) and collagen type X [131].

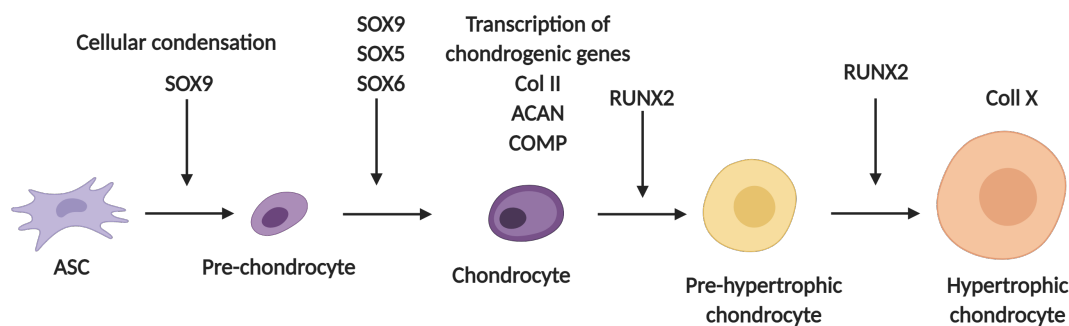


Figure 1.3. Transcriptional control of chondrogenesis.

1.7 Project Overview

1.7.1 Project Rationale

Currently, leading interventions for meniscal injury serve as short-term solutions that provide temporary alleviation of associated symptoms. Ultimately, these treatments lead

to further degeneration of the knee joint and the development of OA. Tissue engineering-based approaches targeting the regeneration of native meniscus have the potential to reverse joint degeneration and avoid the onset of OA. Three-dimensional bioprinting represents a useful tool in fabricating complex and personalized meniscal constructs. One limitation of this approach, however, is that most standard bioinks lack biological cues that can enhance tissue regeneration by providing cell-instruction to direct cell survival and differentiation. Therefore, this study aimed to investigate the cell-instructive effects of incorporating decellularized meniscus with ASCs in 3D printable alginate-based bioinks. Considering the distinct regional variability within the meniscus, the inner and outer regions were processed separately and incorporated into independent bioinks.

1.7.2 Hypothesis

The incorporation of decellularized meniscus within an alginate bioink formulation will enhance the survival and direct the lineage-specific differentiation of encapsulated human ASCs. The inner and outer meniscus-containing bioinks will direct ASC differentiation towards a chondrocyte-like and fibroblast-like phenotype, respectively. These effects may be enhanced through culture in chondrogenic differentiation medium.

1.7.3 Specific Aims

This Master's thesis focused on exploring the effects of the ECM bioink formulations derived from the inner versus outer meniscus on ASC survival and fibrochondrogenic differentiation. Specifically, this is divided into three project aims:

Aim 1: To establish a meniscus decellularization protocol that effectively removes nuclear content while simultaneously retaining ECM components including collagen and GAGs.

Aim 2: To develop region-specific bioink formulations composed of enzyme-digested inner or outer decellularized meniscus incorporated within a proprietary alginate formulation, and assess human ASC viability following encapsulation over time in culture.

Aim 3: To assess the effects of incorporating decellularized inner versus outer meniscus within the bioink on the differentiation of encapsulated ASCs towards a fibrochondrocyte-like phenotype.

Chapter 2

2 Materials and Methods

2.1 Materials

All chemical reagents were purchased from Sigma-Aldrich Canada Ltd. (Oakville, Ontario) unless otherwise indicated.

2.2 Meniscal Decellularization

Porcine knees from animals 5-8 months of age were sourced from the Mount Brydges Abattoir (Mount Brydges, ON, Canada). The menisci were extracted aseptically using a scalpel to remove the bone, muscles, ligaments, and soft tissues surrounding the knee joint. Menisci were cut along the midline to separate the inner and outer regions, which were processed separately for all studies (Figure 2.1). Finally, the tissues were minced into small pieces using a 2.0 mm biopsy punch. The tissues from 6-8 knees were pooled to create a large batch for use in subsequent studies.

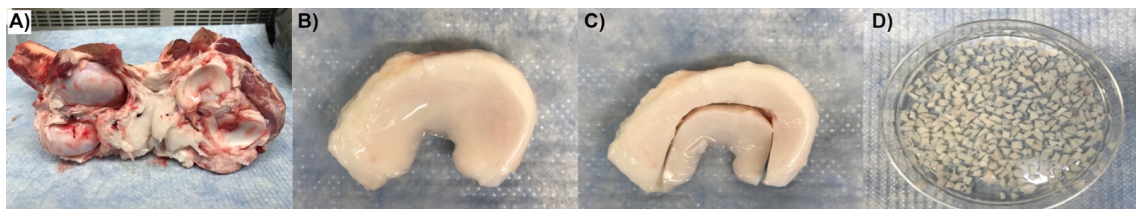


Figure 2.1. Schematic of meniscus extraction and separation of inner and outer regions. A) The porcine knee joint was dissected and the B) menisci were extracted. C) The menisci were cut along the midline to separate the inner and outer regions and D) minced using a 2.0 mm biopsy punch.

Decellularization Protocol A: A new decellularization protocol was developed and tested (Protocol A) that was based on the work of Woods and Gratzner [132] and involved sequential treatment steps including freeze-thaw cycles in hypotonic buffer, Triton X-100 detergent extraction, and enzymatic digestion with deoxyribonuclease (DNase) and ribonuclease (RNase). All solutions were supplemented with 1 % (v/v) antibiotic-antimycotic (ABAM) (Gibco®, Invitrogen, Burlington, ON, Canada) and 0.27 mM phenylmethylsulfonyl fluoride (PMSF) (except enzymatic digestion steps) and all

incubation steps took place at 37 °C under agitation on a Labnet 311DS orbital shaker control system (Labnet International, Inc., Woodbridge, NJ, United States) at 120 rpm.

Approximately 1 g of tissue was subjected to two freeze-thaw cycles (-80 °C overnight/ 37 °C, 120 rpm for 2 hours) in 50 mL of hypotonic buffer (pH 8.0) comprised of 10 mM tris (hydroxymethyl)aminomethane (Tris) and 5 mM ethylenediaminetetraacetic acid (EDTA) in deionized water (dH₂O) (Solution A), which was replaced between each cycle. After the second thaw, the samples were incubated in fresh Solution A for 8 hours. The solution was then replaced with fresh Solution A, and the samples were incubated overnight for 18 hours. Next, the samples were subjected to a high-salt detergent extraction (pH 8.0) in 50 mL of 50 mM Tris buffer supplemented with 1 v/v% Triton X-100 and 1.5 M KCl (Solution B) for 24 hours, with one solution change halfway through processing. The samples were then rinsed three times for 30 minutes in 50 mL of Sorenson's phosphate buffer (SPB) rinsing solution comprised of 0.55 M sodium phosphate dibasic heptahydrate (Na₂HPO₄·7H₂O) and 0.17 M potassium phosphate (KH₂PO₄) (pH 8.0). Next, the samples were enzymatically digested for 2 hours in 50 mL of SPB digest solution comprised of 0.55 M Na₂HPO₄·7H₂O, 0.17 M KH₂PO₄, and 0.049 M magnesium sulphate heptahydrate (MgSO₄·7H₂O) (pH 7.3) supplemented with 300 U/mL DNase Type II (from bovine pancreas) and 20 U/mL RNase Type III (from bovine pancreas). The samples were then subjected to a final detergent extraction in 1 % (v/v) Triton X-100 in 50 mM Tris buffer (pH 8.0) (Solution C) overnight for 18 hours. Solution C was renewed in the morning and the samples were incubated for an additional 8 hours. At the end of the process, the samples were rinsed three times for 30 minutes in dH₂O, frozen at -80 °C in dH₂O, and lyophilized using a Labconco Freezone 4.5 lyophilizer (Labconco, Kansas City, MO, United States) for 48 hours.

Decellularization Protocol B: For comparative purposes, additional meniscal tissue samples were processed following an established protocol from the literature that involved Triton X-100 detergent extraction and enzymatic digestion with DNase and RNase [11]. All solutions were supplemented with 1 % (v/v) antibiotic-antimycotic (ABAM) (Gibco®, Invitrogen, Burlington, ON, Canada). Briefly, 1 g of tissue was incubated in 50 mL of 1% (v/v) Triton X-100 in phosphate buffered saline (PBS) at 4 °C

under agitation on an orbital shaker at 100 rpm for 72 hours. The samples were then rinsed three times for 30 minutes in fresh PBS and enzymatically digested in 200 U/mL DNase and 50 U/mL RNase solution at 37°C, 100 rpm for 24 hours. Finally, the samples were rinsed 6 times for 30 minutes each in PBS, frozen at -80°C in dH₂O, and lyophilized using a Labconco Freezone 4.5 lyophilizer (Labconco, Kansas City, MO, United States) for 48 hours.

2.3 Characterization of Decellularized Tissues

2.3.1 Histological Analyses

Native and decellularized meniscus samples (n=3 cross-sections containing multiple meniscus pieces/batch, N=3 decellularization batches) were rehydrated in PBS and fixed overnight at 4 °C in 4% paraformaldehyde (PFA). The samples were processed for histology at Robart's Molecular Pathology Laboratory (London, ON, Canada), embedded in paraffin, and sectioned (7 µm sections) using a Leica RM2235 microtome (Leica Biosystems, Concord, ON, Canada). Sections were deparaffinized by rinsing in xylene (two times for 5 minutes each) and rehydrated through an ethanol series (100%, 100%, 95%, 70%) followed by dH₂O for 2 minutes each. Sections were stained with toluidine blue to visualize glycosaminoglycan (GAG) content, picrosirius red to visualize collagen, and 4',6-diamidino-2-phenylindole (DAPI) in fluoroshield mounting medium (ab104139, Abcam) to visualize cell nuclei, following standard protocols. Images were obtained using an EVOS XL Core microscope (Thermo Fisher Scientific Inc., Burlington, ON, Canada), a Nikon Optiphot polarizing microscope (Nikon Instruments Inc., Melville, NY, United States), and an EVOS FL fluorescence microscope (Thermo Fisher Scientific Inc., Burlington, ON, Canada) respectively.

2.3.2 Biochemical Analyses

Tissue composition was assessed using a variety of biochemical assays. A PicoGreen® assay was used to quantify the reduction in double-stranded DNA (dsDNA) content following decellularization in comparison to native tissue samples. Collagen content was quantified using a hydroxyproline assay, which detects a predominant amino acid in collagen that serves to stabilize the helical structure [133]. Lastly, a dimethylmethylene

blue assay (DMMB) was used to quantify the GAG content in the native versus decellularized samples (n=3 separately digested samples/batch, N=3 decellularization batches for all assays).

To prepare the samples for the analyses, lyophilized samples were cryo-milled into a fine powder by placing 1 g of each sample into a Retsch 25 mL grinding jar with two 10 mm stainless steel milling balls. The chambers were submerged in liquid nitrogen for 3 minutes, and then milled for 3 minutes at 30 Hz (Retsch Mixer Mill MM 400 milling system). This cycle was repeated three times. Ten mg of each cryomilled sample was then digested in 500 μ L of Tris-EDTA (TE) buffer supplemented with 600 U Proteinase K (Qiagen, Hilden, Germany) for 4 hours at 56 °C in a HERATherm oven (Thermo Fisher Scientific Inc., Burlington, ON, Canada) and vortexed every 15 minutes with a VWR Fixed Speed Vortex Mixer (VWR International LLC., Mississauga, ON, Canada). The enzyme was thermally inactivated by agitating (500 rpm) the samples at 92 °C for 5 minutes.

PicoGreen assay: A Quant-iT™ PicoGreen® assay (Molecular Probes, Burlington, Ontario) was used to quantify the dsDNA content within the native and decellularized tissue samples. Samples were prepared using the DNeasy Blood & Tissue Kit (Qiagen, Hilden, Germany), following the manufacturer's protocols. An eight-point standard curve ranging from 0 ng/mL to 1000 ng/mL was prepared by serial dilution of the λ -DNA standard provided with the PicoGreen® kit in TE buffer. One hundred μ L of each sample (diluted 1:15 in TE buffer (native and Protocol B) or undiluted (Protocol A)) was combined with 100 μ L of Quant-iT™ reagent in technical triplicates and fluorescence was read using a CLARIOstar® microplate reader, according to the manufacturer's instructions. The dsDNA concentration of each sample was determined using the standard curve and was normalized to the dry weight of the tissue.

Hydroxyproline assay: A hydroxyproline (OHP) assay was used to quantify the hydroxyproline concentrations within the native and decellularized tissue samples as a measure of total collagen content. One hundred μ L of each proteinase K-digested sample was hydrolyzed in 100 μ L of 12 M hydrochloric acid for 18 hours at 110 °C and

neutralized with 100 μL of 5.7 M sodium hydroxide. One hundred μL of dH_2O was added and the samples were centrifuged at $400 \times g$ for 1 minute. The supernatant was collected and analyzed as previously described [96]. Briefly, an eight-point standard curve ranging from 0 $\mu\text{g}/\text{mL}$ to 16 $\mu\text{g}/\text{mL}$ was prepared by serial dilution of a hydroxyproline stock (100 $\mu\text{g}/\text{mL}$ in dH_2O) and the samples were diluted 1:200 in dH_2O . Fifty μL of each standard or sample was combined with 50 μL of chloramine-T (0.05 M) in technical triplicates and incubated at room temperature for 20 minutes. Next, 50 μL of perchloric acid (3.15 M) was added and incubated at room temperature for 5 minutes. Finally, 50 μL of Erlich's Reagent (200 mg/mL of 4-dimethylaminobenzaldehyde in 2-methoxyethanol) was added and incubated at 60 $^\circ\text{C}$ for 20 minutes. The plate was cooled at 4 $^\circ\text{C}$ for 5 minutes and absorbance was read using a CLARIOstar[®] microplate reader at 560 nm. The hydroxyproline concentration of each sample was determined using the standard curve and was normalized to the dry weight of the tissue.

Dimethylmethylen blue assay: A DMMB assay was used to quantify the GAG content within the native and decellularized tissue samples, as previously reported [96]. An eight-point standard curve ranging from 0 $\mu\text{g}/\text{mL}$ to 100 $\mu\text{g}/\text{mL}$ was prepared from serial dilutions of a 10 mg/mL chondroitin sulphate stock (Sigma C-6737) in 1 w/v% bovine serum albumin (BSA) in PBS working solution. Samples were diluted 1:20 with the 1% BSA working solution and 10 μL of each was combined with 200 μL of DMMB reagent (0.016 mg/mL in 0.2% formic acid (pH 5.3)) in technical triplicates. Absorbance was read using a CLARIOstar[®] microplate reader at 525 nm. The GAG concentration of each sample was determined using the standard curve and was normalized to the dry weight of the tissue.

2.3.3 Scanning Electron Microscopy

Scanning electron microscopy (SEM) was performed on native and decellularized meniscus samples to visualize extracellular matrix (ECM) ultrastructure following decellularization (n=3 menisci pieces per condition, N=2 batches of separately processed menisci). Briefly, lyophilized tissues were thinly sliced and coated with osmium. Samples were imaged by Dr. Todd Simpson with a LEO 1530 scanning electron microscope at an

accelerating voltage of 1 kV and a working distance of 3.6-3.8 mm (Nanofabrication facility, Western University).

2.3.4 Immunohistochemical Analyses

Lyophilized native and decellularized meniscus samples processed with Protocol A (n=3 cross-sections containing multiple meniscus pieces/batch, N=3 decellularization batches) were rehydrated through an ethanol series (100%, 90%, 70%, 50% (v/v) diluted in PBS) for 30 minutes each and rinsed twice in PBS for 15 minutes at room temperature. Samples were then embedded in Tissue-Tek OCT compound (Sakura Finetek, Torrance, CA, United States) and snap frozen in liquid nitrogen before cryosectioning into 7 μ m sections with a Leica CM3050 S cryostat (Leica Microsystems Inc., Concord, ON, Canada). Following fixation in acetone for 10 minutes at -20°C and blocking in 10% goat serum in tris-buffered saline with 0.1% tween (TBST), sections were stained overnight at 4°C with primary antibodies against collagen type I (dilution 1:100 in TBST with 2% BSA, ab34710, Abcam, Toronto, ON, Canada), collagen type II (dilution 1:200, ab34712, Abcam), collagen type IV (dilution 1:100, ab6586, Abcam), collagen type VI (dilution 1:300, ab6588, Abcam), fibronectin (dilution 1:150, ab23750, Abcam), laminin (dilution 1:200, ab11575, Abcam), and keratan sulphate (dilution 1:200, sc-73518, Santa Cruz Biotechnology). Detection was carried out using an anti-rabbit secondary conjugated to Alexa Fluor 594 (dilution 1:200, ab150080, Abcam) or an anti-mouse secondary conjugated to Alexa Fluor 650 (dilution 1:200, ab96882, Abcam). Porcine skin and bovine nucleus pulposus were used as positive controls and no primary antibody controls were included in all trials (Supplementary Figure A.1 and A.2, Appendix A). Images were acquired with an EVOS FL fluorescence microscope (Thermo Fisher Scientific Inc., Burlington, ON, Canada).

2.4 Human Adipose-Derived Stromal Cell (ASC) Isolation and Culture

Subcutaneous breast and abdominal human adipose tissue samples were obtained with informed consent from patients undergoing lipo-reduction surgeries in London, Ontario with approval from the Human Research Ethics Board at Western University (HSREB#

105426) (Appendix B). The adipose tissue was transported to the lab in sterile PBS supplemented with 20 mg/mL BSA and processed within 2 hours of harvest. ASCs were extracted based on previously-established methods [134].

Briefly, the cauterized pieces were removed, and the tissue was finely minced using surgical scissors. The minced tissue was digested in a solution of 2 mg/mL collagenase type I (Worthington Biochemical Corp., Lakewood, NJ), 3 mM glucose, 25 mM 4-(2-hydroxyethyl)-1-piperazineethanesulfonic acid (HEPES) and 20 mg/mL BSA in Kreb's Ringer Buffer (KRB) under agitation at 100 rpm for 45 minutes at 37 °C. A 250 µm pore-size strainer was used to filter undigested fragments, the filtrate was left to gravity separate for 5 minutes, and the mature adipocyte layer was removed by aspiration. The collagenase was neutralized by the addition of an equal volume of proliferation medium comprised of DMEM/Ham's F12 supplemented with 10% fetal bovine serum (FBS) (Gibco®, Invitrogen, Burlington, ON, Canada) and 100 U/mL of penicillin with 0.1 mg/mL streptomycin (pen- strep) (Gibco®, Invitrogen, Burlington, ON, Canada) and centrifuged at 1200 x g for 5 minutes. The supernatant was aspirated, and the pellet was resuspended in erythrocyte lysing buffer (0.154 M ammonium chloride, 10 mM potassium bicarbonate, and 0.1 M EDTA in sterile dH₂O) and incubated for 10 minutes at room temperature under gentle agitation. The cell suspension was then re-centrifuged and the resultant pellet was resuspended in proliferation medium, filtered through a 100 µm pore-size filter and re-centrifuged. The cell pellet was plated on T-75 tissue culture polystyrene (TCPS) flasks (Corning, NY, United States) at a density of 30,000 cells/cm². After 24 hours, the cells were rinsed with sterile PBS to remove non-adherent cells and debris. The media was changed every 2-3 days, and passage 0 (P0) cells were frozen at approximately 80% confluence.

To prepare the cells for the encapsulation studies, cryopreserved P0 cells were thawed and plated on T-75 flasks at a density of 1.0×10^6 cells/T-75 flask in proliferation medium and cultured at 37 °C (20% O₂, 5% CO₂). After 24 hours, the ASCs were released using trypsin-EDTA (0.25% Trypsin/2.21 mM EDTA from Wisent Inc., Montreal, QC, Canada) and split into new T-75 flasks in a 1:4 ratio. The proliferation media was changed every 2-3 days. At 80% confluence, the cells were plated onto 875

cm² multi-flasks (Corning, NY, United States). Passage 4 (P4) cells were used for all encapsulation studies. The cell viability and density studies were repeated with 3 ASC donors (N=3) and gene expression studies were repeated with 2 ASC donors (N=2) to verify trends (Supplementary Table A.1, Appendix A).

2.5 Fabrication of Composite Alginate-ECM Beads

2.5.1 Pepsin Digestion of Cryomilled Meniscus

To prepare pepsin-digested decellularized meniscus solutions, cryomilled decellularized inner meniscus (DIM) and decellularized outer meniscus (DOM) from Protocol A were added at a concentration of 20 mg/mL to sterile 10 w/w% porcine pepsin (3200-4500 mU/mg protein) in 0.1 M hydrochloric acid and digested for 18 hours at 37 °C under agitation at 120 rpm. The solutions were neutralized with sterile 1 M sodium hydroxide and undigested fragments were removed by filtering through a sterile 40 µm cell strainer (FisherBrand™ CAT#22-363-547). The resultant solutions were stored at 4 °C for a maximum of 48 hours before use.

2.5.2 Cell Encapsulation within Alginate-Based Beads

Composite alginate-ECM beads were fabricated by combining a propriety alginate formulation (AG-10 Matrix, Aspect Biosystems Ltd., Vancouver, British Columbia) with pepsin-digested meniscus and drop-casting the bioinks into a propriety calcium-based crosslinker (CAT-2, Aspect Biosystems Ltd., Vancouver, BC, Canada). Pure alginate beads (ALG) were also synthesized as controls. To generate the composites, the AG-10 Matrix was combined in a 1:1 ratio with pepsin-digested DIM or DOM to obtain a final ECM concentration of 10 mg/mL. For cell encapsulation, human ASCs were combined with the bioinks at a concentration of 3.0×10^6 cells/mL and mixed well through gentle pipetting. The cell-loaded bioinks were transferred into sterile 1 mL syringes and subsequently manually expelled dropwise through a 16 G needle into a 6-well plate containing 5 mL of the CAT-2 crosslinker. The beads were incubated in the crosslinking solution for 10 minutes at 37 °C. The resultant beads were rinsed with sterile proliferation media to remove excess crosslinker and approximately 15-20 beads were transferred into

12-well culture inserts (Greiner Bio-one, Germany) in 3 mL of proliferation medium (1 mL in insert, 2 mL in well) at 37 °C (20% O₂, 5% CO₂).

Chondrogenic differentiation was induced in half of the samples by replacing the proliferation medium with 3 mL of chondrogenic differentiation medium [126] comprised of proliferation medium supplemented with 10 ng/mL recombinant human transforming growth factor- β 1 (TGF- β 1) (BioLegend®, CAT#781804, San Diego, CA, United States), 50 μ g/mL ascorbate-2-phosphate, 6.25 μ g/mL bovine insulin, and 100 nM dexamethasone at 48 hours post-encapsulation. The remaining samples were cultured in proliferation medium. Half of the volume of media (1.5 mL) was changed in both the samples in proliferation media (non-induced) and chondrogenic differentiation media (induced) every 2 days.

2.5.3 Characterization of Bead Size

Bead size was measured using a previously-established method [135]. Briefly, ALG, ALG+DIM, and ALG+DOM beads were prepared following the methods described above, with supplementation of the CAT-2 crosslinker with 0.05% (w/v) Coomassie Brilliant Blue for visualization purposes. Immediately following crosslinking, the beads (n=3 beads per composition, N=3 batches with different cell donors) were imaged at 4X magnification using an EVOS XL Core microscope (Thermo Fisher Scientific Inc., Burlington, ON, Canada). Feret's diameter was measured using the ImageJ analysis software.

2.6 *In vitro* Assessment of Human ASCs Encapsulated in the Bioinks

2.6.1 Confocal Analysis of Cell Viability and Density using the LIVE/DEAD® Assay

ASC viability following encapsulation and culture was assessed through confocal microscopy at 24 hours, 7 days, 14 days, and 28 days post-encapsulation using the LIVE/DEAD® Viability/Cytotoxicity Assay (Invitrogen CAT#L3224), which allows for the visualization of live cells in green by staining with Calcein AM and dead cells in red

through the use of ethidium homodimer-1 (EthD-1). At each timepoint, three beads (n=3 beads from each composition/timepoint, N=3 cell donors) from each bioink (i.e. ALG, ALG+DIM, ALG+DOM) and media formulation (chondrogenic versus proliferation) were collected, rinsed with PBS, and incubated at 37 °C in 4 µM EthD-1 and 2 µM Calcein AM in PBS for 30 minutes. Following incubation, the beads were imaged using the 5X objective at 3 depths separated by 40 µm on a Zeiss LSM800 Confocal Microscope with Airyscan. ImageJ analysis software was used to automatically count the viable cells to determine the ASC density within the beads at 28 days compared to 24 hours post-encapsulation (n=3 beads per group/timepoint in each trial, N=3 trials with different cell donors).

2.6.2 Gene Expression Analysis

For each condition, ALG, ALG+DIM, and ALG+DOM beads cultured in proliferation and chondrogenic differentiation media, approximately 300 µL of beads pooled from multiple wells were collected at 9 and 30 days post-encapsulation (i.e. 7 and 28 days after the induction of chondrogenic differentiation). The cells were released from the alginate through incubation in 25 mM sodium citrate in dH₂O for 45 minutes at 37 °C under agitation at 120 rpm. A cell pellet was obtained by centrifuging at 1200 x g for 5 minutes, and frozen in 1 mL of PureZOL (Bio-Rad Laboratories, Mississauga, ON, Canada). Samples were thawed on ice and sonicated three times using a Model 100 Sonic Dismembrator (Fisher Scientific) in one second bursts. Total RNA was extracted using the Aurum Total RNA Fatty and Fibrous Tissue kit (Bio-Rad Laboratories), according to the manufacturer's instructions. RNA concentration and purity were determined using a Nanodrop 1000 spectrophotometer (Thermo-Scientific), and cDNA was synthesized using the iScript™ cDNA Synthesis Kit (Bio-Rad Laboratories) from 300 ng of input RNA in a 20 µL volume. Controls with no reverse transcriptase were also prepared for each sample.

Gene expression was analyzed by real-time qPCR using the BioRad CFX-384 system. Three separate samples from each bead formulation and culture medium were run in triplicate, with each well containing 0.3 µL of 10 µM forward and reverse primers, 5 µL of 2xSSoAdvanced™ Universal SYBR® Green Supermix (Bio-Rad Laboratories) and

2 μ L of sample. The panel of markers used to assess chondrogenic differentiation consisted of SRY-Box transcription factor 9 (*SOX9*), cartilage oligomeric matrix protein (*COMP*), aggrecan (*ACAN*), collagen type I (*COL I*), collagen type II (*COL II*), and collagen type X (*COL X*) with housekeeping genes glucuronidase beta (*GUSB*) and ribosomal protein L 13a (*RPL13A*). The primers were previously validated for efficiency and specificity, and their sequences are provided in Table 2.1. The following protocol was used: enzyme activation at 95 °C for 2 minutes, followed by denaturation at 95 °C for 10 seconds and annealing and elongation at 60 °C for 30 seconds, repeated for 40 cycles. Transcript levels were analyzed using the $\Delta\Delta$ CT method, with normalization of each sample to the geometric mean of the housekeeping genes and using the ALG samples cultured in chondrogenic differentiation medium for 7 days as the calibrator (n=3 bead samples processed separately at each timepoint/trial, N=2 trials with different ASC donors).

Table 2.1: RT-qPCR Primer Sequences.

Gene	Primer Sequence (5' to 3')
<i>SOX9</i>	FWD: AGCGAACGCACATCAAGAC REV: CTGTAGGCGATCTGTTGGGG
<i>COMP</i>	FWD: GCCTGCATCCAGACGGAGAG REV: GTGGGCGTTGCACTCGTTG
<i>ACAN</i>	FWD: TGAGGAGGGCTGGAACAAGTACC REV: GGAGGTGCTAATTGCAGGGAACA
<i>COL I</i>	FWD: AAGAGGAAGGCCAAGTCGGAG REV: CACACGTCTCGGTCATGGTA
<i>COL II</i>	FWD: CCAGATGACCTTCCTACGCC REV: TTCAGGGCAGTGTACGTGAAC
<i>COL X</i>	FWD: CAGGCATAAAAGGCCCACTA REV:GGTGGTCCAGAAGGTCCAGAAGGACCTG
<i>GUSB</i>	FWD: ACGCAGAAAATATGTGGTTGGA REV: GCATCTCGTCGGTGACTGTT
<i>RPL13A</i>	FWD: TCGGTCTGAAGCCTACAAGA REV: GTTCTTCTCGGCCTGTTTCC

2.6.3 Immunohistochemical Characterization of ECM Markers within Alginate-Based Beads

IHC was used to qualitatively assess the presence of key chondrogenic ECM components in induced and non-induced ALG, ALG+DIM, and ALG+DOM beds at 30 days post-encapsulation (i.e. 28 days after the induction of chondrogenic differentiation). Briefly, beads were collected at each timepoint and fixed in 4% paraformaldehyde with 10 mM

calcium chloride and 0.1 M sodium cacodylate for 4 hours at 4°C. The samples were then washed in a solution of 0.1 M sodium cacodylate with 50 mM barium chloride for 18 hours at 4°C and sent to Robarts Molecular Pathology Laboratory (London, ON, Canada) for histological processing. Upon return, samples were embedded in paraffin and sectioned (7 µm sections) using a Leica RM2235 microtome (Leica Biosystems). Sections were deparaffinized by rinsing in xylene (two times for 5 minutes each) and rehydrated in an ethanol series (100%, 100%, 95%, 70%) and dH₂O for 2 minutes each.

For heat-mediated antigen retrieval, sections were placed in slide mailers containing 1x DAKO Target Retrieval Solution (DAKO Canada Inc., Burlington, ON, Canada). The slide mailers were heated at 95°C in a double boiler system for 10 minutes. Following antigen retrieval, fixation in acetone for 10 minutes at -20°C, and blocking with 10% goat serum in TBST, the sections were stained overnight at 4°C with primary antibodies against collagen type I (dilution 1:100 in TBST with 10% goat serum, ab34710, Abcam, Toronto, ON, Canada), collagen type II (dilution 1:400, ab34712, Abcam), fibronectin (dilution 1:150, ab23750, Abcam), and keratan sulphate (dilution 1:200, sc-73518, Santa Cruz Biotechnology). Detection was carried out using an anti-rabbit secondary conjugated to Alexa Fluor 594 (dilution 1:200, ab150080, Abcam) or an anti-mouse secondary conjugated to Alexa Fluor 650 (dilution 1:200, ab96882, Abcam) (n=3 cross-sections containing multiple beads/trial, N=2 trials with different ASC donors). Inner native meniscus was used as a positive control and no primary antibody controls were included in all trials. Images were acquired using an EVOS FL fluorescence microscope (Thermo Fisher Scientific Inc., Burlington, ON, Canada).

2.7 Statistical Analyses

All numerical data are expressed as mean ± standard deviation (SD). All statistical analyses were performed using GraphPad Prism 7 (GraphPad Software, San Diego, CA). All statistical analyses were performed by two-way ANOVA with a Tukey's post-hoc comparison of the means. Differences of $p < 0.05$ were considered statistically significant.

Chapter 3

3 Results

3.1 Comparison of Protocols to Decellularize Porcine Meniscal Tissues

The first aim of this project was to establish a porcine meniscus decellularization protocol that effectively removed cellular content from both the inner and outer regions of the tissues, and preserved the extracellular matrix (ECM) composition and ultrastructure. The inner and outer regions were processed independently to develop region-specific bioinks in order to assess whether the ECM sourcing had an effect on the survival and differentiation of encapsulated human adipose-derived stromal cells (ASCs).

Briefly, the new decellularization protocol, Protocol A, consisted of dissecting menisci from porcine knees, which were then cut along the midline to separate the inner and outer regions, minced with a biopsy punch, and treated with a 5-day decellularization protocol. Protocol A included the use of freeze-thaw cycles to mechanically aid in tissue decellularization, cell lysis through hypotonic and hypertonic solutions, enzymatic digestion with deoxyribonuclease (DNase) and ribonuclease (RNase), and detergent extraction with Triton X-100. Additionally, the novel Protocol A was compared to an established meniscus decellularization protocol taken from the literature, Protocol B, that involved extended detergent extraction with Triton X-100 combined with enzymatic digestion with DNase and RNase [11]. Decellularized samples from both protocols were collected and characterized using histological techniques and quantitative biochemical assays in comparison to native tissue controls.

To assess cell extraction, cell nuclei were visualized using 4',6-diamidino-2-phenylindole (DAPI) fluorescent staining (Figure 3.1A). Representative images illustrate that in comparison to native tissues, samples processed with Protocol A exhibited enhanced cell removal in both regions, with no detectable nuclei remaining in the tissues at the end of processing. In contrast, residual cell nuclei were visualized throughout both regions of the samples processed with Protocol B. Regional variability was observed throughout these samples wherein cell nuclei detection was heterogeneous throughout the tissue. To

corroborate these findings, a PicoGreen® assay was used to quantify the presence of double-stranded DNA (dsDNA) in the native versus decellularized samples (Figure 3.1B). While both protocols significantly reduced the dsDNA content, Protocol A removed significantly more dsDNA than Protocol B in both regions, with an average of 0.7 ± 0.3 ng/mg and 0.6 ± 0.2 ng/mg detected in the inner and outer regions respectively.

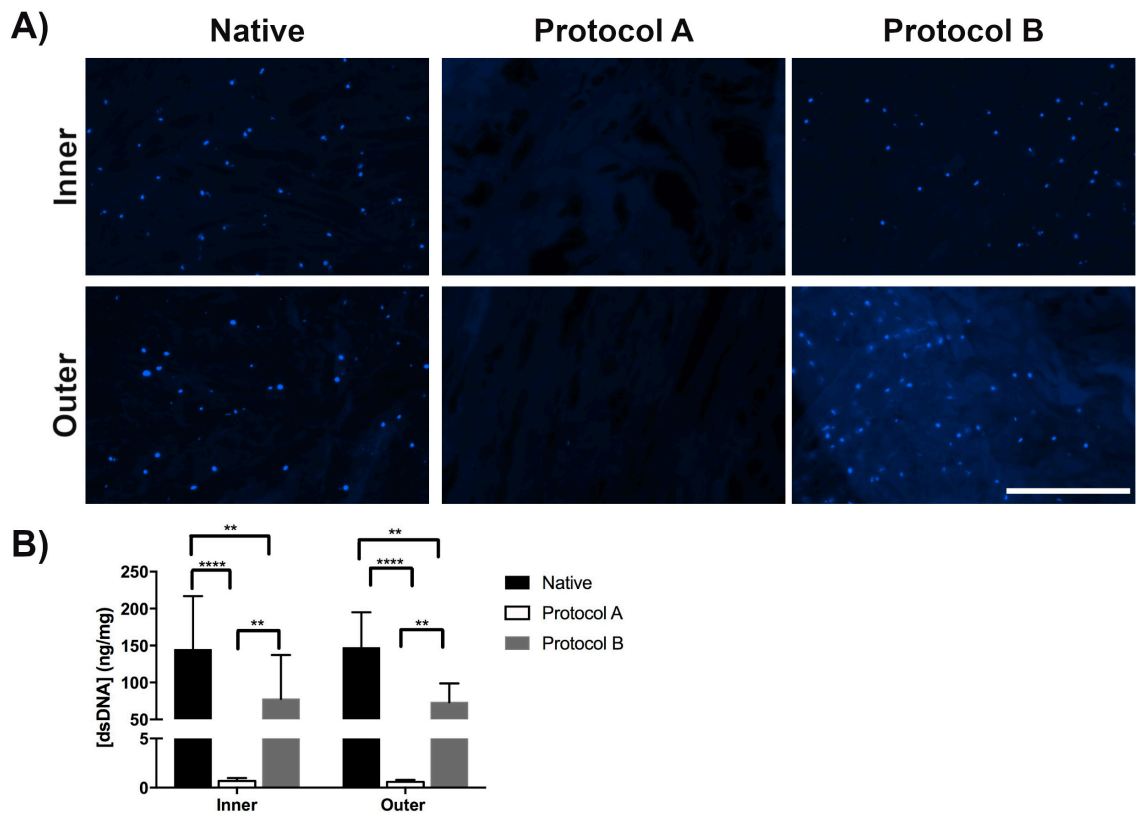


Figure 3.1. Cell extraction was enhanced in the meniscus samples processed with decellularization Protocol A. **A)** Representative DAPI nuclear staining of inner and outer meniscus samples following decellularization in comparison to native tissue controls showing enhanced removal of cell nuclei in the samples processed with Protocol A (n=3 cross-sections containing multiple meniscus pieces/batch, N=3 decellularization batches). Scale bar=200 μ m. **B)** Quantitative analysis of double-stranded DNA (dsDNA) content in the native and decellularized meniscus samples using the PicoGreen assay confirmed that Protocol A was more effective at extracting cells from the tissues. Values are reported based on dry weight. (n=3 separately digested samples/batch, N=3 decellularization batches). Two-way ANOVA; **p<0.01, ****p<0.0001.

The distribution of collagen in the samples processed with both protocols was visualized using picrosirius red staining. Imaging through circularly polarized light microscopy revealed dense networks of collagen comprised of a combination of thicker fibers visualized through red-orange staining and thinner fibers that appeared yellow-green in colour. Similar patterns were seen in both the native and decellularized tissues, with the exception of a qualitative reduction in the yellow-green staining in the tissues from the outer region processed with Protocol B, suggesting a loss in thin fibers or a potentially a change in the organization of the collagen (Figure 3.2A). A hydroxyproline assay was used to quantitatively analyze collagen content (Figure 3.2B). In the inner region, the hydroxyproline content in the samples processed with both protocols remained similar to the native tissues. In contrast, there was a significant enrichment in hydroxyproline content within the outer region in the samples decellularized with both protocols.

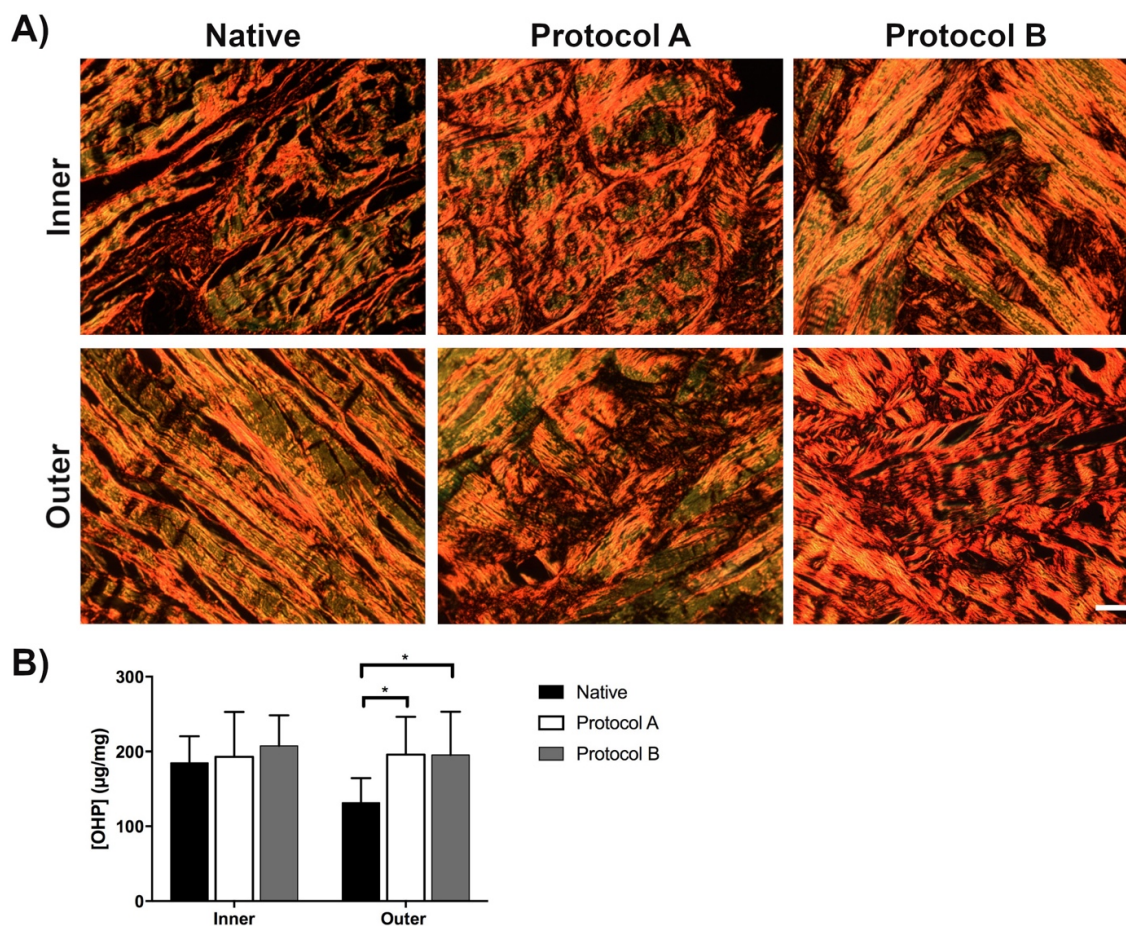


Figure 3.2. Collagen content remained similar in the inner region and was enriched in the outer region following decellularization with both protocols. **A)** Representative picrosirius red staining showing that the tissues processed with Protocol A contained a dense network of collagen fibers with similar staining patterns to the native tissue samples in both regions. The tissues processed with Protocol B exhibited similar staining patterns in the inner region but qualitatively less yellow-green staining in the outer region, suggesting a loss of thin fibers or potentially a change in the organization of the collagen. (n=3 cross-sections containing multiple meniscus pieces/batch, N=3 decellularization batches). Scale bar=200 µm. **B)** Quantification of total collagen content through the hydroxyproline assay showed similar levels in the decellularized inner meniscus samples relative to the native tissue controls. In contrast, a significant enrichment in hydroxyproline content was observed in the decellularized outer meniscus samples processed with both protocols. Values are reported based on dry weight. (n=3 separately digested samples/batch, N=3 decellularization batches). Two-way ANOVA; *p<0.05.

Analysis of glycosaminoglycan (GAG) content through toluidine blue staining exhibited qualitatively more intense staining in both regions in the samples processed with Protocol A as compared to those processed with Protocol B (Figure 3.3A). Similarly, quantitative analysis of GAG content using the dimethylmethylene blue (DMMB) assay determined that Protocol A retained significantly more GAG in the inner region than Protocol B (Figure 3.3B). Additionally, in the outer region, a significant loss of GAG content relative to the native tissues was only observed in the samples processed with Protocol B.

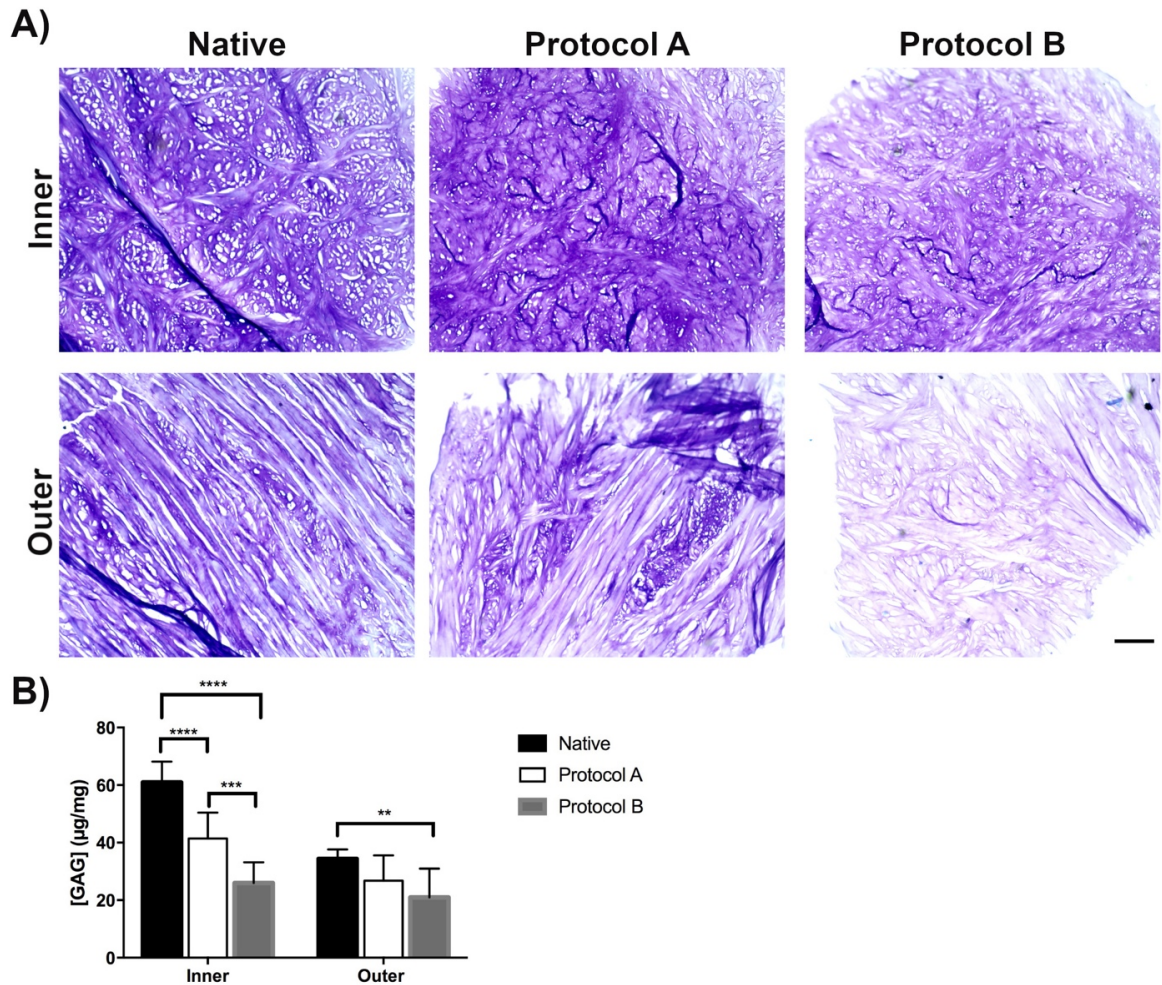


Figure 3.3. Protocol A enhanced the retention of glycosaminoglycan (GAG) content in the processed tissues. **A)** Representative toluidine blue staining showing more intense staining of GAGs (purple) in the decellularized meniscus samples processed with Protocol A (n=3 cross-sections containing multiple meniscus pieces/batch, N=3 decellularization batches). Scale bar=200 µm. **B)** Quantitative analysis with the DMMB assay showing that the inner meniscus samples decellularized with Protocol A contained significantly more sulphated GAG content than those processed with Protocol B. A significant reduction in GAG content was observed in the outer meniscus samples decellularized with Protocol B relative to the native tissue controls. Values are reported based on dry weight. (n=3 separately digested samples/batch, N=3 decellularization batches). Two-way ANOVA; ** p<0.01, ***p<0.001, ****p<0.0001.

Scanning electron microscopy (SEM) images revealed that all samples possessed a complex fibrous ECM ultrastructure, with no obvious differences between the samples processed with the two decellularization protocols or relative to the native tissue controls (Figure 3.4).

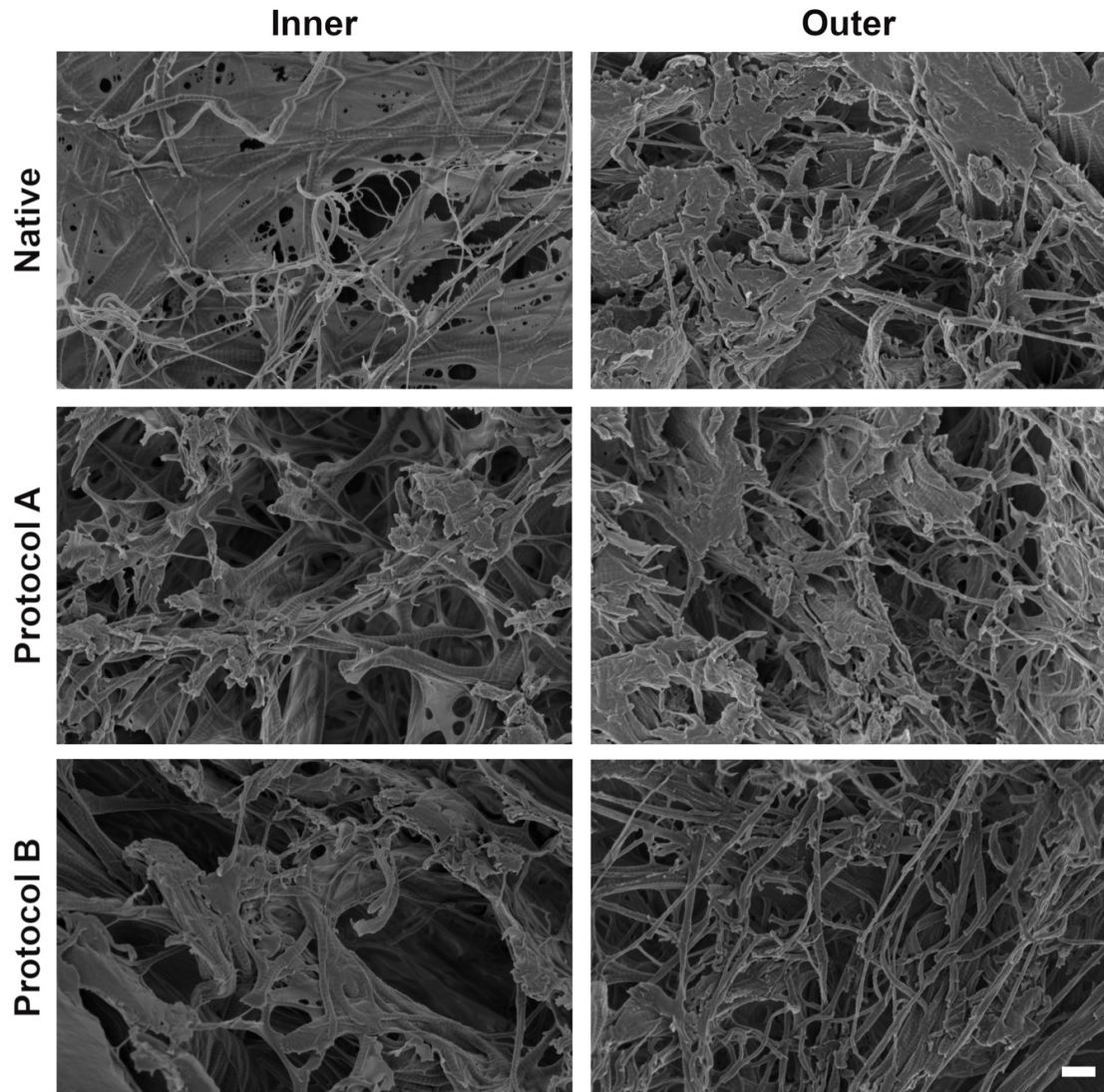


Figure 3.4. Scanning electron microscopy (SEM) images of native and decellularized meniscus showing that all samples had a complex fibrous ECM ultrastructure. Scale bar=400 nm.

Taken together, the results confirmed that the novel Protocol A was more effective at extracting nuclear content and retaining GAGs in both regions compared to Protocol B. As such, all subsequent studies included samples processed with Protocol A only.

3.2 Immunohistochemical Characterization of the ECM Composition within the Decellularized Meniscus

Immunohistochemical analyses were used to further investigate the presence and distribution of ECM components in the inner and outer regions of the native tissues and following decellularization with Protocol A (Figure 3.5). Staining for collagen type I (Coll I), collagen type II (Coll II), collagen type IV (Coll IV), collagen type VI (Coll VI), keratan sulphate (KS), fibronectin (FN), and laminin (LN) showed qualitatively similar patterns between the native and decellularized meniscus samples in both regions. Some regional variations between markers were consistently observed. Specifically, in the inner region, KS staining was qualitatively more intense. Furthermore, in the outer region, Coll I and FN staining were qualitatively more intense (positive antibody controls shown in Supplementary Figure A.1 and A.2, Appendix A).

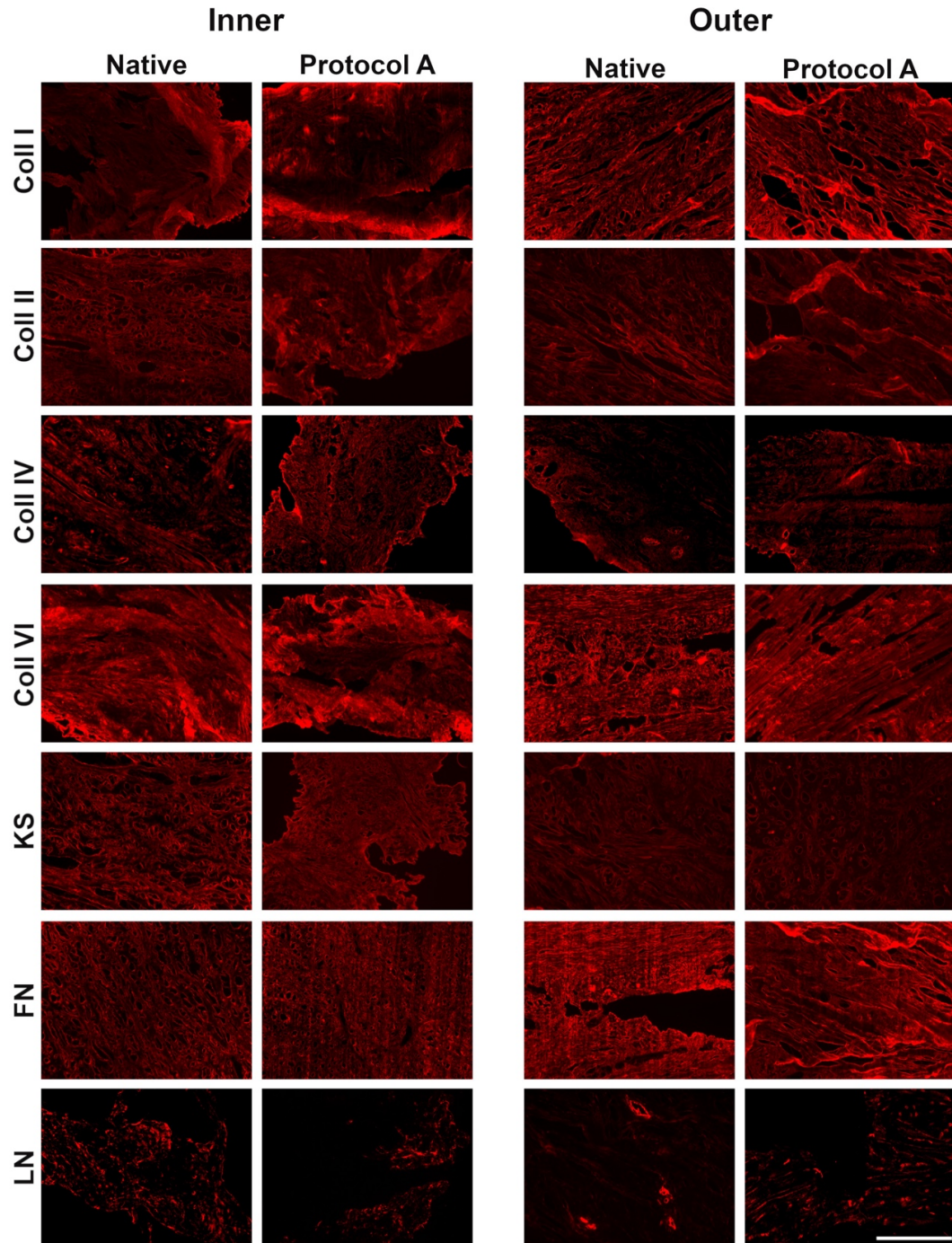


Figure 3.5. Immunohistochemical analyses confirmed the presence of key ECM components following decellularization. Representative staining showed similar patterns between native and decellularized meniscus processed using Protocol A for all ECM markers investigated (n=3 cross-sections containing multiple meniscus pieces/batch, N=3 decellularization batches). Scale bar=400 μ m. Abbreviations: Coll I=collagen type I, Coll II=collagen type II, Coll IV=collagen type IV, Coll VI=collagen type VI, KS=keratan sulphate, FN=fibronectin, LN=laminin.

3.3 Bead Synthesis Through Dropcasting of the Alginate-Based Bioinks

Decellularized inner meniscus (DIM) and decellularized outer meniscus (DOM) samples generated by Protocol A were lyophilized, cryomilled, and enzymatically digested using pepsin. The resultant solubilized ECM was combined with a proprietary alginate formulation generously provided by Aspect Biosystems Ltd. to generate region-specific bioinks (ALG+DIM and ALG+DOM) containing a final ECM concentration of 10 mg/mL, based on the initial dry mass of the decellularized tissues within the digests. In addition, alginate (ALG) alone was applied as a control. Each bioink was combined with human ASCs at a density of 3.0×10^6 cells/mL and dropcast into the propriety crosslinker to form beads (Figure 3.6). The average bead size for all three bioinks was similar, with Feret's diameters measuring 3.75 ± 0.46 mm, 3.69 ± 0.39 mm, and 3.33 ± 0.35 mm for the ALG, ALG+DIM, and ALG+DOM beads respectively.

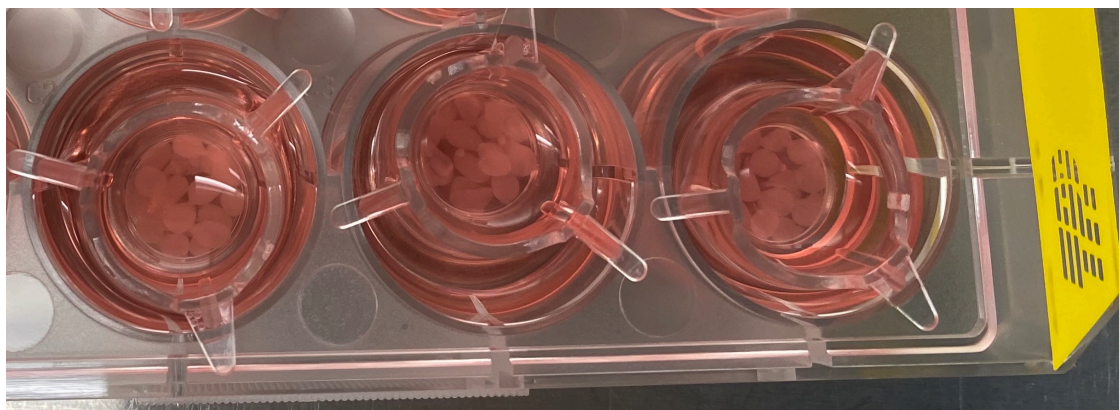


Figure 3.6. Macroscopic image of alginate-based beads post-encapsulation shows similar appearance of all formulations. Qualitatively there were no differences between the appearance of ALG, ALG+DIM, and ALG+DOM beads.

3.4 Viability and Retention of Human ASCs Encapsulated and Cultured in the Alginate-Based Beads

The LIVE/DEAD[®] assay with confocal imaging was used to assess the viability of the human ASCs encapsulated within the ALG, ALG+DIM, and ALG+DOM beads at 24 hours, 7 days, 14 days, and 28 days post-encapsulation and culture in proliferation medium (Figure 3.7A) or chondrogenic differentiation medium (Figure 3.8A). In all

conditions, the ASCs remained highly viable throughout the culture period. After 28 days of *in vitro* culture in chondrogenic differentiation medium, an apparent increase in the volume of some cells was observed. Most notably, this was seen with the ASCs in the ALG+DIM beads but also to a lesser degree in the ALG+DOM and ALG beads. Qualitatively, the ASC density appeared to decline over time in the ALG alone beads. To verify this observation, the viable ASC density at 24 hours and 28 days post-encapsulation was quantified using ImageJ for the samples cultured in proliferation medium (Figure 3.7B) and chondrogenic differentiation medium (3.8B). In proliferation medium, there was a significant increase in ASC density within the ALG+DIM group from 24 hours to 28 days. In both media formulations, the ASC density within the ALG+DIM and ALG+DOM beads was significantly higher than in the ALG alone beads at 28 days.

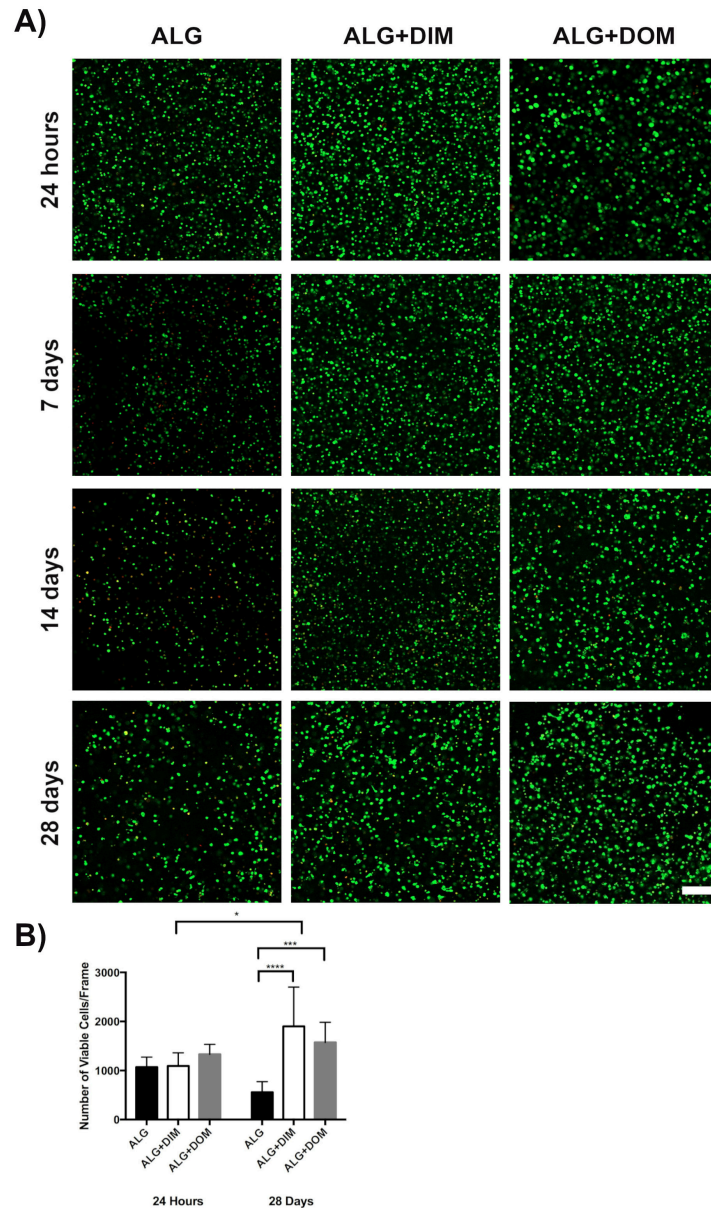


Figure 3.7. LIVE/DEAD staining confirmed that the human ASCs remained highly viable following encapsulation and culture in proliferation media for 28 days. **A)** Representative images showing calcein⁺ live (green) and EthD-1⁺ dead (red) ASCs in the ALG, ALG+DIM, and ALG+DOM beads support that high cell viability was maintained throughout the culture period. (n=3 beads per timepoint/trial, N=3 trials with different cell donors). Scale bar=200 μ m. **B)** The ASC density, reported as cells/frame at 5X magnification, was significantly higher at 28 days within the ALG+DIM and ALG+DOM beads as compared to the ALG beads. From 24 hours to 28 days there was a significant increase in the ASC density in ALG+DIM beads. (n=2 images counted for 3 beads per timepoint/trial, N=3 trials with different cell donors). Two-way ANOVA; ***p<0.001, ****p<0.0001.

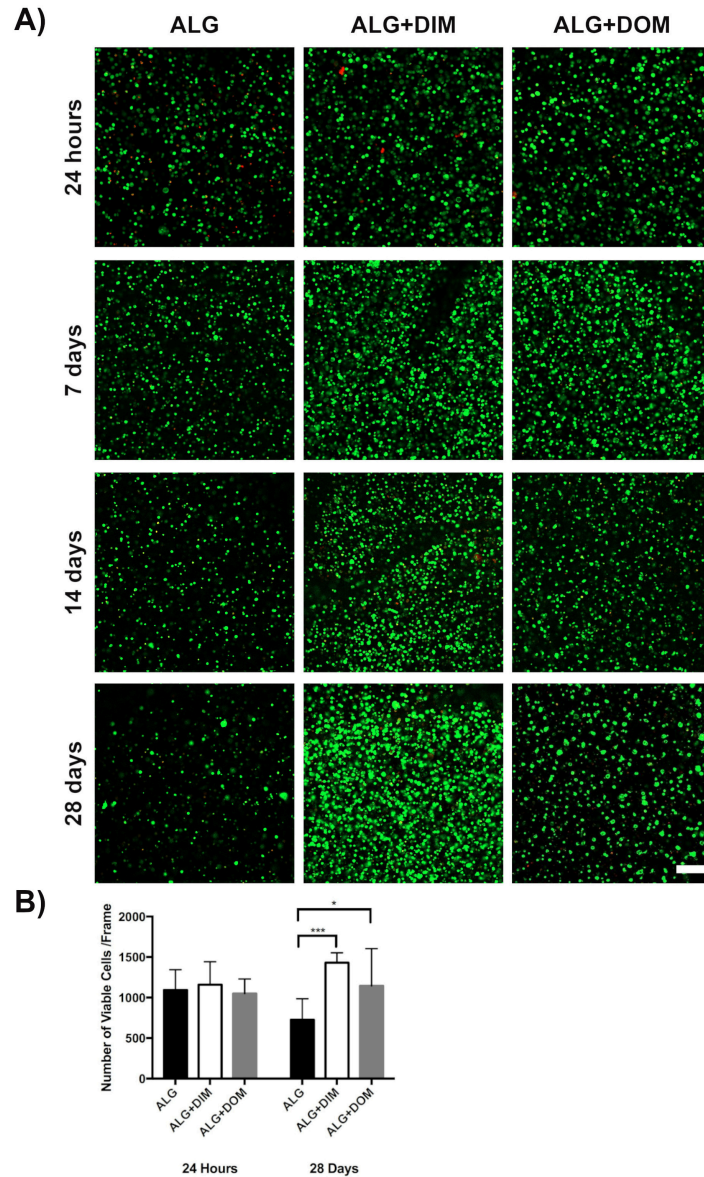


Figure 3.8. LIVE/DEAD confirmed that the human ASCs remained highly viable following encapsulation and culture in chondrogenic differentiation media for 28 days. **A)** Representative images showing Calcein⁺ live (green) and EthD-1⁺ dead (red) ASCs in the ALG, ALG+DIM, and ALG+DOM beads support that high cell viability was maintained throughout the culture period. (n=3 beads per timepoint/trial, N=3 trials with different cell donors). Scale bar=200 μ m. **B)** Following 28 days of *in vitro* culture in chondrogenic differentiation medium the ASC density was significantly higher in the ALG+DIM and ALG+DOM beads as compared to the ALG alone (reported as cells/frame at 5X magnification). (n=2 images counted for 3 beads per timepoint/trial, N=3 trials with different cell donors). Two-way ANOVA; *p<0.05, ***p<0.001.

3.5 Chondrogenic Gene Expression in the Human ASCs Cultured in the Alginate-Based Beads

RT-qPCR analysis was used to assess a panel of genes associated with chondrogenesis including: *SOX9* as a key transcription factor that regulates chondrogenesis; *COMP*, *ACAN*, *Coll I*, and *Coll II* as markers of chondrocyte ECM production; and *Coll X* as a marker of chondrocyte hypertrophy. Samples were analyzed at 7 and 28 days after the induction of chondrogenic differentiation (i.e. 9 and 30 days of total culture post-encapsulation). Relative gene expression from 2 donors is presented in heatmaps using the 7-day alginate beads cultured in chondrogenic differentiation medium as the calibrator.

While there was donor variability in the response, similar patterns of relative gene expression were observed in both donors, with higher expression of most of the markers in the samples that had been cultured in chondrogenic differentiation medium for 28 days (Figure 3.9). Notably, in this subset of samples, *Coll II* and *ACAN* were more highly expressed in the ALG+DOM beads as compared to the ALG beads for both donors, suggesting that the incorporation of the solubilized DOM may have had a positive effect on cartilage-specific ECM expression.

The analysis of the 7-day samples also revealed some interesting trends. More specifically, *SOX9* expression was enhanced in the samples cultured in proliferation medium, suggesting that 3-D culture for 7 days within the alginate gels had an inductive effect on the expression of this transcription factor. In addition, there was elevated expression of *Coll II* and *ACAN* in the ALG+DIM and ALG+DOM beads, as well as *COMP* in the ALG+DOM beads, compared to the ALG beads after 7 days of culture in chondrogenic differentiation medium for both of the cell donors, supporting that the incorporation of the ECM within the bioink may have had a bioactive effect on the induction of chondrogenic differentiation.

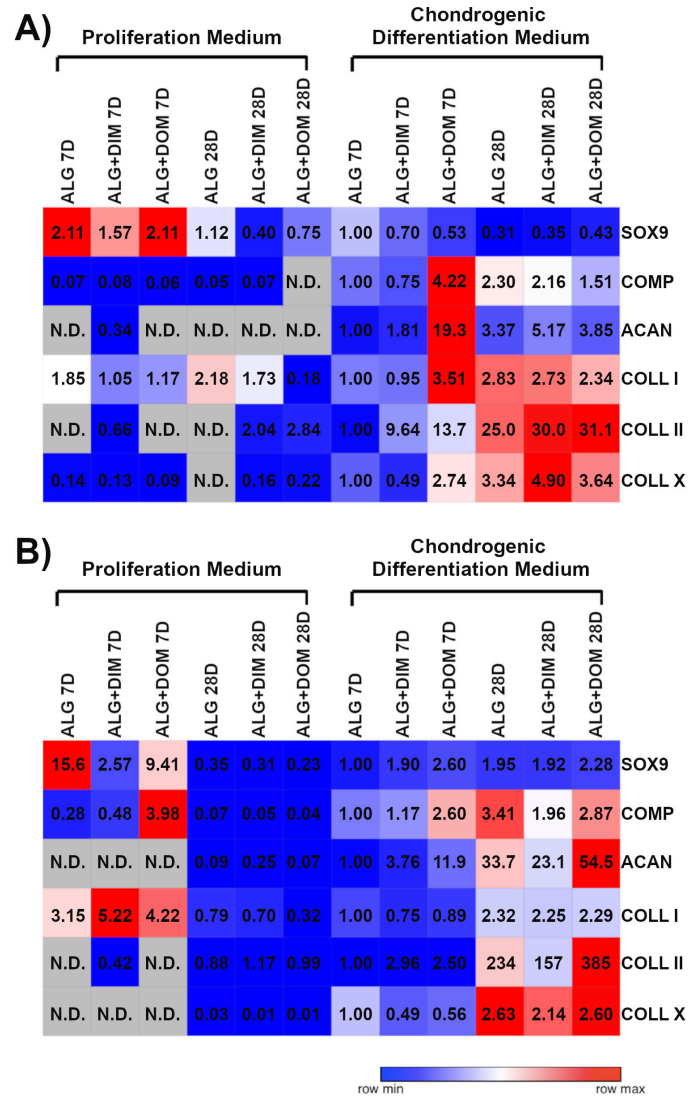


Figure 3.9. Chondrogenic ECM gene expression was enhanced in the human ASCs encapsulated within the alginate-based beads following 28 days of culture in chondrogenic differentiation medium. Relative gene expression for **A)** cell donor 1 and **B)** cell donor 2 with ASCs encapsulated in alginate +/- ECM beads. The ASCs were encapsulated in the alginate beads and cultured in proliferation medium for 48 h, and then transferred into chondrogenic differentiation medium for an additional 7 or 28 days, or maintained in proliferation medium as a control. Analysis was performed on *SOX9* as a key transcription factor associated with the induction of chondrogenesis; *COMP*, *ACAN*, *Coll I*, and *Coll II* as markers of chondrocyte ECM production; and *Coll X* as a marker of chondrocyte hypertrophy. Data was analyzed using the $\Delta\Delta C_t$ method with normalization to the geometric mean of the stable housekeeping genes *RPL13A* and *GUSB*, and using the 7-day alginate beads cultured in chondrogenic differentiation medium as the calibrator. Data is presented as a heatmap (n=3 bead samples processed separately at each timepoint/trial, N=2 trials with different ASC donors). N.D.=Not detected.

3.6 Immunohistochemical Analysis of Chondrogenic ECM Expression in the Alginate-Based Beads

Immunohistochemical staining was used to visualize ECM marker expression within the alginate-based beads following *in vitro* culture in proliferation medium for 30 days (Figure 3.10) or proliferation medium for 2 days followed by 28 days in chondrogenic differentiation medium (Figure 3.11). Most of the markers were not detected in the beads cultured in proliferation medium, with the exception of fibronectin, which appeared to be qualitatively more highly expressed in ALG+DIM beads. In contrast, collagen type I, collagen type II, and fibronectin were abundantly expressed in the ALG+DIM and ALG+DOM beads that were cultured in chondrogenic differentiation medium, suggesting that the incorporation of the ECM within the alginate had a positive effect on matrix production. Interestingly, qualitatively higher levels of expression were observed for collagen I, collagen II and keratan sulphate in the ALG+DOM beads relative to ALG+DIM beads. Faint staining for keratan sulphate was observed only in the ALG+DOM samples, suggesting there was limited GAG accumulation in any of the samples under the conditions in the current study (positive antibody controls shown in Supplementary Figure A.3, Appendix A).

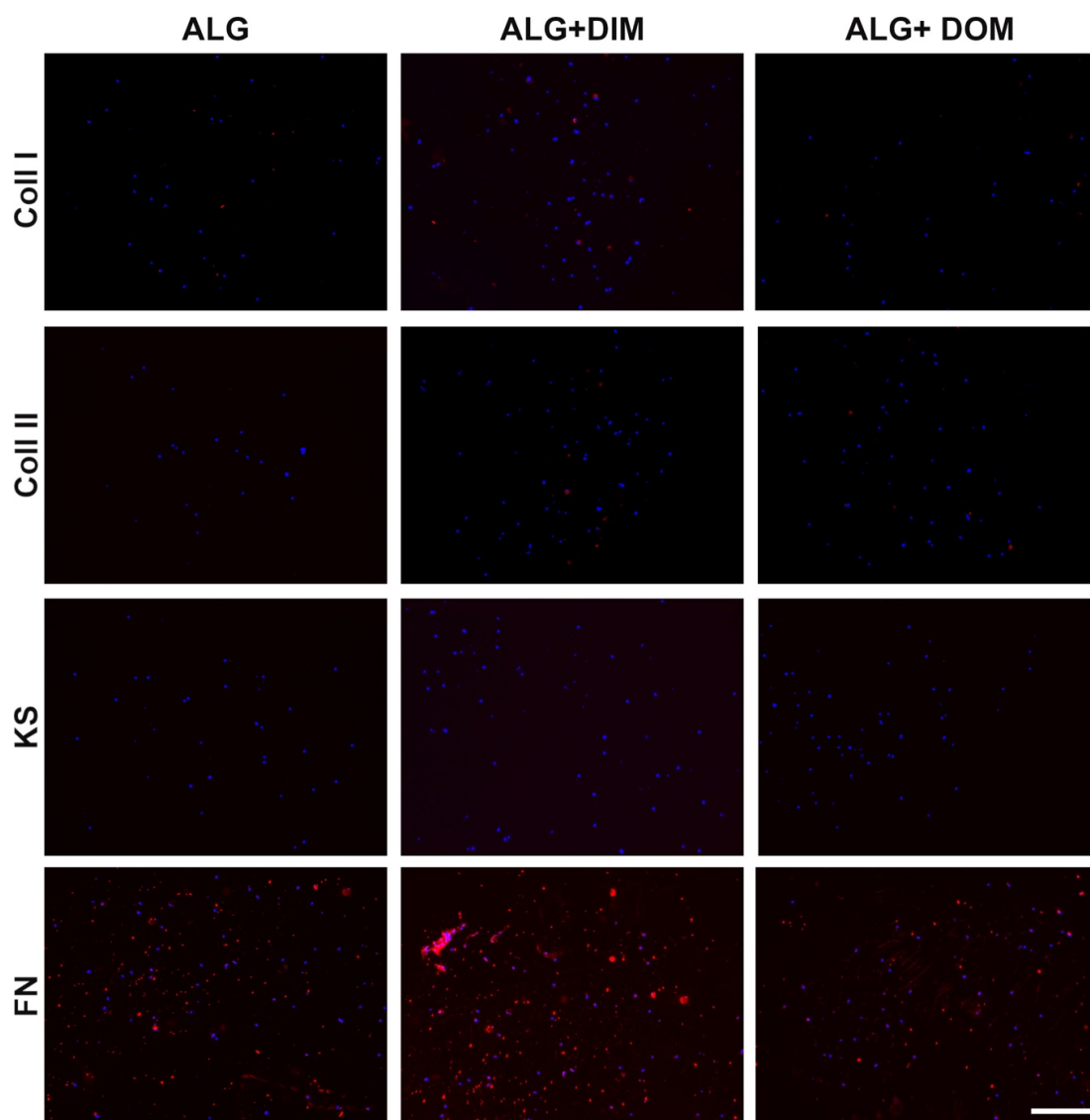


Figure 3.10. Immunohistochemical staining showing limited ECM marker expression within the alginate-based beads following 30 days of culture in proliferation medium. Representative images of the ECM markers (red) with DAPI counterstaining (blue) to localize the human ASCs. Fibronectin expression was qualitatively enhanced in the ALG+DIM group. (n=3 cross-sections containing multiple beads/trial, N=2 trials with different ASC donors). Abbreviations: Coll I=collagen type I, Coll II=collagen type II, KS=keratan sulphate, FN=fibronectin. Scale bar= 200 μ m.

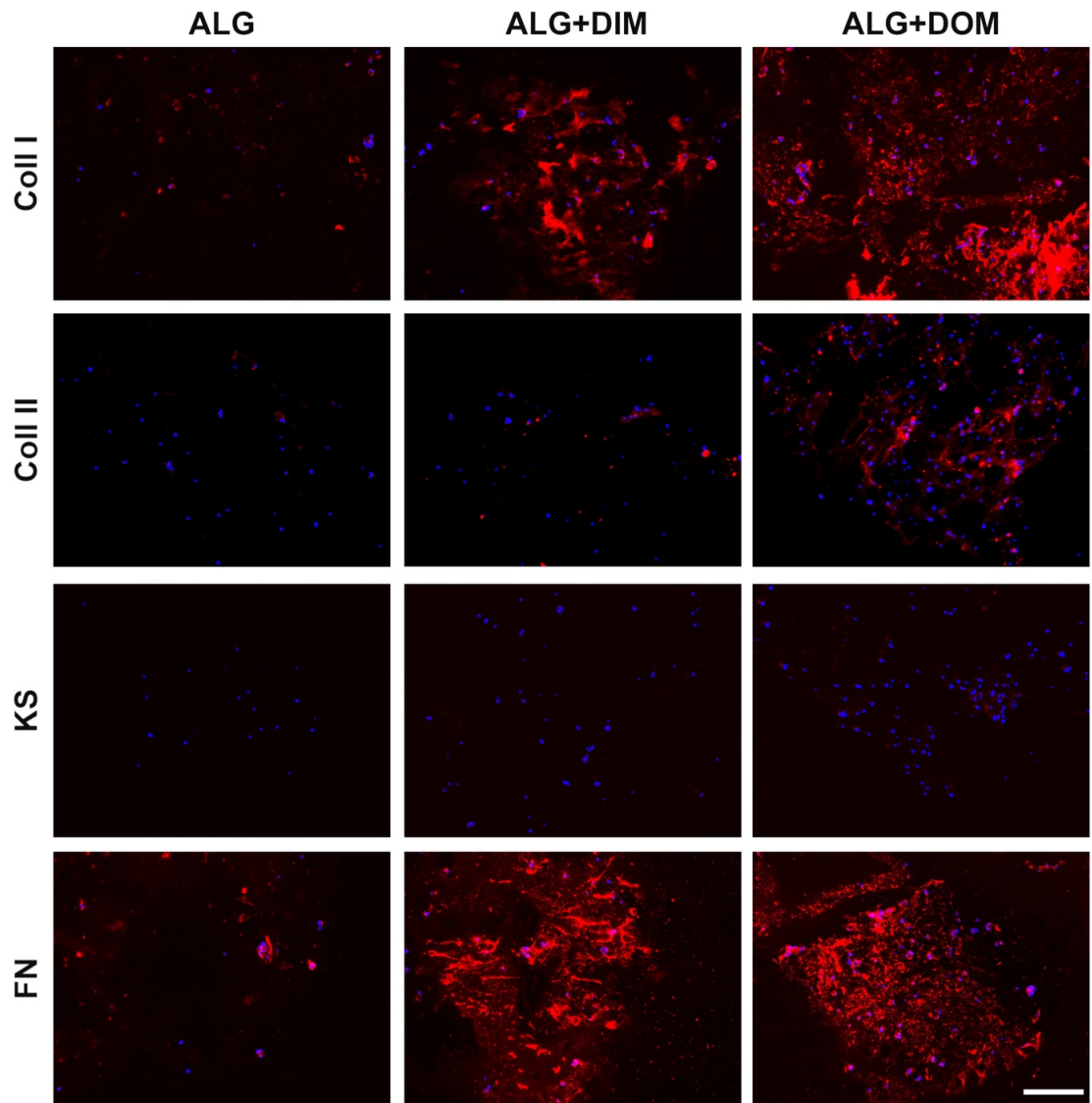


Figure 3.11. Immunohistochemical staining showing enhanced ECM marker expression within the composite alginate + ECM beads following 28 days of culture in chondrogenic medium. The samples were cultured in proliferation medium for 48 h post-encapsulation before being transferred into differentiation medium for 28 days. Representative images of the ECM markers (red) with DAPI counterstaining (blue) to localize the human ASCs showing qualitatively enhanced ECM staining for collagen I, collagen II and fibronectin within the ALG+DIM and ALG+DOM beads and faint staining for keratan sulphate within the ALG+DOM beads relative to the ALG controls. (n=3 cross-sections containing multiple beads/trial, N=2 trials with different ASC donors). Abbreviations: Coll I=collagen type I, Coll II=collagen type II, KS=keratan sulphate, FN=fibronectin. Scale bar= 200 μ m.

Chapter 4

4 Discussion

The menisci play a critical role in the knee joint by providing shock absorption, load transmission, joint lubrication, and joint stability [12], [136]. Notably, the menisci are the most frequently injured structures in the knee and due to their relatively acellular and avascular composition, they have a limited capacity for self-repair. As such, surgical interventions targeting the meniscus are among the most frequently performed procedures in the orthopaedic field. Specifically, meniscectomy is the most commonly used technique, which is linked to altered biomechanics of the joint that can ultimately lead to the onset of osteoarthritis (OA) [21], [137]. OA inflicts significant health and economic burdens on society, as it is the second most prevalent chronic condition in Canada and is associated with major expenditures [56], [138]. For these reasons, there is a critical need for novel and effective treatment approaches that promote structural and functional meniscal regeneration.

The application of three-dimensional (3D) bioprinting is of interest in the field of meniscal tissue engineering, as it can be used to create personalized constructs through a highly controlled fabrication process [75]. Additionally, the material to be printed, known as a bioink, can be made from a variety of materials and may also incorporate various cell types. In particular, alginate is a biomaterial derived from seaweed that has been extensively used in the field of tissue engineering as it possesses many favorable qualities including low toxicity, high water content, and the capacity to support the viability of encapsulated cell populations [77], [139]. From a commercial perspective, alginate is relatively inexpensive and widely available, reducing the risk of bottlenecks in the manufacturing process. Importantly, alginate is easily and rapidly crosslinked with divalent cations such as calcium, avoiding the exposure of cells to harsh treatments during encapsulation. The release of cells from alginate is also easily achieved through the use of chelating agents, allowing for a simple recovery and collection of the encapsulated cells for analysis.

While alginate can provide a cell-supportive microenvironment, it lacks biological cues that can help to direct cell functions including proliferation, differentiation and matrix production that may be favorable for meniscal regeneration [140]. As such the generation of alginate-based composites harnessing the innate bioactivity of the extracellular matrix (ECM) holds promise to address this limitation. In particular, decellularization can be used to obtain tissue-specific ECM for this application. Overall, the goals of decellularization are to remove cellular and nuclear content while preserving the composition and ultrastructure of the native tissue as much as possible.

Every tissue in the body has unique properties, in terms of cellularity and composition, and tailored approaches to decellularization are critical. To date, many decellularization protocols targeting the meniscus have employed the use of harsh ionic detergents and acids, such as sodium dodecyl sulphate (SDS) [68], [110], [111], [141] and peracetic acid [112], as well as enzymatic treatment with proteolytic enzymes including trypsin and collagenase [113]. Although effective at extracting cells, SDS can cause denaturation of ECM proteins, alterations in ECM structure and mechanical properties, and the removal of glycosaminoglycans (GAGs) and growth factors [109], [142]. In addition, the presence of residual detergent may elicit cytotoxic effects [109], [142]. Treatment with peracetic acid has also been shown to denature proteins and strip tissue of growth factors [109], [142], and enzymes can degrade collagens and GAGs, affecting their structure and bioactivity [109], [142].

Taking these considerations into account, this project aimed to develop a new meniscal decellularization protocol (Protocol A) that maximized cell extraction while retaining native ECM constituents. The approach was based on protocols developed by Woods and Gratzer to decellularize porcine bone-anterior cruciate ligament grafts [132]. Briefly, their methods involved hypotonic cell lysis, high salt detergent extraction with 1 v/v% Triton X-100, enzymatic digestion with deoxyribonuclease (DNase) and ribonuclease (RNase), and a final extraction with 1 v/v% Triton X-100. While applying a similar combination of treatments, a number of modifications were made in developing the new protocol for the meniscus, including the addition of freeze-thaw cycles to promote cell

lysis, shortened incubation steps that were all performed at 37 °C instead of room temperature, and higher concentration of DNase and RNase.

Decellularization Protocol A was compared to a recent protocol from the literature (Protocol B), which also analyzed the inner and outer regions of the meniscus independently [11]. This protocol was selected as the comparator because it also relied on treatment with the non-ionic detergent Triton X-100 [11], which is known to be gentler than stronger anionic detergents such as SDS and can better preserve the ECM structure and composition [92], [132], [143], [144]. In addition, this previous study demonstrated that urea extracts from the decellularized inner region promoted the fibrochondrogenic differentiation of human bone marrow-derived MSCs encapsulated within polyethylene glycol hydrogels, while extracts from the outer region promoted a more fibroblastic phenotype associated with enhanced collagen type I expression [11].

In terms of cell extraction, qualitative analysis using DAPI staining clearly revealed that Protocol A enhanced cell removal in both regions, compared to Protocol B. These findings were corroborated by the PicoGreen® analysis of double-stranded DNA (dsDNA) content. The broader combination of treatments, including the addition of freeze-thaw cycles in hypotonic solution at the beginning of the process, along with the overall extended treatment time may have contributed to the enhanced efficacy of Protocol A [88]. Freeze-thawing forms ice crystals that mechanically disrupt cell membranes, ultimately causing lysis [85], [142], and this process can be augmented by hypotonic solution treatment, which causes an influx of water into the cell [88]. These initial steps may have rendered the nuclear content more accessible to the subsequent washing and digestion steps. In addition, Protocol A incorporated the use of a chelating agent (EDTA) to sequester ions and impede cell binding to the ECM, which may have also helped to promote cell extraction [88].

Collagen is the most abundant protein in mammalian tissues, where it plays a vital role in providing strength, resilience, and structure, as well as in modulating cellular processes including adhesion and migration [145]. Picrosirius red staining revealed that the samples processed with Protocol A showed similar collagen staining patterns to the native tissues

in both regions. In contrast, samples from the outer region processed with Protocol B showed a qualitative reduction in yellow-green staining, potentially indicating a loss of thin collagen fibers, or a change in collagen organization following decellularization [146]. These changes may have been caused by the extended treatment time in Triton X-100 [109], [147] or potentially due to the lack of inclusion of protease inhibitors in Protocol B to counteract the intracellular proteases that are released by lysed cells [88], [92], [132]. The hydroxyproline assay results indicated that the samples processed with both protocols had similar levels of collagen in the inner region and an enrichment of collagen in the outer region relative to the native tissues. This enrichment is likely attributed to the relative increase in collagen levels due to the loss of cellular and other ECM components during decellularization.

Glycosaminoglycans (GAGs) are another key ECM component that have the capacity to modulate cellular processes both directly through cell binding and indirectly through the sequestration of growth factors [69]. In addition, their hydrophilic nature plays a critical role in maintaining tissue hydration and contributes to the compressive resistance of the meniscal tissues [1]. Toluidine blue staining revealed qualitatively less intense staining for GAGs in the samples decellularized with Protocol B, which was verified by the dimethylmethylene blue (DMMB) assay results. In addition to causing changes in collagen, a number of studies have reported that processing with Triton X-100 can result in the loss of GAGs [132], [148], [149]. As such, is likely that the additional 30 hours of processing time in Triton X-100 in Protocol B contributed to the observed changes in the ECM composition.

Immunohistochemical analyses were used to visualize the presence and distribution of ECM components in both regions of the meniscus. For all markers, similar staining patterns were observed between the native and decellularized samples in each respective region. However, some regional variations were observed including more intense staining for collagen type I in the outer region. In dry weight, collagen type I makes up approximately 30% of the inner bovine meniscus, and 80% of the outer meniscus [5]. In contrast, collagen type II is estimated to represent approximately 42% of the dry weight of inner meniscus, and less than 1% of the outer meniscus [5]. Surprisingly, this contrast

was not reflected in the qualitatively similar collagen type II staining intensities visualized in this study. However, research investigating the specific localization of collagen type II has indicated that it is primarily found in the inner region horns, which was not controlled for in this study [150], [151]. As such, it would be interesting to explore the effects of deriving materials specifically from that region in future studies in order to generate inner composites that have a more distinct cartilage-like composition.

Although the staining patterns for collagen type II were similar, there was qualitatively more intense staining for keratan sulphate in the inner region in both the native and decellularized tissue samples. In the meniscus, keratan sulphate is one of the most abundant GAG side chains within aggrecan [1], [5], which is the major large proteoglycan found within the tissues that contributes to its characteristic load-bearing properties [5], [152]. Regional variability in proteoglycan expression is also expected, with higher levels reported in the inner and central regions of the tissues [5].

Interestingly, staining for fibronectin appeared qualitatively enhanced in the outer region of both the native and decellularized tissues. While there is limited information on the localization of fibronectin within the meniscus, it is well-recognized that it plays an important role in mediating cell attachment to matrix constituents such as collagens and GAGs [5], [17], [153]. Interestingly, during chondrogenesis, fibronectin expression and matrix assembly has been shown to occur prior to and during cell condensation and differentiation [154], [155]. It is therefore postulated that fibronectin is necessary for chondrogenesis by initiating and maintaining cell-cell connections, and/or organizing the developing cartilage matrix [154], [155].

Of the other proteins investigated, network-forming collagen type IV and laminin are known to be co-localized in the pericellular matrix of chondrocyte-like cells in the inner region, as well as in the basement membrane surrounding the vasculature in the outer region [156], [157]. Microfibrillar collagen type VI has also been reported to be abundantly expressed in the meniscus, where it can be found in association with both collagen type I and II bundles, as well as within the pericellular matrix [158], [159]. All

three proteins are known to have bioactive effects in mediating cell phenotype and function [158], [159].

While the pepsin digestion used to solubilize the ECM would have substantially altered the ECM structure and composition, the findings of the *in vitro* studies clearly support that the pepsin-digested decellularized meniscus had bioactive effects on the ASCs encapsulated within the alginate-based bioinks. Notably, peptides derived from the proteolytic digestion of ECM proteins, termed matrikines, are well-known to have biological activity and can modulate cell functions including growth, proliferation and differentiation [69]. It is postulated that the differing composition within the two regions contributed to the varying effects observed between the alginate incorporating the decellularized inner meniscus (ALG+DIM) and decellularized outer meniscus (ALG+DOM).

LIVE/DEAD® staining with confocal microscopy revealed that there was a significantly higher density of viable ASCs in the ALG+DIM and ALG+DOM beads as compared to the alginate only controls (ALG) after 28 days of culture in either proliferation or chondrogenic differentiation media. Furthermore, in proliferation medium, the density of ASCs within the ALG+DIM beads was significantly higher at 28 days as compared to 24 hours. Taken together, these results suggest that the incorporation of the digested ECM may have promoted cell survival and/or proliferation, or provided adhesive cues that supported cell retention within the beads.

The LIVE/DEAD® images also revealed some morphological changes in the encapsulated ASCs that were cultured in chondrogenic differentiation medium for 28 days, most notably in ALG+DIM beads, where an increase in cell size and/or cell clustering was observed. These findings are consistent with reports of increasing cell volume throughout the progressive stages of chondrogenic differentiation [160]–[163]. Based on the IHC analysis, there was greater cell clustering in the regions where there was enhanced matrix accumulation, although further studies would be needed to interpret whether this was a cause or an effect.

Interestingly, the RT-qPCR results revealed that expression of *SOX9* was enhanced in the 7-day samples cultured in proliferation media. *SOX9* is a transcription factor that is expressed during cellular condensation and at the early stages of chondrogenesis [127], [129], [164]. This finding suggests that culturing within the alginate-based beads had an inductive effect on the expression of this transcription factor. However, the low levels of expression of all of the chondrogenic markers in the samples cultured in proliferation medium at 28 days indicate that the 3-D culture platforms were insufficient on their own to induce a robust chondrogenic response. Notably, *SOX9* remained relatively low in the samples that were cultured in chondrogenic medium. Glucocorticoids, including dexamethasone, have been shown to promote chondrogenic differentiation and the early and transient upregulation of *SOX9* [165]–[167]. As such, it would be interesting to explore differences in the expression levels under chondrogenic conditions at earlier time points in future studies to provide a more comprehensive understanding of the progression of chondrogenic differentiation.

While culturing in differentiation medium had the most marked effect on chondrogenic gene expression, the RT-qPCR studies provided further evidence that the incorporated ECM had bioactive effects in mediating the chondrogenic differentiation of the encapsulated ASCs. More specifically, after 7 days of culture in chondrogenic differentiation medium, increased expression of *ACAN* and *Coll II* was observed in the ALG+DIM and ALG+DOM beads, and *COMP* in the ALG+DOM, compared to ALG alone, for both of the cell donors studied. Further, in comparing the expression levels in the 28-day chondrogenic samples, both of these markers were also consistently more highly expressed in the ALG+DOM beads relative to the ALG alone.

The gene expression findings are aligned with the IHC results that showed markedly enhanced ECM accumulation in the composite bioinks after 28 days of culture in chondrogenic differentiation medium. More specifically, collagen type I, collagen type II, and fibronectin expression were qualitatively enhanced in the ALG+DOM and ALG+DIM beads compared to the ALG alone, with more intense staining in the ALG+DOM group. As previously discussed, fibronectin plays important roles in the initiation of chondrogenesis, as well as in the organization of the developing cartilage

matrix [154], [155]. As such, an enhanced presence of fibronectin-derived peptides within the pepsin-digested DOM may have stimulated the production of fibrocartilaginous ECM by the encapsulated ASCs. Interestingly, a previous study investigating the effects of incorporating a recombinant fibronectin fragment on the *in vitro* chondrogenic differentiation of bovine bone marrow-derived mesenchymal stromal cells (MSCs) encapsulated within agarose hydrogels showed that the fragment impeded proteoglycan synthesis and GAG accumulation [168], consistent with the very low levels of keratan sulphate staining observed under the conditions in the current study. An enhanced presence of fibronectin-derived peptides in the ALG+DOM group may have also contributed to a downregulation in fibronectin expression under proliferation conditions relative to the ALG+DIM group, similar to what has been reported in terms of collagen production when cells are cultured on collagen-based scaffolds [169].

Overall, the current study contributes to a growing body of evidence that supports that the ECM can have region-specific cell-instructive effects on MSC differentiation when incorporated within 3-D scaffolds [69]. Our findings are similar to a recent study that demonstrated that scaffolds derived from decellularized human meniscus provided a supportive microenvironment for the fibrochondrogenic differentiation of human synovial fluid-derived MSCs when cultured in medium containing inductive growth factors [170]. Similarly, another study investigating the effects of soluble urea extracts from decellularized inner versus outer bovine meniscus showed that both had positive effects on the proliferation and fibrochondrogenic differentiation of human bone marrow MSCs in 2-D culture [171]. Further, when the cells were encapsulated in 3-D methacrylated gelatin hydrogels, supplementation of the chondrogenic medium with the urea extracts was shown to accelerate chondrogenic differentiation [171]. Interestingly, the extracts from the inner meniscus had a more marked effect at timepoints up to day 21, but chondrogenic marker expression was similar between both ECM-supplemented groups at 42 days [171].

Future studies should explore the phenotypic stability of the cells, and probe strategies to further augment fibrocartilaginous ECM production including increasing the concentration of ECM incorporated in the gels, the effects of varying oxygen tensions

[172], as well as supplementation of the medium with additional growth factors such as growth differentiation factor-5 (GDF-5) [173]. In addition, bioprinting studies should be performed to assess the potential of the bioinks to fabricate customized constructs with defined geometries, including applying both the ALG+DIM and ALG+DOM bioinks in combination to create constructs with a varying composition that mimics the native tissues.

Chapter 5

5 Conclusion

5.1 Summary of Findings

In the first aim, a novel protocol (Protocol A) was applied to decellularize the inner and outer regions of the porcine meniscus that effectively extracted cellular and nuclear content while preserving key extracellular matrix (ECM) components including collagens, glycosaminoglycans (GAGs), laminin, and fibronectin. Methods used in this protocol included freeze-thaw cycles to mechanically induce cell lysis, hypotonic and hypertonic solutions to lyse cells by osmotic shock, enzymatic digestion with DNase and RNase, and washes with the non-ionic detergent Triton X-100. Protocol A was compared to an established protocol from the literature (Protocol B) that also relied on Triton X-100 detergent extraction combined with DNase and RNase digestion, and was previously used in studies comparing the cell-instructive effects of the decellularized inner and outer regions of the meniscus on human bone marrow-derived mesenchymal stromal cells (MSCs) encapsulated within 3-D hydrogels [11].

As confirmed by 4',6-diamidino-2-phenylindole (DAPI) fluorescent staining and the PicoGreen® assay, Protocol A was more effective at extracting cellular content than Protocol B in both regions. Tissues processed with both protocols incorporated qualitatively similar dense networks of collagen, with the exception of the outer region of Protocol B, which showed an altered presence or arrangement of thin collagen fibers based on picrosirius red staining. Quantitatively, the tissues processed with both protocols had an enrichment in collagen content in the outer region relative to the native tissues, likely associated with a relative increase in collagen due to the loss of cells and other ECM components during decellularization. Protocol A enhanced the retention of GAGs based on toluidine blue staining and confirmed by the dimethylmethylene blue (DMMB) assay. Immunohistochemical analyses of key ECM markers revealed meniscal tissues decellularized by Protocol A presented similar staining patterns and intensities compared to native tissue controls. Notably, collagen type I and fibronectin staining were

more intense in the outer region, while more intense staining for keratan sulphate was observed in the inner region.

In the second aim, decellularized inner (DIM) or outer (DOM) meniscus processed with Protocol A was pepsin-digested and incorporated at a concentration of 10 mg/mL into a proprietary alginate (ALG) solution, creating ALG+DIM and ALG+DOM bionks. A bioink comprised of ALG alone was also included as a control. A proprietary crosslinker was used to encapsulate human adipose-derived stromal cells (ASCs) within the alginate-based beads at a density of 3.0×10^6 cells/mL. The beads were then cultured in proliferation or chondrogenic differentiation media for up to 30 days. The LIVE/DEAD® assay confirmed that the cells within the ALG, ALG+DIM, and ALG+DOM beads cultured in both media types remained highly viable throughout the *in vitro* culture period. A significantly higher cell density was observed in the ECM-containing bioinks at 28 days in both media formulations relative to the alginate alone, and a significant increase in the cell density was found from 24 hours to 28 days within the ALG+DIM beads cultured in proliferation medium. Taken together, these findings indicate the incorporation of the pepsin-digested ECM had bioactive effects on promoting cell survival and/or proliferation, or adhesive cues to remain in the beads.

In the final aim, gene expression of the ASCs cultured in proliferation and chondrogenic differentiation media was analyzed using RT-qPCR targeting genes associated with chondrogenesis. *SOX9* was upregulated at 7 days of culture in proliferation medium, which may suggest an inductive effect of the 3D culture platform. However, this effect did not contribute to any notable expression of chondrogenic markers at either the gene or protein levels in the samples cultured for 28 days in proliferation medium, indicating that the ECM alone was insufficient to induce a chondrogenic differentiation response. Increased levels of aggrecan and collagen type II gene expression were seen at 7 days of culture in chondrogenic differentiation medium in the ALG+DIM and ALG+DOM beads, and *COMP* in ALG+DOM beads, compared to ALG alone, supporting that the ECM may have provided instructive cues to direct chondrogenic differentiation. This interpretation is further corroborated by the higher levels of *Coll II* and *ACAN* expression that were observed in the ALG+DOM beads cultured in chondrogenic differentiation medium from

28 days relative to the ALG alone group for both of the cell donors included in the study. Immunohistochemical analyses revealed that the ALG+DIM and ALG+DOM beads cultured in chondrogenic differentiation medium showed enhanced staining for collagen type I, collagen type II, and fibronectin relative to the ALG beads, with qualitatively higher levels of expression in the ALG+DOM group. In addition, the ALG+DOM beads also demonstrated faint staining for keratan sulphate. Based on the abundant staining, it was concluded that there was enhanced fibrocartilaginous matrix formation when the human ASCs were cultured within the ALG+DOM beads and confirmed that the region-dependent bioinks had distinct effects on ECM accumulation within the hydrogels.

5.2 Conclusions and Significance

A novel decellularization protocol was demonstrated to effectively remove cellular and nuclear content, while preserving native ECM constituents including collagens, GAGs, laminin and fibronectin, from both the inner and outer regions of porcine meniscus. The decellularized tissues generated with this protocol could be applied to generate a wide range of ECM-derived bioscaffolds, including porous foams, microcarriers, coatings, and hydrogels, using methods established in the Flynn lab with other decellularized tissue sources [96], [123], [174]–[178]. The findings in this thesis also support that the pepsin-digested meniscus ECM had bioactive effects on mediating the proliferation and fibrochondrogenic differentiation of human ASCs encapsulated within alginate-based hydrogels. Overall, this body of work contributes relevant new insight into a growing body of evidence that supports that region-specific ECM can be harnessed to direct cell phenotype and function within tissue-engineered scaffolds.

5.3 Future Directions

The work in this thesis served a basis to understanding the potential effects of meniscus ECM on the viability and chondrogenic differentiation of human ASCs encapsulated within alginate-based beads. Future studies should focus on the effects of varying ECM concentrations within the beads, redefining parameters for separating more distinct regions of the menisci, as well as investigating the conjugation of the ECM to the alginate to ensure the fragments remain inside the beads during *in vitro* culture [179], [180]. A

more in-depth understanding of the mechanism that guides the differential response between the two regions could also be an interesting aspect to explore in future work. A potential approach to this may be to explore the effects of bioinks made from pepsin-digested purified collagen and fibronectin, used independently and in combination.

Additionally, since enzymatic digestion with pepsin may result in time-dependent alterations to the ECM [181], it would be interesting to evaluate the bioactivity of ECM digested with pepsin for varying amounts of time. From a cellular perspective, it is understood that ASCs exhibit a reduced capacity to differentiate beyond passage 5 [182]. Therefore, gene expression studies should analyze the use of ASCs from earlier passages and should be repeated on additional cell donors to verify trends. The application of other cell types including bone marrow-derived MSCs, meniscal fibrochondrocytes, or cartilage cells could also be studied to determine which cell type enhances fibrochondrogenic ECM production. Furthermore, RT-qPCR should include additional timepoints, especially an earlier timepoint, to provide more insight on the progression of cell differentiation. Collagen type X expression should be analyzed using immunohistochemistry to assess the degree of cell hypertrophy.

Lastly, this study focused on verifying that the addition of meniscus ECM to alginate-based beads is able to influence ASC viability and differentiation. Future studies that aim to explore 3D bioprinting of meniscus constructs containing this ECM should investigate modifications to the bioink that would retain its bioactivity while more accurately representing the mechanical properties of native meniscus. Additional studies could also assess the cell-instructive effects of combining both bioinks.

References

- [1] A. J. S. Fox, A. Bedi, and S. A. Rodeo, “The Basic Science of Human Knee Menisci: Structure, Composition, and Function,” *Sports Health*, vol. 4, no. 4, pp. 340–351, 2012.
- [2] J. K. Bryceland, A. J. Powell, and T. Nunn, “Knee Menisci: Structure, Function, and Management of Pathology,” *Cartilage*, vol. 8, no. 2, pp. 99–104, 2017.
- [3] I. D. McDermott, F. Sharifi, A. M. J. Bull, C. M. Gupte, R. W. Thomas, and A. A. Amis, “An anatomical study of meniscal allograft sizing,” *Knee Surgery, Sport. Traumatol. Arthrosc.*, vol. 12, no. 2, pp. 130–135, 2004.
- [4] B. Shaffer, S. Kennedy, J. Klimkiewicz, and L. Yao, “Preoperative sizing of meniscal allografts in meniscus transplantation,” *Am. J. Sports Med.*, vol. 28, no. 4, pp. 524–533, 2000.
- [5] E. A. Makris, P. Hadidi, and K. A. Athanasiou, “The knee meniscus: structure-function, pathophysiology, current repair techniques, and prospects for regeneration”, *Biomaterials*, vol. 32, pp.7411-7431, 2011.
- [6] K. A. Athanasiou and J. Sanchez-Adams, "The knee meniscus: A complex tissue of diverse cells", *Cellular and molecular bioeng.* vol. 2, no. 3, pp. 332-340, 2009.
- [7] K. Messner and J. Gao, “The menisci of the knee joint. Anatomical and functional characteristics, and a rationale for clinical treatment,” *J. Anat.*, vol. 193, no. 2, pp. 161–178, 1998.
- [8] D. Learmonth, “Aspects of the knee: Meniscal injury and surgery,” *Trauma*, vol. 2, no. 3, pp. 223–230, 2000.
- [9] J. Sanchez-Adams and K. A. Athanasiou, “The knee meniscus: A complex tissue of diverse cells,” *Cell. Mol. Bioeng.*, vol. 2, no. 3, pp. 332–340, 2009.
- [10] R. Verdonk, J. Espregueira-Mendes, and J. C. Monllau, “Meniscal

- transplantation,” *Meniscal Transplant.*, pp. 1–117, 2013.
- [11] K. Shimomura, B. B. Rothrauff, and R. S. Tuan, “Region-Specific Effect of the Decellularized Meniscus Extracellular Matrix on Mesenchymal Stem Cell – Based Meniscus Tissue Engineering,” pp. 604–611, 2016.
- [12] M. A. Sweigart and K. A. Athanasiou, “Toward tissue engineering of the knee meniscus,” *Tissue Eng.*, vol. 7, no. 2, pp. 111–129, 2001.
- [13] H. S. Cheung, “Distribution of type I, II, III and v in the pepsin solubilized collagens in bovine menisci,” *Connect. Tissue Res.*, vol. 16, no. 4, pp. 343–356, 1987.
- [14] P. G. Scott, T. Nakano, and C. M. Dodd, “Isolation and characterization of small proteoglycans from different zones of the porcine knee meniscus,” *Biochim. Biophys. Acta - Gen. Subj.*, vol. 1336, no. 2, pp. 254–262, 1997.
- [15] E. A. Makris, P. Hadidi, and K. A. Athanasiou, “The knee meniscus: structure-function, pathophysiology, current repair techniques, and prospects for regeneration,” *Biomaterials*, vol. 32, pp.7411-7431, 2011.
- [16] T. Nakano, C. M. Dodd, and P. G. Scott, “Glycosaminoglycans and proteoglycans from different zones of the porcine knee meniscus,” *J. Orthop. Res.*, vol. 15, no. 2, pp. 213–220, 1997.
- [17] C. A. McDevitt and R. J. Webber, “The ultrastructure and biochemistry of meniscal cartilage,” *Clin. Orthop. Relat. Res.*, no. 252, pp. 8–18, 1990.
- [18] P. C. M. Verdonk *et al.*, “Characterisation of human knee meniscus cell phenotype,” *Osteoarthr. Cartil.*, vol. 13, no. 7, pp. 548–60, 2005.
- [19] T. Furumatsu, T. Kanazawa, Y. Yokoyama, N. Abe, and T. Ozaki, “Inner Meniscus Cells Maintain Higher Chondrogenic Phenotype Compared with Outer Meniscus Cells Inner Meniscus Cells Maintain Higher Chondrogenic Phenotype Compared with Outer Meniscus Cells,” *Connective tissue research*, vol. 8207,

2011.

- [20] E. Bari *et al.*, “Freeze-Dried Secretome for Cell-Free Regenerative Nanomedicine: A Validated GMP-Compliant Process,” *Cells*, pp. 1–22, 2018.
- [21] B. Bilgen, C. T. Jayasuriya, and B. D. Owens, “Current Concepts in Meniscus Tissue Engineering and Repair,” *Advanc Healthc Mater.*, vol 7, 2018.
- [22] M. J. Salata, A. E. Gibbs, and J. K. Sekiya, “A systematic review of clinical outcomes in patients undergoing meniscectomy,” *Am. J. Sports Med.*, vol. 38, no. 9, pp. 1907–1916, 2010.
- [23] Y. Chen *et al.*, “Current advances in the development of natural meniscus scaffolds: innovative approaches to decellularization and recellularization,” *Cell Tissue Res.*, vol. 370, no. 1, pp. 41–52, 2017.
- [24] M. Englund, A. Guermazi, and S. L. Lohmander, “The Role of the Meniscus in Knee Osteoarthritis: a cause or consequence?,” *Radiol. Clin. North Am.*, vol. 47, no. 4, pp. 703–712, 2009.
- [25] L. B. Williams and A. B. Adesida, “Angiogenic approaches to meniscal healing,” *Injury*, vol. 49, no. 3, pp. 467–472, 2018.
- [26] T. J. Fairbank, “Knee joint changes after meniscectomy.,” *J. Bone Joint Surg. Am.*, vol. 30 B, no. 4, pp. 664–670, 1948.
- [27] M. Englund and L. S. Lohmander, “Risk factors for symptomatic knee osteoarthritis fifteen to twenty-two years after meniscectomy,” *Arthritis Rheum.*, vol. 50, no. 9, pp. 2811–2819, 2004.
- [28] P. Beaufils, R. Becker, S. Kopf, O. Matthieu, and N. Pujol, “The knee meniscus: Management of traumatic tears and degenerative lesions,” *EFORT Open Rev.*, vol. 2, no. 5, pp. 195–203, 2017.
- [29] R. H. Brophy, B. Zhang, L. Cai, R. W. Wright, L. J. Sandell, and M. F. Rai,

- “Transcriptome comparison of meniscus from patients with and without osteoarthritis,” *Osteoarthr. Cartil.*, vol. 26, no. 3, pp. 422–432, 2018.
- [30] P. A. MacMullan and G. M. McCarthy, “The meniscus, calcification and osteoarthritis: A pathologic team,” *Arthritis Res. Ther.*, vol. 12, no. 3, pp. 12–13, 2010.
- [31] K. P. H. Pritzker, “Counterpoint: Hydroxyapatite crystal deposition is not intimately involved in the pathogenesis and progression of human osteoarthritis,” *Curr. Rheumatol. Rep.*, vol. 11, no. 2, pp. 148–153, 2009.
- [32] B. A. Derfus *et al.*, “The high prevalence of pathologic calcium crystals in pre-operative knees,” *J. Rheumatol.*, vol. 29, no. 3, pp. 570–574, 2002.
- [33] H. S. Cheung, “Biologic effects of calcium-containing crystals,” *Curr Opin Rheumatol.*, pp. 336–340, 2005.
- [34] P. C. M. Verdonk, M. E. E. Van Laer, and R. Verdonk, “Meniscus Replacement: From Allograft to Tissue Engineering,” *Sport. - Sport.*, vol. 24, no. 2, pp. 78–82, 2008.
- [35] C. T. Vangsness, J. F. Ii, J. Boyd, D. T. Dellaero, C. R. Mills, and M. Leroux-Williams, “Adult Human Mesenchymal Stem Cells Delivered via,” *J. Bone Jt. Surg.*, vol. 96, pp. 90–98, 2014.
- [36] W. E. GARRETT *et al.*, “American Board of Orthopaedic Surgery Practice of the Orthopaedic Surgeon,” *J. Bone Jt. Surgery-American Vol.*, vol. 88, no. 3, pp. 660–667, 2006.
- [37] R. J. Williams, K. K. Warner, F. A. Petrigliano, H. G. Potter, J. Hatch, and F. A. Cordasco, “MRI evaluation of isolated arthroscopic partial meniscectomy patients at a minimum five-year follow-up,” *HSS J.*, vol. 3, no. 1, pp. 35–43, 2007.
- [38] Y. L. Gu and Y. Bin Wang, “Treatment of meniscal injury: A current concept review,” *Chinese J. Traumatol. - English Ed.*, vol. 13, no. 6, pp. 370–376, 2010.

- [39] H. Andersson-Molina, H. Karlsson, and P. Rockborn, "Arthroscopic partial and total meniscectomy: A long-term follow-up study with matched controls," *Arthroscopy*, vol. 18, no. 2, pp. 183–189, 2002.
- [40] W. Niu, W. Guo, S. Han, Y. Zhu, S. Liu, and Q. Guo, "Cell-Based Strategies for Meniscus Tissue Engineering," *Stem Cells International*, 2016.
- [41] C. Chrysanthou *et al.*, "Meniscal repair using fibrin clot from autologous blood: description of the surgical technique," *J. Res. Pract. Musculoskelet. Syst.*, vol. 02, no. 03, pp. 89–94, 2018.
- [42] M. Karia, Y. Ghaly, N. Al-Hadithy, S. Mordecai, and C. Gupte, "Current concepts in the techniques, indications and outcomes of meniscal repairs," *Eur. J. Orthop. Surg. Traumatol.*, vol. 29, no. 3, pp. 509–520, 2019.
- [43] J. M. Fox, K. G. Rintz, and R. D. Ferkel, "Trephination of incomplete meniscal tears," *Arthroscopy*, vol. 9, no. 4, pp. 451–455, 1993.
- [44] Z. Zhang and J. A. Arnold, "Trephination and suturing of avascular meniscal tears: A clinical study of the trephination procedure," *Arthroscopy*, vol. 12, no. 6, pp. 726–731, 1996.
- [45] G. A. Paletta, S. P. Arnoczky, and R. F. Warren, "The repair of osteochondral defects using an exogenous fibrin clot: An experimental study in dogs," *Am. J. Sports Med.*, vol. 20, no. 6, pp. 725–731, 1992.
- [46] L. E. Scordino and T. M. DeBerardino, "Biologic Enhancement of Meniscus Repair," *Clin. Sports Med.*, vol. 31, no. 1, pp. 91–100, 2012.
- [47] T. L. Wickiewicz, "Arthroscopic Meniscal Repair With Fibrin Clot of Complete," *Arthroscopy*, vol. 14, no. 4, pp. 360–365, 1998.
- [48] T. Kamimura and M. Kimura, "Repair of horizontal meniscal cleavage tears with exogenous fibrin clots," *Knee Surgery, Sport. Traumatol. Arthrosc.*, vol. 19, no. 7, pp. 1154–1157, 2011.

- [49] K. Ishida *et al.*, “The regenerative effects of platelet-rich plasma on meniscal cells in vitro and its in vivo application with biodegradable gelatin hydrogel,” *Tissue Eng.*, vol. 13, no. 5, pp. 1103–1112, 2007.
- [50] J. W. Griffin, M. M. Hadeed, B. C. Werner, D. R. Diduch, E. W. Carson, and M. D. Miller, “Platelet-rich Plasma in Meniscal Repair: Does Augmentation Improve Surgical Outcomes?,” *Clin. Orthop. Relat. Res.*, vol. 473, no. 5, pp. 1665–1672, 2015.
- [51] H. Pereira *et al.*, “Meniscal allograft transplants and new scaffolding techniques,” *EFORT Open Rev.*, vol. 4, no. 6, pp. 279–295, 2019.
- [52] S. R. Lee, J. G. Kim, and S. W. Nam, “The Tips and Pitfalls of Meniscus Allograft Transplantation,” *Knee Surg. Relat. Res.*, vol. 24, no. 3, pp. 137–145, 2012.
- [53] K. A. Milachowski, K. Weismeier, and C. J. Wirth, “Homologous meniscus transplantation - Experimental and clinical results,” *Int. Orthop.*, vol. 13, no. 1, pp. 1–11, 1989.
- [54] A. H. Gomoll and T. Minas, “Meniscal Allograft Transplantation,” *A Prim. Cartil. Repair Jt. Preserv. Knee*, pp. 193–199, 2011.
- [55] E. Kon *et al.*, “Tissue engineering for total meniscal substitution: Animal study in sheep model,” *Tissue Eng. - Part A.*, vol. 14, no. 6, pp. 1067–1080, 2008.
- [56] B. Haddad, B. Haddad, S. Konan, A. Adesida, and W. S. Khan, “A Systematic Review of Tissue Engineered Meniscus and Replacement Strategies: Preclinical Models,” *Curr. Stem Cell Res. Ther.*, vol. 8, no. 3, pp. 232–242, 2013.
- [57] T. Yamasaki, M. Deie, R. Shinomiya, Y. Yasunaga, S. Yanada, and M. Ochi, “Transplantation of meniscus regenerated by tissue engineering with a scaffold derived from a rat meniscus and mesenchymal stromal cells derived from rat bone marrow,” *Artif. Organs*, vol. 32, no. 7, pp. 519–524, 2008.
- [58] F. T. Moutos and F. Guilak, “Functional properties of cell-seeded three-

- dimensionally woven poly(ϵ -Caprolactone) scaffolds for cartilage tissue engineering,” *Tissue Eng. - Part A*, vol. 16, no. 4, pp. 1291–1301, 2010.
- [59] Y. Moriguchi *et al.*, “Repair of meniscal lesions using a scaffold-free tissue-engineered construct derived from allogenic synovial MSCs in a miniature swine model,” *Biomaterials*, vol. 34, no. 9, pp. 2185–2193, 2013.
- [60] M. Li, M. J. Mondrinos, X. Chen, M. R. Gandhi, F. K. Ko, and P. I. Lelkes, “Elastin Blends for Tissue Engineering Scaffolds,” *J. Biomed. Mater. Res. Part A*, vol. 79, no. 4, pp. 963–73, 2006.
- [61] A. I. Caplan and J. E. Dennis, “Mesenchymal stem cells as trophic mediators,” *J. Cell. Biochem.*, vol. 98, no. 5, pp. 1076–1084, 2006.
- [62] K. Shimomura, S. Hamamoto, D. A. Hart, H. Yoshikawa, and N. Nakamura, “Meniscal repair and regeneration: Current strategies and future perspectives,” *J. Clin. Orthop. Trauma*, vol. 9, no. 3, pp. 247–253, 2018.
- [63] C. Scotti, M. T. Hirschmann, P. Antinolfi, I. Martin, and G. M. Peretti, “Meniscus repair and regeneration: Review on current methods and research potential,” *Eur. Cells Mater.*, vol. 26, pp. 150–170, Sep. 2013.
- [64] A. Leroy, P. Beaufils, B. Faivre, C. Steltzlen, P. Boisrenoult, and N. Pujol, “Actifit® polyurethane meniscal scaffold: MRI and functional outcomes after a minimum follow-up of 5 years,” *Orthop. Traumatol. Surg. Res.*, vol. 103, no. 4, pp. 609–614, 2017.
- [65] S. T. Beyer, A. Bsoul, A. Ahmadi, and K. Walus, “3D alginate constructs for tissue engineering printed using a coaxial flow focusing microfluidic device,” *Transducers Eurosensors XXVII 17th Int. Conf. Solid-State Sensors, Actuators Microsystems*, pp. 1206–1209, 2013.
- [66] R. Resmi, J. Parvathy, A. John, and R. Joseph, “Injectable self-crosslinking hydrogels for meniscal repair: A study with oxidized alginate and gelatin,” *Carbohydr. Polym.*, vol. 234, 2020.

- [67] S. Zaffagnini *et al.*, “Two-Year Clinical Results of Lateral Collagen Meniscus Implant: A Multicenter Study,” *Arthrosc. - J. Arthrosc. Relat. Surg.*, vol. 31, no. 7, pp. 1269–1278, 2015.
- [68] T. W. Stapleton *et al.*, “Development and characterization of an acellular porcine medial meniscus for use in tissue engineering,” *Tissue Eng. - Part A.*, vol. 14, no. 4, pp. 505–518, 2008.
- [69] K. P. Robb, A. Shridhar, and L. E. Flynn, “Decellularized Matrices As Cell-Instructive Scaffolds to Guide Tissue-Specific Regeneration,” *ACS Biomater.*, 4, 11, 2018.
- [70] Z. Yu *et al.*, “Development of decellularized meniscus extracellular matrix and gelatin/chitosan scaffolds for meniscus tissue engineering,” *Biomed. Mater. Eng.*, vol. 30, no. 2, pp. 125–132, 2019.
- [71] J. Wu, Q. Ding, A. Dutta, Y. Wang, Y. Huang, and H. Weng, “Acta Biomaterialia An injectable extracellular matrix derived hydrogel for meniscus repair and regeneration,” *Acta Biomater.*, vol. 16, pp. 49–59, 2015.
- [72] C. Yu *et al.*, “Rapid 3D bioprinting of decellularized extracellular matrix with regionally varied mechanical properties and biometric microarchitecture,” *Biomater* pp. 310–321, 2019.
- [73] N. Faramarzi *et al.*, “Patient-specific bioinks for 3D bioprinting of tissue engineering scaffolds,” *Adv Healthc Mater.*, vol. 7, no. 11, pp. 1–17, 2019.
- [74] F. Pati *et al.*, “Printing three-dimensional tissue analogues with decellularized extracellular matrix bioink,” *Nat. Commun.*, vol. 5, pp. 1–11, 2014.
- [75] S. V. Murphy and A. Atala, “3D bioprinting of tissues and organs,” *Nat. Biotechnol.*, vol. 32, no. 8, pp. 773–785, 2014.
- [76] C. Mota, S. Camarero-Espinosa, M. B. Baker, P. Wieringa, and L. Moroni, “Bioprinting: From Tissue and Organ Development to in Vitro Models,” *Chem.*

Rev., 120, pp. 10547-10607, 2020.

- [77] K. Y. Lee and D. J. Mooney, "Alginate: Properties and biomedical applications," *Prog. Polym. Sci.*, vol. 37, no. 1, pp. 106–126, 2012.
- [78] J. Li, M. Chen, X. Fan, and H. Zhou, "Recent advances in bioprinting techniques: Approaches, applications and future prospects," *J. Transl. Med.*, vol. 14, no. 1, pp. 1–15, 2016.
- [79] E. Abelseh, L. Abelseh, L. De La Vega, S. T. Beyer, S. J. Wadsworth, and S. M. Willerth, "3D Printing of Neural Tissues Derived from Human Induced Pluripotent Stem Cells Using a Fibrin-Based Bioink," *ACS Biomater. Sci. Eng.*, vol. 5, no. 1, pp. 234–243, 2019.
- [80] A. Bsoul, S. Pan, E. Cretu, B. Stoeber, and K. Walus, "Design, microfabrication, and characterization of a moulded PDMS/SU-8 inkjet dispenser for a Lab-on-a-Printer platform technology with disposable microfluidic chip," *Lab Chip*, vol. 16, no. 17, pp. 3351–3361, 2016.
- [81] H. Baharvand, A. Samandian, S. Abbasalizadeh. "Bioprocess Development for Mass Production of Size-Controlled Human Pluripotent Stem Cell Aggregates in Stirred Suspension Bioreactor," *Tissue eng.* vol. 120947, no. 514, pp. 1–55, 2013.
- [82] Wadsworth et al., "United States Patent Application Publication Pub No. US 2019/0314552 A1," 2019.
- [83] S. Y. Nam and S. H. Park, "ECM based bioink for tissue mimetic 3D bioprinting," *Adv. Exp. Med. Biol.*, vol. 1064, pp. 335–353, 2018.
- [84] K. Dzobo, K. S. C. M. Motaung, and A. Adesida, "Recent trends in decellularized extracellular matrix bioinks for 3D printing: An updated review," *Int. J. Mol. Sci.*, vol. 20, no. 18, pp. 1–28, 2019.
- [85] F. Kabirian and M. Mozafari, "Decellularized ECM-derived bioinks: Prospects for the future," *Methods*, vol. 171, pp. 108–118, 2020.

- [86] X. Ma *et al.*, “Rapid 3D bioprinting of decellularized extracellular matrix with regionally varied mechanical properties and biomimetic microarchitecture,” *Biomaterials*, vol. 185, pp. 310–321, 2018.
- [87] C. T. D. Dickman *et al.*, “Functional characterization of 3D contractile smooth muscle tissues generated using a unique microfluidic 3D bioprinting technology,” *Faseb J.*, vol. 34, no. 1, pp. 1652–1664, 2020.
- [88] T. W. Gilbert, T. L. Sellaro, and S. F. Badylak, “Decellularization of tissues and organs,” *Biomaterials*, vol. 27, no. 19, pp. 3675–3683, 2006.
- [89] A. Gilpin and Y. Yang, “Decellularization Strategies for Regenerative Medicine: From Processing Techniques to Applications,” *Biomed Res. Int.*, vol. 2017, 2017.
- [90] J. Hodde, A. Janis, D. Ernst, D. Zopf, D. Sherman, and C. Johnson, “Effects of sterilization on an extracellular matrix scaffold: Part I. Composition and matrix architecture,” *J. Mater. Sci. Mater. Med.*, vol. 18, no. 4, pp. 537–543, 2007.
- [91] S. B. Lumpkins, N. Pierre, and P. S. McFetridge, “A mechanical evaluation of three decellularization methods in the design of a xenogeneic scaffold for tissue engineering the temporomandibular joint disc,” *Acta Biomater.*, vol. 4, no. 4, pp. 808–816, 2008.
- [92] P. Crapo, T. Gilbert, and S. Badylak. “An Overview of Tissue and Whole,” *Biomaterials*, vol. 32, no. 12, pp. 3233–3243, 2012.
- [93] J. Aamodt, and D. Grainger. “ Extracellular matrix-based scaffolds and the host response” *Biomaterials*, vol. 176, no. 3, pp. 139–148, 2016.
- [94] T. W. Gilbert, J. M. Freund, and S. F. Badylak, “Quantification of DNA in Biologic Scaffold Materials,” *J. Surg. Res.*, vol. 152, no. 1, pp. 135–139, 2009.
- [95] B. N. Brown *et al.*, “Comparison of three methods for the derivation of a biologic scaffold composed of adipose tissue extracellular matrix,” *Tissue Eng. - Part C Methods*, vol. 17, no. 4, pp. 411–421, 2011.

- [96] P. Morissette, A. Grant, D. W. Hamilton, and L. E. Flynn, “Matrix composition in 3-D collagenous bioscaffolds modulates the survival and angiogenic phenotype of human chronic wound dermal fibroblasts,” *Acta Biomater.*, vol. 83, pp. 199–210, 2019.
- [97] Y. Sun, “Histological Examination of Collagen and Proteoglycan Changes in Osteoarthritic Menisci,” *Open Rheumatol. J.*, vol. 6, no. 1, pp. 24–32, 2012.
- [98] C. Frantz, K. M. Stewart, and V. M. Weaver, “The extracellular matrix at a glance,” *J. Cell Sci.*, vol. 123, no. 24, pp. 4195–4200, 2010.
- [99] S. Ricard-Blum and R. Salza, “Matricryptins and matrikines: Biologically active fragments of the extracellular matrix,” *Exp. Dermatol.*, vol. 23, no. 7, pp. 457–463, 2014.
- [100] J. Mauney, B. R. Olsen, and V. Volloch, “Matrix remodeling as stem cell recruitment event: A novel in vitro model for homing of human bone marrow stromal cells to the site of injury shows crucial role of extracellular collagen matrix,” *Matrix Biol.*, vol. 29, no. 8, pp. 657–663, 2010.
- [101] G. E. Davis, K. J. Bayless, M. J. Davis, and G. A. Meininger, “Regulation of tissue injury responses by the exposure of matricryptic sites within extracellular matrix molecules,” *Am. J. Pathol.*, vol. 156, no. 5, pp. 1489–1498, 2000.
- [102] B. N. Brown and S. F. Badylak, “Extracellular matrix as an inductive scaffold for functional tissue reconstruction,” *Transl. Res.*, vol. 163, no. 4, pp. 268–285, 2014.
- [103] F. Gattazzo, A. Urciuolo, and P. Bonaldo, “Extracellular matrix: A dynamic microenvironment for stem cell niche,” *Biochim. Biophys. Acta - Gen. Subj.*, vol. 1840, no. 8, pp. 2506–2519, 2014.
- [104] D. Li, J. Zhou, F. Chowdhury, j. Cheng, N. Wang. “Role of mechanical factors in fate decisions of stem cells,” *Regen Med* 6(2) 229-240, 2011.
- [105] T. Luo, K. Mohan, P. A. Iglesias, and D. N. Robinson, “Molecular mechanisms of

- cellular mechanosensing,” *Nat. Mater.*, vol. 12, no. 11, pp. 1064–1071, 2013.
- [106] B. Brown, K. Lindberg, J. Reing, D. B. Stolz, and S. F. Badylak, “The basement membrane component of biologic scaffolds derived from extracellular matrix,” *Tissue Eng.*, vol. 12, no. 3, pp. 519–526, 2006.
- [107] B. Brown, C. Barnes, R. Kasick, R. Michel, et al. "Surface Characteristics of extracellular matrix scaffolds," *Biomaterials* 31(3):428-437, 2009.
- [108] Q. L. Loh and C. Choong, “Three-dimensional scaffolds for tissue engineering applications: Role of porosity and pore size,” *Tissue Eng. - Part B Rev.*, vol. 19, no. 6, pp. 485–502, 2013.
- [109] P. F. Gratzer, "Decellularized extracellular matrix", *Encyclopedia of biomedical engineering*, vol. 1, 2019.
- [110] A. Azhim, T. Ono, Y. Fukui, Y. Morimoto, K. Furukawa, and T. Ushida, “Preparation of decellularized meniscal scaffolds using sonication treatment for tissue engineering,” *Proc. Annu. Int. Conf. IEEE Eng. Med. Biol. Soc. EMBS*, pp. 6953–6956, 2013.
- [111] G. H. Sandmann *et al.*, “Generation and characterization of a human acellular meniscus scaffold for tissue engineering,” *J. Biomed. Mater. Res. - Part A*, vol. 91, no. 2, pp. 567–574, 2009.
- [112] K. J. Stabile *et al.*, “An Acellular, Allograft-Derived Meniscus Scaffold in an Ovine Model,” *Arthrosc. - J. Arthrosc. Relat. Surg.*, vol. 26, no. 7, pp. 936–948, 2010.
- [113] R. J. Butler, S. Marchesi, T. Royer, and I. S. Davis, “The Effect of a Subject-Specific Amount of Lateral Wedge on Knee,” *J. Orthop. Res. Sept.*, vol. 25, no. June, pp. 1121–1127, 2007.
- [114] A. Jakolevich, K. Petrakova, G. Frolova, "Analysis of precursor cells for osteogenic and hematopoietic tissues" *Transplantation*, vol. 6, no. 2, 1968.

- [115] R. Hass, C. Kasper, S. Böhm, and R. Jacobs, "Different populations and sources of human mesenchymal stem cells (MSC): A comparison of adult and neonatal tissue-derived MSC," *Cell Commun. Signal.*, vol. 9, no. 1, p. 12, 2011.
- [116] S. A. Wexler, C. Donaldson, P. Denning-Kendall, C. Rice, B. Bradley, and J. M. Hows, "Adult bone marrow is a rich source of human mesenchymal 'stem' cells but umbilical cord and mobilized adult blood are not," *Br. J. Haematol.*, vol. 121, no. 2, pp. 368–374, 2003.
- [117] K. Lakshmi Kanth, S. Sanivarapu, S. Moogla, and R. S. Kutcham, "Adipose tissue - adequate, accessible regenerative material," *Int. J. Stem Cells*, vol. 8, no. 2, pp. 121–127, 2015.
- [118] J. M. Gimble, B. A. Bunnell, E. S. Chiu, and F. Guilak, "Concise review: Adipose-derived stromal vascular fraction cells and stem cells: Let's not get lost in translation," *Stem Cells*, vol. 29, no. 5, pp. 749–754, 2011.
- [119] P. Bourin, B. Bunnell, L. Casteilla, M. Dominici et al. "Stromal cells from the adipose tissue-derived stromal vascular fraction and culture expanded adipose-tissue derived stromal cells: a joint statement of the International Federation for Adipose Therapeutics and Science and the International Society for Cellular Therapy" *Cytotherapy. 1862*, vol. 15, no. 6, pp. 5–5, 2014.
- [120] K. Kornicka, K. Marycz, K. A. Tomaszewski, M. Marędziak, and A. Smieszek, "The Effect of Age on Osteogenic and Adipogenic Differentiation Potential of Human Adipose Derived Stromal Stem Cells (hASCs) and the Impact of Stress Factors in the Course of the Differentiation Process," *Oxid. Med. Cell. Longev.*, vol. 2015, 2015.
- [121] M. S. Choudhery, M. Badowski, A. Muise, J. Pierce, and D. T. Harris, "Donor age negatively impacts adipose tissue-derived mesenchymal stem cell expansion and differentiation," *J. Transl. Med.*, vol. 12, no. 1, pp. 1–14, 2014.
- [122] V. Van Harmelen *et al.*, "Effect of BMI and age on adipose tissue cellularity and

- differentiation capacity in women,” *Int. J. Obes.*, vol. 27, no. 8, pp. 889–895, 2003.
- [123] V. Russo, C. Yu, P. Belliveau, A. Hamilton, and L. E. Flynn, “Comparison of Human Adipose-Derived Stem Cells Isolated from Subcutaneous, Omental, and Intrathoracic Adipose Tissue Depots for Regenerative Applications,” *Stem Cells Transl. Med.*, vol. 3, no. 2, pp. 206–217, 2014.
- [124] E. D. Rosen and B. M. Spiegelman, “Molecular Regulation of Adipogenesis,” *Annu Rev Cell Dev Biol.*, vol. 16, pp. 145-171, 2000.
- [125] J. P. Stromps, N. E. Paul, B. Rath, M. Nourbakhsh, J. Bernhagen, and N. Pallua, “Chondrogenic differentiation of human adipose-derived stem cells: A new path in articular cartilage defect management?,” *Biomed Res. Int.*, vol. 2014, 2014.
- [126] M. Neupane, C.-C. Chang, M. Kiupel, and V. Yuzbasiyan-Gurkan, “Isolation and Characterization of Canine Adipose-Derived Mesenchymal Stem Cells,” *Tissue Eng. Part A*, vol. 0, no. 0, p. 080422095744451, 2008.
- [127] T. Ikeda *et al.*, “Distinct roles of Sox5, Sox6, and Sox9 in different stages of chondrogenic differentiation,” *J. Bone Miner. Metab.*, vol. 23, no. 5, pp. 337–340, 2005.
- [128] V. Lefebvre, R. R. Behringer, and B. De Crombrughe, “L-Sox5, Sox6 and SOx9 control essential steps of the chondrocyte differentiation pathway,” *Osteoarthr. Cartil.*, vol. 9, no. SUPPL. A, pp. 69–75, 2001.
- [129] M. B. Goldring, K. Tsuchimochi, and K. Ijiri, “The control of chondrogenesis,” *J. Cell. Biochem.*, vol. 97, no. 1, pp. 33–44, 2006.
- [130] J. Frith and P. Genever, “Transcriptional control of mesenchymal stem cell differentiation,” *Transfus. Med. Hemother.*, vol. 35, no. 3, pp. 216–21627, 2008.
- [131] S. Chen, P. Fu, R. Cong, H. S. Wu, and M. Pei, “Strategies to minimize hypertrophy in cartilage engineering and regeneration,” *Genes Dis.*, vol. 2, no. 1,

pp. 76–95, 2015.

- [132] T. Woods and P. F. Gratzner, “Effectiveness of three extraction techniques in the development of a decellularized bone-anterior cruciate ligament-bone graft,” *Biomaterials*, vol. 26, no. 35, pp. 7339–7349, 2005.
- [133] P. Li and G. Wu, “Roles of dietary glycine , proline , and hydroxyproline in collagen synthesis and animal growth,” *Amino Acids*, vol. 50, no. 1, pp. 29–38, 2018.
- [134] L. E. Flynn, G. D. Prestwich, J. L. Semple, and K. A. Woodhouse, “Proliferation and differentiation of adipose-derived stem cells on naturally derived scaffolds,” *Biomaterials*, vol. 29, no. 12, pp. 1862–1871, 2008.
- [135] S. L. Huang and Y. S. Lin, “The Size Stability of Alginate Beads by Different Ionic Crosslinkers,” *Adv. Mater. Sci. Eng.*, vol. 2017, 2017.
- [136] M. Englund and L. S. Lohmander, “Meniscectomy and osteoarthritis: what is the cause and what is the effect?,” *Fut. Rheumatol.*, vol. 1, no. 2, pp. 207–215, 2006.
- [137] M. M. Pillai, J. Gopinathan, R. Selvakumar, and A. Bhattacharyya, “Human Knee Meniscus Regeneration Strategies: a Review on Recent Advances,” *Curr. Osteoporos. Rep.*, vol. 16, no. 3, pp. 224–235, 2018.
- [138] I. Wong *et al.*, “Position Statement of the Arthroscopy Association of Canada (AAC) Concerning Arthroscopy of the Knee Joint—September 2017,” *Orthop. J. Sport. Med.*, vol. 6, no. 2, pp. 1–4, 2018.
- [139] M. Jalayeri, A. Pirnia, E. P. Najafabad, A. M. Varzi, and M. Gholami, “Evaluation of alginate hydrogel cytotoxicity on three-dimensional culture of type A spermatogonial stem cells,” *Int. J. Biol. Macromol.*, vol. 95, pp. 888–894, 2017.
- [140] K. Markstedt, A. Mantas, I. Tournier, H. Martínez Ávila, D. Hägg, and P. Gatenholm, “3D bioprinting human chondrocytes with nanocellulose-alginate bioink for cartilage tissue engineering applications,” *Biomacromolecules*, vol. 16,

- no. 5, pp. 1489–1496, 2015.
- [141] J. Wua *et al.*, “An injectable extracellular matrix derived hydrogel for meniscus repair and regeneration,” *Acta Biomater.*, vol. 16, no. 1, pp. 49–59, 2015.
- [142] T. J. Keane, I. T. Swinehart, and S. F. Badylak, “Methods of tissue decellularization used for preparation of biologic scaffolds and in vivo relevance,” *Methods*, vol. 84, pp. 25–34, 2015.
- [143] L. J. White *et al.*, “The impact of detergents on the tissue decellularization process: A ToF-SIMS study,” *Acta Biomater.*, vol. 50, pp. 207–219, 2017.
- [144] G. Agmon, K. L. Christman, and S. Diego, “Controlling stem cell behaviour with decellularized extracellular matrix scaffolds,” *Curr Opin Solid State Mater Sci.*, pp. 1–23, 2017.
- [145] L. Cen, W. Liu, L. Cui, W. Zhang, and Y. Cao, “Collagen tissue engineering: Development of novel biomaterials and applications,” *Pediatr. Res.*, vol. 63, no. 5, pp. 492–496, 2008.
- [146] R. Lattouf *et al.*, “Picrosirius Red Staining: A Useful Tool to Appraise Collagen Networks in Normal and Pathological Tissues,” *J. Histochem. Cytochem.*, vol. 62, no. 10, pp. 751–758, 2014.
- [147] J. Hwang *et al.*, “Molecular assessment of collagen denaturation in decellularized tissues using a collagen hybridizing peptide,” *Acta Biomater.*, vol. 53, pp. 268–278, 2017.
- [148] J. S. Cartmell and M. G. Dunn, “Effect of chemical treatments on tendon cellularity and mechanical properties,” *J. Biomed. Mater. Res.*, vol. 49, no. 1, pp. 134–140, 2000.
- [149] B. Mendoza-Novelo *et al.*, “Decellularization of pericardial tissue and its impact on tensile viscoelasticity and glycosaminoglycan content,” *Acta Biomater.*, vol. 7, no. 3, pp. 1241–1248, 2011.

- [150] J. Melrose, S. Smith, M. Cake, R. Read, and J. Whitelock, "Comparative spatial and temporal localisation of perlecan, aggrecan and type I, II and IV collagen in the ovine meniscus: An ageing study," *Histochem. Cell Biol.*, vol. 124, no. 3–4, pp. 225–235, 2005.
- [151] T. Mine, K. Ihara, H. Kawamura, R. Date, and K. Umehara, "Collagen expression in various degenerative meniscal changes: an immunohistological study.," *J. Orthop. Surg. (Hong Kong)*, vol. 21, no. 2, pp. 216–220, 2013.
- [152] C. Kiani, L. Chen, Y. J. Wu, A. J. Yee, and B. B. Yang, "Structure and function of aggrecan," *Cell Res.*, vol. 12, no. 1, pp. 19–32, 2002.
- [153] R. R. Miller and C. A. McDevitt, "Thrombospondin in ligament, meniscus and intervertebral disc," *BBA - Gen. Subj.*, vol. 1115, no. 1, pp. 85–88, 1991.
- [154] P. Singh and J. E. Schwarzbauer, "Fibronectin matrix assembly is essential for cell condensation during chondrogenesis," *J. Cell Sci.*, vol. 127, no. 20, pp. 4420–4428, 2014.
- [155] P. Singh and J. E. Schwarzbauer, "Fibronectin and stem cell differentiation - lessons from chondrogenesis," *J. Cell Sci.*, vol. 125, no. 16, pp. 3703–3712, 2012.
- [156] C. B. Foldager, W. S. Toh, A. H. Gomoll, B. R. Olsen, and M. Spector, "Distribution of Basement Membrane Molecules, Laminin and Collagen Type IV, in Normal and Degenerated Cartilage Tissues," *Cartilage*, vol. 5, no. 2, pp. 123–132, 2014.
- [157] L. F. Yousif, J. Di Russo, and L. Sorokin, "Laminin isoforms in endothelial and perivascular basement membranes," *Cell Adhes. Migr.*, vol. 7, no. 1, pp. 101–110, 2013.
- [158] M. Cescon, F. Gattazzo, P. Chen, and P. Bonaldo, "Collagen VI at a glance," *J. Cell Sci.*, vol. 128, no. 19, pp. 3525–3531, 2015.
- [159] E. J. Vanderploeg, C. G. Wilson, S. M. Imler, C. H. Y. Ling, and M. E. Levenston,

- “Regional variations in the distribution and colocalization of extracellular matrix proteins in the juvenile bovine meniscus,” *J. Anat.*, vol. 221, no. 2, pp. 174–186, 2012.
- [160] L. Shum and G. Nuckolls, “The life cycle of chondrocytes in the developing skeleton,” *Arthritis Res.*, vol. 4, no. 2, pp. 94–106, 2002.
- [161] A. C. Hall, “The Role of Chondrocyte Morphology and Volume in Controlling Phenotype—Implications for Osteoarthritis, Cartilage Repair, and Cartilage Engineering,” *Curr. Rheumatol. Rep.*, vol. 21, no. 8, 2019.
- [162] P. H. G. Chao, A. C. West, and C. T. Hung, “Chondrocyte intracellular calcium, cytoskeletal organization, and gene expression responses to dynamic osmotic loading,” *Am. J. Physiol. - Cell Physiol.*, vol. 291, no. 4, 2006.
- [163] A. M. DeLise, L. Fischer, and R. S. Tuan, “Cellular interactions and signaling in cartilage development,” *Osteoarthr. Cartil.*, vol. 8, no. 5, pp. 309–334, 2000.
- [164] I. Sekiya *et al.*, “Dexamethasone enhances SOX9 expression in chondrocytes,” *J. Endocrinol.*, vol. 169, no. 3, pp. 573–579, 2001.
- [165] T. Takano, M. Takigawa, and F. Suzuki, “Stimulation by glucocorticoids of the differentiated phenotype of chondrocytes and the proliferation of rabbit costal chondrocytes in culture,” *J. Biochem.*, vol. 97, no. 4, pp. 1093–1100, 1985.
- [166] W. Horton, T. Miyashita, K. Kohno, J. R. Hassell, and Y. Yamada, “Identification of a phenotype-specific enhancer in the first intron of the rat collagen II gene,” *Proc. Natl. Acad. Sci. U. S. A.*, vol. 84, no. 24, pp. 8864–8868, 1987.
- [167] R. Quarto, G. Campanile, R. Cancedda, and B. Dozin, “Thyroid hormone, insulin, and glucocorticoids are sufficient to support chondrocyte differentiation to hypertrophy: A serum-free analysis,” *J. Cell Biol.*, vol. 119, no. 4, pp. 989–995, 1992.
- [168] J. Connelly, T. Petrie, A. Garcia, M. Levenston “Fibronectin- and Collagen-

Mimetic Ligands Regulate BMSC Chondrogenesis in 3D Hydrogels," *Eur Cell Mater.*, 22: 168-177, 2018.

- [169] M. Ivarsson, A. Mcwhirter, T. K. Borg, and K. Rubin, "Type I collagen synthesis in cultured human fibroblasts: Regulation by cell spreading, platelet-derived growth factor and interactions with collagen fibers," *Matrix Biol.*, vol. 16, no. 7, pp. 409–425, 1998.
- [170] Y. Liang *et al.*, "Chondrogenic differentiation of synovial fluid mesenchymal stem cells on human meniscus-derived decellularized matrix requires exogenous growth factors," *Acta Biomater.*, vol. 80, pp. 131–143, 2018.
- [171] B. B. Rothrauff, K. Shimomura, R. Gottardi, P. G. Alexander, and R. S. Tuan, "Anatomical region-dependent enhancement of 3-dimensional chondrogenic differentiation of human mesenchymal stem cells by soluble meniscus extracellular matrix," *Acta Biomater.*, vol. 49, pp. 140–151, 2017.
- [172] C. Henrionnet *et al.*, "* Hypoxia for Mesenchymal Stem Cell Expansion and Differentiation: The Best Way for Enhancing TGF β -Induced Chondrogenesis and Preventing Calcifications in Alginate Beads," *Tissue Eng. Part A*, vol. 23, no. 17–18, pp. 913–922, 2017.
- [173] K. Endo, N. Fujita, T. Nakagawa, and R. Nishimura, "Comparison of the effect of growth factors on chondrogenesis of canine mesenchymal stem cells," *J. Vet. Med. Sci.*, vol. 81, no. 8, pp. 1211–1218, 2019.
- [174] A. Kornmuller, C. F. C. Brown, C. Yu, and L. E. Flynn, "Fabrication of Extracellular Matrix-derived Foams and Microcarriers as Tissue-specific Cell Culture and Delivery Platforms," no. April, pp. 1–11, 2017.
- [175] C. Yu, A. Kornmuller, C. Brown, T. Hoare, and L. E. Flynn, "Biomaterials Decellularized adipose tissue microcarriers as a dynamic culture platform for human adipose-derived stem / stromal cell expansion," *Biomaterials*, vol. 120, pp. 66–80, 2017.

- [176] S. A. Young *et al.*, “Biomaterials Mechanically resilient injectable scaffolds for intramuscular stem cell delivery and cytokine release,” *Biomaterials*, vol. 159, pp. 146–160, 2018.
- [177] L. E. Flynn, “Biomaterials The use of decellularized adipose tissue to provide an inductive microenvironment for the adipogenic differentiation of human adipose-derived stem cells,” *Biomaterials*, vol. 31, no. 17, pp. 4715–4724, 2010.
- [178] T. Tian, Y. Han, S. Toutounji, B. G. Amsden, and L. E. Flynn, “Biomaterials Adipose-derived stromal cells mediate in vivo adipogenesis , angiogenesis and inflammation in decellularized adipose tissue bioscaffolds,” *Biomaterials*, vol. 72, pp. 125–137, 2015.
- [179] J. A. Rowley, G. Madlambayan, and D. J. Mooney, “Alginate hydrogels as synthetic extracellular matrix materials,” *Biomaterials*, vol. 20, no. 1, pp. 45–53, 1999.
- [180] J. T. Connelly, A. J. García, and M. E. Levenston, “Inhibition of in vitro chondrogenesis in RGD-modified three-dimensional alginate gels,” *Biomaterials*, vol. 28, no. 6, pp. 1071–1083, 2007.
- [181] R. A. Pouliot *et al.*, “Porcine Lung-Derived Extracellular Matrix Hydrogel Properties Are Dependent on Pepsin Digestion Time,” *Tissue Eng. - Part C Methods*, vol. 26, no. 6, pp. 332–346, 2020.
- [182] Y. Zhao, S. D. Waldman, and L. E. Flynn, “The effect of serial passaging on the proliferation and differentiation of bovine adipose-derived stem cells,” *Cells Tissues Organs*, vol. 195, no. 5, pp. 414–427, 2012.

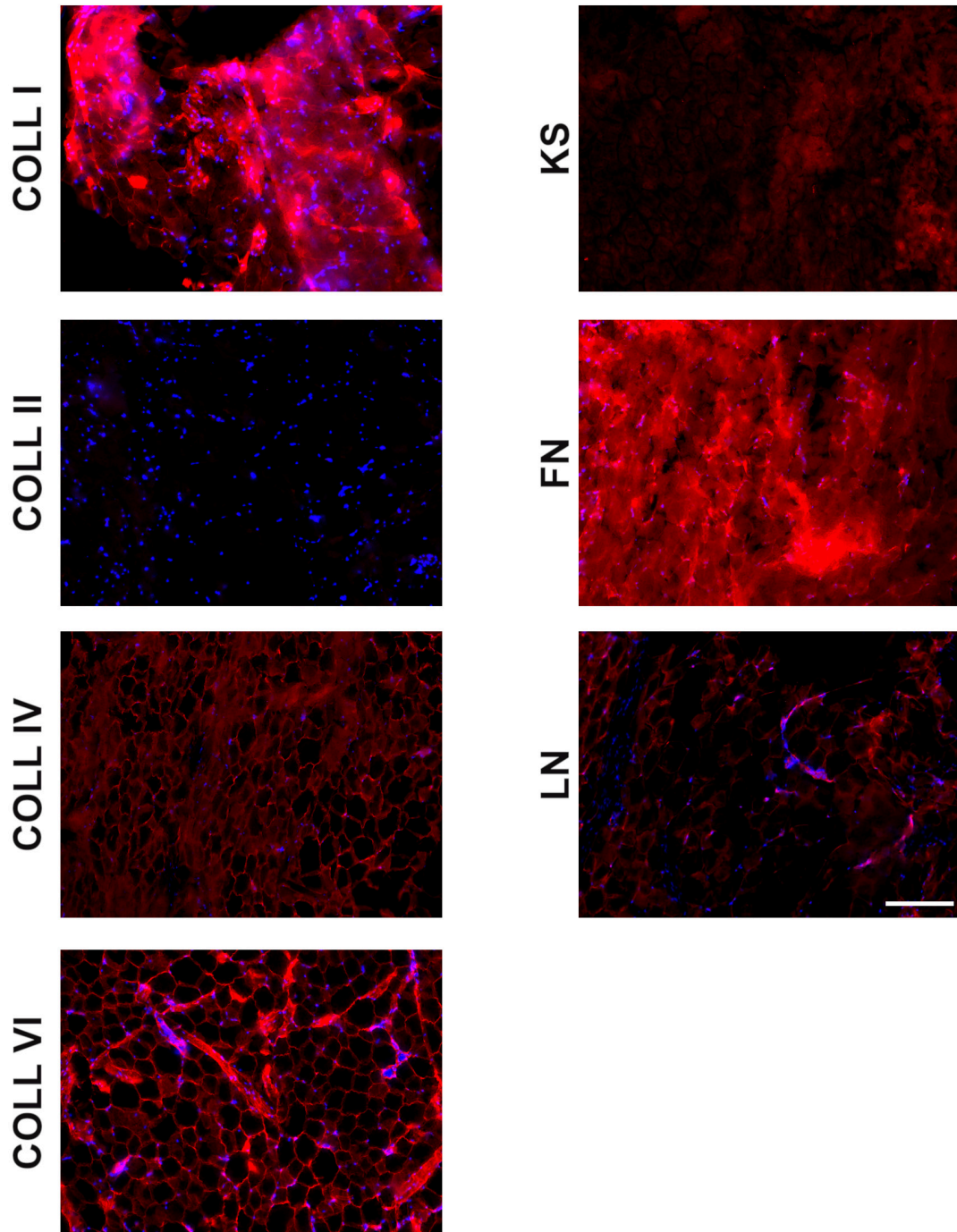
Appendix A: Supplementary Data

Supplementary Table A. 1: ASC Donor Information

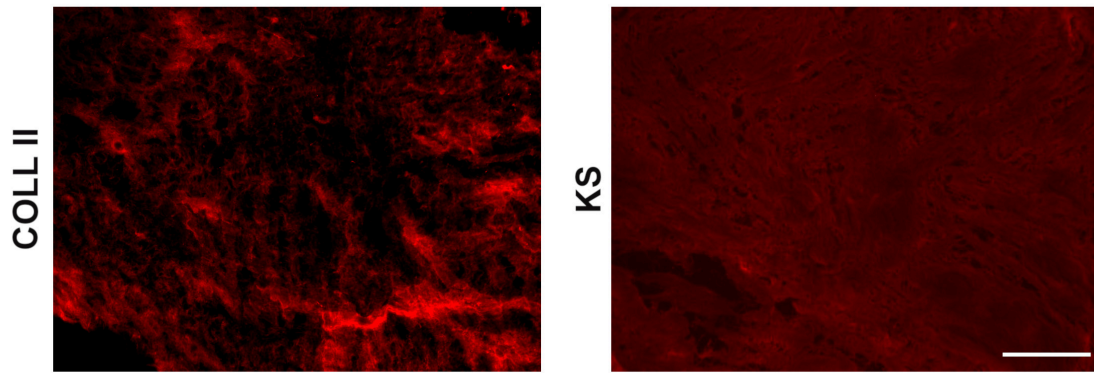
Donor	Gender	Age	Weight (kg)	Height (cm)	Surgical Site
1*	Female	37	86.1	175	Breast
2*	Female	49	68.7	158	Breast
3†	Female	63	87.0	161	Breast

*Donors used in viability and gene expression studies

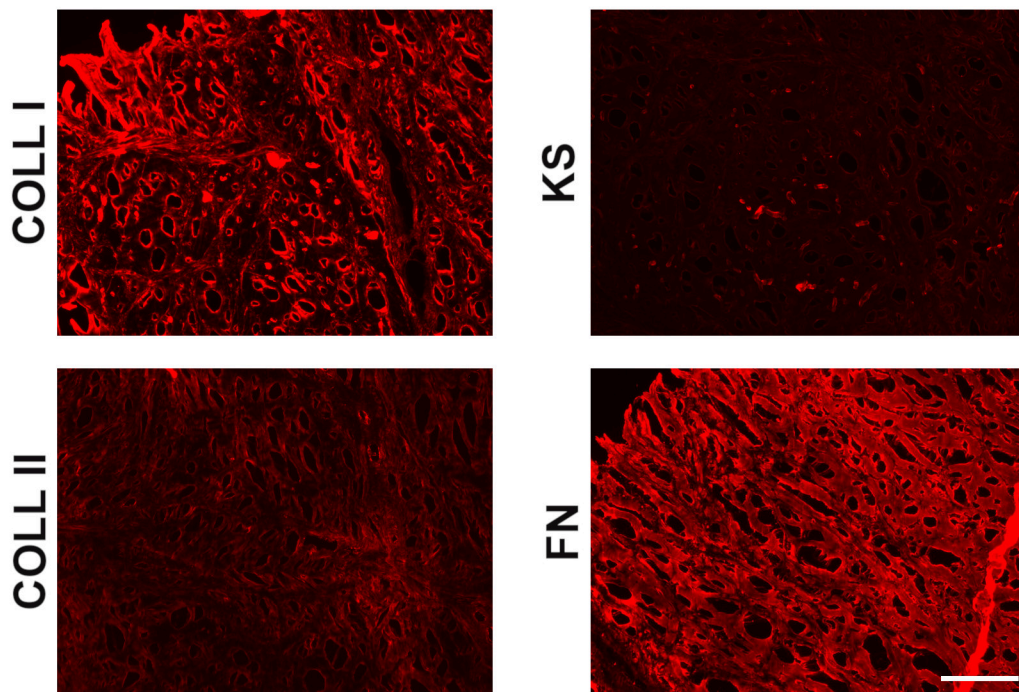
†Donor used only in viability study



Supplementary Figure A.1. Immunohistochemical staining of porcine skin was used as a positive control for meniscus staining. ECM markers (red) are counterstained with DAPI (blue) to visualize cell nuclei. Abbreviations: Coll I=collagen type I, Coll II=collagen type II, Coll IV=collagen type IV, Coll VI=collagen type VI, KS=keratan sulphate, FN=fibronectin, LN=laminin. Scale bar= 200 μ m.



Supplemental Figure A.2. Immunohistochemical staining of native bovine nucleus pulposus as a positive control for meniscus staining. Abbreviations: Coll II=collagen type II, KS=keratan sulphate. Scale bar= 200 μ m.



Supplementary Figure A.3. Immunohistochemical staining of native porcine inner meniscus was used as a positive control for alginate bead staining. Abbreviations: Coll I=collagen type I, Coll II=collagen type II, KS=keratan sulphate, FN=fibronectin. Scale bar= 200 μ m.

Appendix B: Research Ethics Board Approval



Date: 17 July 2020

To: Dr. Lauren Flynn

Project ID: 105426

Study Title: Tissue Engineering with Adipose-derived Stem Cells

Application Type: Continuing Ethics Review (CER) Form

Review Type: Delegated

REB Meeting Date: 04/Aug/2020

Date Approval Issued: 17/Jul/2020

REB Approval Expiry Date: 13/Aug/2021

Dear Dr. Lauren Flynn,

The Western University Research Ethics Board has reviewed the application. This study, including all currently approved documents, has been re-approved until the expiry date noted above.

REB members involved in the research project do not participate in the review, discussion or decision.

Western University REB operates in compliance with, and is constituted in accordance with, the requirements of the TriCouncil Policy Statement: Ethical Conduct for Research Involving Humans (TCPS 2); the International Conference on Harmonisation Good Clinical Practice Consolidated Guideline (ICH GCP); Part C, Division 5 of the Food and Drug Regulations; Part 4 of the Natural Health Products Regulations; Part 3 of the Medical Devices Regulations and the provisions of the Ontario Personal Health Information Protection Act (PHIPA 2004) and its applicable regulations. The REB is registered with the U.S. Department of Health & Human Services under the IRB registration number IRB 00000940.

Please do not hesitate to contact us if you have any questions.

Sincerely,

The Office of Human Research Ethics

Note: This correspondence includes an electronic signature (validation and approval via an online system that is compliant with all regulations).

Appendix C: Figure Permissions

License Number	4974260644582
License date	Dec 22, 2020
Licensed Content Publisher	Elsevier
Licensed Content Publication	Biomaterials
Licensed Content Title	The knee meniscus: Structure–function, pathophysiology, current repair techniques, and prospects for regeneration
Licensed Content Author	Eleftherios A. Makris, Pasha Hadidi, Kyriacos A. Athanasiou
Licensed Content Date	Oct 1, 2011
Licensed Content Volume	32
Licensed Content Issue	30
Licensed Content Pages	21
Start Page	7411
End Page	7431
Type of Use	reuse in a thesis/dissertation
Portion	figures/tables/illustrations
Number of figures/tables/illustrations	2
Format	electronic
Are you the author of this Elsevier article?	No
Will you be translating?	No
Title	Master's Thesis on 3D printable bioink containing decellularized meniscus
Institution name	Western University
Expected presentation date	Feb 2021
Portions	Figure 2 and Figure 3
	Ms. Sheridan Doherty

Curriculum Vitae

Name: Sheradan Lana Doherty

Post-secondary Education and Degrees: Queen's University
Kingston, Ontario, Canada
2014-2018 B.Sc. (Honours Specialization in Biochemistry)

The University of Western Ontario
London, Ontario, Canada
2018-2021 M.E.Sc. Candidate (Biomedical Engineering)

Honours and Awards: CMHR Transdisciplinary Bone and Joint Training Award
2018-2020

CONNECT! NSERC CREATE Program in Soft Connective Tissue
Regeneration/Therapy Training Award
2018-2020

Western Graduate Research Scholarship
2018-2020

Student's Choice TA Award
The University of Western Ontario
2018

Student's Choice TA Award
The University of Western Ontario
2019

Related Work Experience Teaching Assistant
The University of Western Ontario
2018-2019

Internship
Aspect Biosystems
Vancouver, British Columbia, Canada
2019